2008

Probing Structural Differences of Recombinant Prion Isoforms Using Fluorescence Spectroscopy

Jessica Louise Gilbert
The University of Montana

PROBING STRUCTURAL DIFFERENCES OF RECOMBINANT PRION ISOFORMS USING FLUORESCENCE SPECTROSCOPY

By

JESSICA LOUISE GILBERT

B.A. Biology, University of Montana, Missoula, MT, 2006

Thesis

presented in partial fulfillment of the requirements
for the degree of

Master of Science
in Biochemistry

The University of Montana
Missoula, MT

Spring 2009

Approved by:

Perry Brown, Associate Provost for Graduate Education
Graduate School

Dr. Michele A. McGuirl, Chair
Division of Biological Sciences

Dr. Scott Wetzel
Division of Biological Sciences

Dr. Bruce Bowler
Chemistry Department

Gilbert, Jessica, M.S., Spring 2009

Major
Biochemistry

Probing Structural Differences of Recombinant Prion Isoforms Using Fluorescence Spectroscopy

Chairperson: Dr. Michele A. McGuirl

Conversion of prion protein (PrP) from its normal, cellular isoform, PrP^{C}, to an infectious, misfolded, fibrillar isoform, PrP^{Sc}, is responsible for various neurodegenerative diseases in a variety of mammalian hosts. Although the structure of PrP^{C} is well studied, the structure of PrP^{Sc} is not known. Obtaining structural information on the misfolded isoform of prion may lead to preventative therapies and treatments of prion diseases. In this study, six single-tryptophan mutants of recombinant PrP were expressed, purified, and refolded into PrP^{C} or two misfolded isoforms of prion, PrP^{β} and PrP^{F}. Solvent accessibilities of the six tryptophan residues were probed among the three isoforms using various tryptophan fluorescence techniques. For all six mutants, solvent accessibility was shown to decrease following conversion to the misfolded isoforms. Tryptophan accessibility data was used to evaluate two computational models of PrP^{Sc}, the β-helix model and the β-spiral model, and was also compared with experimental data in literature. Although neither computational model entirely fit the data, the Surewicz model of parallel, in-register β-strands comprising residues ~160-220 was in agreement with tryptophan accessibilities of residues within this area. However, more structural detail of this experimentally-based model is needed before the two data sets can be fully compared.

Table of Contents

List of Tables

List of Figures

CHAPTER 1: INTRODUCTION

In the1900s, a group of diseases was discovered that would challenge the way scientists view infectious agents. From the first successful transmission studies and the similarities observed among various diseases, to the controversial definition of a prion and the long fought struggle for functional and structural data on multiple isoforms, prion protein and its related diseases continue to hold great enigma in the scientific community. This chapter gives an introduction to the prion protein starting with the history and discovery of different prion diseases and the definition of the infectious agent. This chapter also gives an overview of the various isoforms of the prion protein (PrP): the cellular PrP^{C}, the infectious PrP^{Sc}, and the *in vitro* PrP^{β} and PrP^{F}. This chapter then concludes with a section on structural models of PrP^{Sc} and studies focused on elucidating the structure of the infectious isoform along with the goal and aims of my thesis as related to the theoretical models of PrP^{Sc}.

1-1. History, Discovery and Definition of Infectious Agent

The history of prion diseases, known also as transmissible spongiform encephalopathies (TSEs), starts as early as the 18^{th} century, but the discovery and definition of the proteinaceous infectious particle took until 1982 and nearly a century of research before being revealed. Because of the multiple TSE diseases and their variability between host species and among similar species, the road to discovery was by no means fast and straightforward. It took the work of many scientists who first observed commonalities in diseases spanning different host species, who developed more advanced and more accessible means of research, and who looked beyond the established understanding of infectious agents to uncover the unifying etiology of transmissible

spongiform encephalopathies. This section chronicles the journey of various researchers attempting to pinpoint the cause of emerging TSE diseases while unearthing commonalities, advancing scientific techniques and redefining the way science views infectious agents.

(A) History of TSE Diseases

Scrapie Prion disease has origins in the 1730s with the recognition of a disease afflicting sheep, given the name scrapie [1, 2]. For reviews on prion see [2-13]. Diseased animals exhibited abnormal behavior such as disinterest, disorientation, cessation of food intake, loss of coordination in the hindquarters, and scraping or rubbing against fixed objects. The latter behavior lends the name of the disease [13, 14]. A major histological abnormality was observed in the appearance of spongiform vacuolation in brain matter of infected animals. The cause of scrapie infection would not be uncovered for many years, but the speculation that it was a transmissible illness was suggested in a German publication in 1759 stressing the importance of isolating infected sheep from the herd [1] and later in 1932 when sheep contracted scrapie after grazing in a field previously inhabited by infected sheep [15]. The transmissible nature of this disease was confirmed in 1936 when Cuille and Chelle used intraocular injections containing preparations of spinal fluid from diseased sheep to infect healthy sheep [16]. They were able to reproducibly show sheep-to-sheep scrapie transmissibility with an incubation period of 14-22 months [8, 14, 16]. While the infectious nature of scrapie had been demonstrated, the causative agent was not yet identified, but accidental incidents of transmission provided some insight into the nature of this disease. Publications by Cuille and Chelle in 1939 [13, 17] and later by William Gordon in 1946 [18] demonstrated inadvertent

infection of healthy sheep from inoculation with a vaccine containing serum from scrapie-infected animals. An important aspect of these accidental transmissions was that the vaccines proved infectious even after the typical treatment of formalin and heat, which was used to destroy bacterial contaminants [11, 18]. These occurrences along with infection of sheep from materials passed through antibacterial filters [9, 14] left scientists speculating that the disease was caused by a slow virus exhibiting an unusually long incubation time [11, 19, 20].

Research with TSE diseases was slow. Because of the long incubation times and low transmissibility in sheep (~25%), it was difficult for scrapie research to be accessible to many scientists [14]. In 1959, Pattison successfully infected goats with scrapie using brain inoculum from diseased sheep with 100% success [14, 21]. This significantly increased research and data collection, as it required fewer animals. It wasn't until 1961 when Chandler showed transmission to mice that the door opened even wider for less expensive, shorter, more accessible laboratory experiments on scrapie [22].

Kuru In the 1950's the anthropologists Ronald and Catherine Berndt were the first to describe a disease afflicting the Fore people of Papua-New Guinea, called kuru by the natives meaning "to shiver" [3]. This disease involved partial paralysis, involuntary twitching, a feeling of coldness and the hallmark trait of shivering. The Fore practiced ritual cannibalism and would eat the remains of dead relatives as a sign of respect and mourning. When kuru was first discovered [23], there was much debate concerning the etiology. Was it an inherited disease, effects from toxic exposure, caused by dietary or environmental factors, an infection [9]? Although Carleton Gajdusek was on the forefront

of kuru investigation and published the first report in 1957 [24], it took the insight of William Hadlow in 1959 for the first major piece to fall into place [9, 11].

Hadlow was a veterinary neuropathologist working on scrapie in England when his colleague from Rocky Mountain Laboratory in Hamilton, MT mentioned an exhibit at the London Wellcome Medical Museum pertaining to a strain of brain disease in the Fore people of New Guinea. As Hadlow viewed the exhibit, he was struck by the similarities in neuro-histologic pictures of infected brains; the vacuolated neurons and spongiform degeneration were much like those in scrapie-infected brains. Following these observations, Hadlow wrote a letter to the Lancet entitled "Kuru and Scrapie" and sent a copy to Gajdusek in 1959 strongly suggesting further tests to inoculate kuru in primates [3, 9, 19].

CJD Just as kuru and scrapie had been linked by Hadlow, in 1959 neuropathologist Igor Klatzo published his speculations concerning similarities between kuru and another TSE known as Creuztfeldt-Jakob disease (CJD) [9, 11, 25]. Like Hadlow, Klatzo was struck by the histological similarities in brains of infected individuals. Creuztfeldt-Jakob disease was first documented in the 1920s by physicians Creutzfeldt and Jakob. In these cases, patients developed symptoms of dementia followed by rapid death. Further cases of this type followed, and the cause was either left as a mystery or described as the result of an unknown agent [26].

In 1966, at the prompting of William Hadlow, Gajdusek was successful in transmitting kuru to primates by intracerebral inoculation [27]. He then demonstrated the successful transmission of CJD to primates in 1968 [28]. Gajdusek's accomplishment was a major step for investigators of TSE diseases, and in 1976 he won a Nobel Prize for

"discovering new mechanisms of disease causes and dissemination" [29, 30]. Traditionally, transmissibility is required to classify a bona fide prion disease [3].

GSS and FFI The first familial TSE disease was diagnosed in 1928. It appeared similar to CJD but differed in such aspects as duration of disease and age of onset. This disease, known as Gerstmann-Straussler-Scheinker Syndrome (GSS) and named for the founding researchers, originated from an Austrian family in 1928 [31] and 1936 [32], but its classification as a TSE did not occur until 1981 when Masters showed transmission to primates using brain tissue inoculation [33]. Later studies isolated mutations in the prion gene responsible for the onset of disease, showing GSS to be a caused by genetic factors [7]. In 1989, Hsiao was the first to identify a mutation (P102L) genetically linked with GSS [34].

Another familial TSE was identified in 1986. An Italian family reported symptoms including insomnia, which worsened until the patients were completely unable to sleep, leading to death in 1 or 2 years following onset. This disease had reportedly been in the wife's family for over 200 years [9, 35] and was termed fatal familial insomnia (FFI). FFI was also classified as a TSE disease after later being shown to be transmissible [36, 37]. In 1992, the identification of a mutation in the prion protein (D178N) allowed for classification of FFI as a genetically inherited disease [38].

BSE and vCJD Although a variety of TSE diseases had emerged in the 1900s, the incidence of infection in humans was low and, according to some neurologists, non-existent. This quickly changed with the appearance of bovine spongiform encephalopathy (BSE) and subsequent disease transmission to humans in the form of variant CJD (vCJD). In the 1980s, hundreds of thousands of cows were affected yearly

(mostly in Europe), increasing up to nearly 2 million cows in 2007. This outbreak was thought to be caused by contaminated feed made from rendered carcasses. It had huge repercussions including bans on import and export of beef products and along with the slaughtering of infected animals resulted in staggering economic costs [3, 5, 10]. Besides the havoc wreaked on the cattle industry, a variant form of CJD (vCJD) was first described in 1996; widespread panic concerning humans ingesting contaminated meat and contracting vCJD after long incubation periods brought to light the importance of TSE research and prevention [13, 39]. Other diseases such as feline spongiform encephalopathies, exotic ungulate encephalopathy (EUE), and transmissible mink encephalopathy were caused by the outbreak of BSE and the dispersion of contaminated beef products to captive animals in zoos and other industries [3, 5].

Chronic Wasting Disease Another noteworthy prion disease affecting animals is chronic wasting disease (CWD) in elk and mule deer. Manifestations of CWD include small growth size, changes in behavior, head tremors and unusual sleepiness. The existence of CWD is especially troublesome to hunters as it is present and spreading via horizontal transfer among free-range animals in North America [40]. So far, there is no evidence supporting the transmission of CWD to humans, but with the experience of BSE and transmission across the species barrier causing vCJD, it has been a valid concern [12, 13].

(B) History of Prion Discovery and Definition

Due to the work and insight of several researchers, transmission was shown to be a common factor linking seemingly disparate diseases like kuru, scrapie and CJD to a common etiology, but the isolation and identification of the causative agent still remained

elusive. It was through advancement of scientific techniques and approaches coupled with the ability to theorize outside the established scientific dogma that the responsible agent was finally discovered. This section highlights some of the advancements in TSE investigation that paved the way for scientific discoveries involving the definition of a prion and the mechanism of prion propagation.

History of Prion Discovery The transmissibility research led to intense efforts to identify the causative agent. Studies had shown that scrapie was transmissible even after treating the samples with heat, formalin, RNase, and DNase [14, 41]. In 1966, Tikvah Alper demonstrated that the infectious agent could also withstand high doses of radiation known to destroy the nucleic acid components of other infectious agents [9, 11, 42, 43]. Studies by Alper showed the minimum molecular weight still possessing infectivity was ~200,000 Da, a size known to be too small for a virus or other cellular pathogens [43, 44]. These data suggested that the infectious agent might be novel.

In the forefront of research was another player waiting to make his grand entrance. In 1972, Stanley Prusiner, a resident in neurology became interested in TSE diseases after one of his patients died from CJD. Intrigued by the radiation studies of Alper, which strongly supported an infectious agent devoid of nucleic acid, Prusiner became interested in the structure of the infectious agent and the prospect of a captivating research project [45]. Prusiner realized that his best shot to identify the structure of the causative agent was to purify the infectious agent from brain homogenates of diseased animals [11]. Purification techniques typically involved subjecting brain homogenates to differential centrifugation or other fractionation techniques followed by assays of infectivity for each fraction by intracerebral inoculation into mice. Endpoint infectivity

assays were performed in which a series of dilutions were inoculated into mice and the highest positive dilution was determined after waiting for the animals to become sick. Due to the long incubation time for mice and the numbers required for meaningful endpoint titration assays, these experiments were difficult to run in parallel and could take an entire year for results [11, 46].

Help arrived in 1975 when successful inoculation of scrapie into Syrian hamsters was demonstrated [47]. By developing an incubation time assay in place of the endpoint titration assay, the time required for experiments was ~ 70 days vs 360 days for endpoint titration assays in mice. Incubation time was defined as the time between inoculation and onset of disease symptoms. It became possible with this assay to determine the prion titer in the innoculum as there is an inverse relationship between titer and length of incubation [48]. This not only significantly shortened the time between experiments, but also the development of the incubation time assay significantly decreased the numbers of animals needed for experiments [11].

Successful purification was achieved in 1982 by enriching fractions of Syrian hamster brain for scrapie infectivity [46]. The agent found was a 27-30kDa protease-resistant core of a protein that was called PrP^{Sc} (with "Sc" designating the scrapie origin). Partial resistance of PrP^{Sc} to proteolysis became a tool for sample enrichment and characterization.

Protein-Only Hypothesis The first enunciation of a protein-only hypothesis occurred in 1967 by a mathematician by the name of John Griffith, who published modeling studies concerning the infectious agent of scrapie [49]. One of his models involved the possibility that the agent could be an aberrant form of a protein that forms

conformational templates and replicates following self-association mechanisms [10, 49, 50]. In this model, disease could arise through spontaneous formation of an aberrant protein or it could occur by transmission of a protein template from an exogenous source. Griffith's mathematical logic coupled with the scientific data showing that the infectious agent was a protein, paved the way for a new outlook on infectious agents and propagation of disease.

Scrapie infectivity was shown to diminish after adding agents that disrupted protein structure by hydrolysis, modification or denaturation, but no decrease in infectivity was observed following treatments that alter nucleic acids [44]. Because of these and similar studies coupled with the small size of the infectious particle, Prusiner thought it appropriate to give this novel agent a name distinguishing it from viruses. The word prion was coined and was defined as a **pro**teinaceous **in**fectious particle that lacks a nucleic acid component. Prusiner was quick to add that the possibility that a small but essential ligand bound to PrP^{Sc} could not be eliminated from his purified preparations [46]. Prusiner won a Nobel Prize in Medicine in 1997 for pioneering the discovery of an entirely new disease-causing agent and the underlying principles of their mode of action [51].

Following purification and identification of PrP^{Sc} came the sequencing of the protein in 1985. cDNA probes confirmed that the prion gene was expressed in healthy adult brains as well as diseased brains, and the likely scenario that normal and infectious prion differed only in their conformation was as heretical as the protein-only hypothesis. Up until that time, conventional dogma was that one gene made one protein with one

structure [11]. Logical evidence for a protein-only mechanism of disease had been expressed before, however, and was not entirely inconceivable.

Emerging scientific evidence continues to confirm the protein-only theory of prion disease and propagation. Although the exact mechanism is still not fully understood, current models exist that attempt to explain the mechanism of conversion. Barring a few variations on a similar theme, the model for prion conversion and aggregation involves a protein-misfolding event followed by the autocatalytic conversion of normal cellular prion (PrP^{C}) into PrP^{Sc}. This begins a chain reaction that results in an accumulation of PrP^{Sc}. These aggregate to form insoluble fibrils. PrP^{C} can either spontaneously misfold, catalyzing the formation and subsequent aggregation of other PrP^{Sc} molecules or PrP^{C} can misfold upon interaction with a misfolded PrP^{Sc} seed [13].

The conversion from PrP^{C} to PrP^{Sc} is accompanied by an increase in β-sheet secondary structure as measured by CD and FTIR [5, 52, 53]. From his sedimentation experiments, Prusiner had observed non-ideal behavior of PrP^{Sc}, and attributed this to a hydrophobic nature of the scrapie agent [54, 55]. The formation of hydrophobic β-sheets explains the potential for fibril and amyloid plaque accumulation, as hydrophobic interactions would propagate the aggregation of misfolded monomers. There has been conjecture concerning the presence of a cofactor or protein X that assists in the misfolding process [56], and this scenario has not yet been ruled out [57] . In any case, it is the autocatalytic mechanism of prion misfolding using PrP^{C} as a substrate that provides a self-replicating model for prion propagation and transmissibility.

Support and Debate Regarding Protein-Only Hypothesis Although viewed by some as heretical, the protein-only hypothesis and mechanism of disease propagation

was backed by many pieces of evidence. It has been shown that scrapie infectivity copurifies with PrP^{Sc}, is maintained in samples where no other particle is detected, and significantly decreases with agents that disrupt protein structure (urea, guanidine, trypsin, hydrolyzing agents) or bind to PrP (anti-PrP antibodies) [58]. Unlike viral diseases, procedures targeted to nucleic acids (radiation, nucleases) produce no decrease in infectivity, the infectious agent elicits no immune response such as inflammation or antigen presentation and no virus has ever been consistently seen in association with the disease [7].

Supporting genetic evidence for the protein-only hypothesis includes the absence of disease and PrP^{Sc} propagation in mice devoid of the PrP gene even after inoculation with brain homogenate from scrapie infected mice [59]. Genetic studies also show that most, if not all, of the familial TSE diseases are associated with mutations in the prion gene. The fact that familial diseases caused by mutation in the prion gene are able to be further transmitted adds additional support to the protein-only hypothesis [13, 50]. Also, a study by Meyer-Luehmann et al. has provided evidence that Alzheimer's disease can be transmitted in mice via intracerebral injections of amyloid-β containing brain extracts from diseased individuals [60]. This provides major support for the protein-only hypothesis as it shows the possibility that other amyloid diseases exhibiting abnormal protein components and aggregation like Alzheimer's, type 2 diabetes, and Parkinson's may be rendered infectious in the laboratory setting.

Arguments concerning the protein-only hypothesis still exist. Based on conventional biology, information is encoded in nucleic acid and not proteins. Therefore, the existence of strains exhibiting diverse phenotypes in prion diseases has been a strong

argument supporting a nucleic acid component. Scrapie and other TSEs occur in multiple strains. Strains are defined by differences in incubation time, the distribution of vacuole formation and amyloid deposits in the brain, and clinical symptoms [5, 12, 50]. This disparity has been attributed to conformational differences between PrP^{Sc} in the various strains; the information regarding the phenotypic differences is encoded in the conformation of PrP^{Sc}, which is replicated as it recruits PrP^{C} substrate. Studies have shown that PrP^{Sc} from various strains exhibit different denaturation profiles, sizes of proteinase K resistant fragments as well as different glycosylation patterns [5, 61]. The mechanistic details regarding how conformational variations give rise to different phenotypic properties of disease still remain unknown.

The most important piece of information that was missing in support of the protein-only hypothesis is the generation of infectious prion in the test tube. If prion protein is the sole causative agent of disease, then it should be possible to form infectious PrP^{Sc} from recombinant, normal PrP. While recombinant PrP^{C} can be misfolded to form fibrils, infectivity studies with this isoform have been largely unsuccessful. Inoculation of fibrils formed *in vitro* into mice overexpressing the prion protein has been shown to cause disease [62], but it is known that animals overexpressing prion can develop disease spontaneously [13].

Perhaps the closest technique to show formation of infectious PrP^{Sc} *in vitro* is the use of protein misfolding cyclic amplification or PMCA. PMCA is a technique based on work done by Caughey and coworkers [63] and further refined by Soto [64] that is analogous to using PCR for DNA amplification. In PMCA, a PrP^{Sc} seed is incubated with an excess of wild type PrP^{C} and the mixture is incubated and then sonicated in successive

rounds. The incubation allows for the formation and aggregation of prion fibrils. Sonication methods fragment the fibrils, creating new seeds. The amount of PrP^{Sc} created depends on the number of cycles performed while samples containing no PrP^{Sc} seed do not show amplification of aggregated protein [64]. Requirements for PMCA and the retention of infectivity are substrate PrP^{C} and normal, uninfected brain homogenate along with a seed of PrP^{Sc}. Dilutions studies using PrP^{Sc} infected brain homogenate along with PrP^{C} for substrate showed continued amplification even when the mixture contained no trace of the initial infected brain homogenate [65]. This shows that replication can occur in a cell-free system without the presence of the initial seed, providing further support for the protein-only hypothesis [66]. To date, infectivity has not been shown from assays using pure PrP^{C} substrate without the cellular factors present in brain homogenates or by using recombinant PrP^{C} as a substrate. This supports the idea that an additional factor is required for pathology of the disease. While the creation of infectivity in the test tube has not yet been conclusively attained, with the PMCA assay it should be possible to identify factors necessary for the formation of infectious fibrils *in vitro* [12, 13].

1-2. Prion Isoforms

Prion protein is unusual in that it can exist in multiple, stable conformational states called isoforms. Disease is associated with the conversion of the cellular isoform, PrP^{C} into a misfolded, infectious isoform, PrP^{Sc}, which is chemically indistinguishable from PrP^{C} differing only in conformation [12]. Furthermore, the diverse phenotypes of various strains and diseases caused by the same protein are thought to be structurally determined. While NMR has elucidated the structure of PrP^{C}, the structure of the

misfolded, infectious isoform is not yet known. This section reviews the structure and biology of PrP^C along with hypotheses concerning the normal function of this protein in the body. Also contained in this section is information regarding the misfolded isoform of PrP^{Sc} along with two other stable isoforms used in laboratory settings, the β-oligomeric isoform, PrP^{β} and the recombinant fibrillar isoform, PrP^F.

(A) Cellular Prion, PrP^C

Structure and Biology Before examining the known information and questions concerning the disease-causing, infectious isoform of prion, it is important to take a look at the normal, cellular prion isoform found in mammalian species [5]. PrP^C is the cellular isoform of prion found primarily in the nervous system but is also found in bone marrow, blood, lymph nodes, and other organs [6]. Human prion is a 253 amino acid protein encoded by a gene with a single exon and one open reading frame [5]. A 22 amino acid leader sequence instructs the targeting of translation into the endoplasmic reticulum (ER) where the protein is processed for eventual secretion. In the ER, the N-terminal leader sequence is cleaved, a disulfide bond is formed between residues 179 and 214, N-linked oligosaccharides are added at Asn181 and 197, and a GPI anchor is attached after the cleavage of the C-terminal hydrophobic residues [67]. The post-translationally modified protein then travels through the Golgi where the sugars are trimmed and modified. The protein is then transported to the plasma membrane via endocytic vesicles. PrP^C is mainly a GPI-linked, extracellular surface protein located in lipid rafts, but a small minority of PrP^C constitutively cycles to and from endocytic compartments mediated by clathrin coated vesicle uptake [67]. In certain cases, prion protein can also exist as a transmembrane protein due to disruptions in translocation

events [68] or due to protein mutations causing familial prion disease [11]. PrP can be mono, di, or unglycosylated, and this variation may be associated with differential neuronal distribution and can distinguish various strains of prion disease [69]. Discovery of the prion gene, its recombinant expression in E. *coli* and purification has led to the elucidation of PrP^C structure through NMR [70] and X-ray crystallography [71] techniques. Recombinant PrP lacks the glycosylation and GPI anchor, but it is accepted as an accurate representation of PrP^C [72]. Although sequence and other slight variations exist, the major structural features of PrP^C among multiple species are highly conserved and are defined by two domains [6, 70]. NMR structures from Syrian Hamster prion show that residues 23-119 comprise a highly unstructured N-terminal domain containing multiple copies of an eight-residue repeating sequence P-H-G-G-G-W-G-Q (octarepeat). Residues 125-228 define the well-structured, globular, α-helical, C-terminal domain. Residues 113-128 comprise a highly conserved alanine-rich hydrophobic cluster that lacks regular secondary structure and is quite dynamic [11, 68, 70]. PrP^C contains three α-helices, Helix A, B, and C, spanning residues 144-156, 172-194, 200-227, respectively, and two short, anti-parallel β-strands, S1 and S2 spanning residues 129-131 and 161-163, respectively [70] (See Figures 1-1 and 1-2).

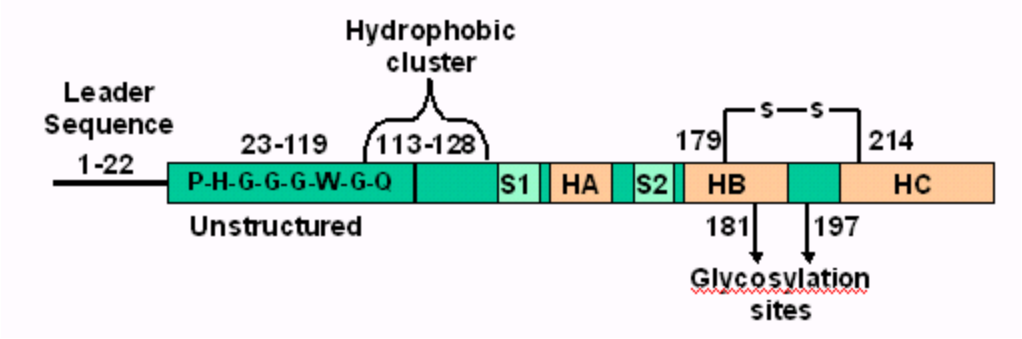

Figure 1-1. Depiction of prion sequence and structural elements showing: leader sequence that is cleaved prior to secretion, the unstructured, N-terminal domain containing the octarepeat sequences, the hydrophobic cluster and the three α-helices (HA, HB, HC) and two β-strands (S1 and S2) along with the disulfide bond and two glycosylation sites.

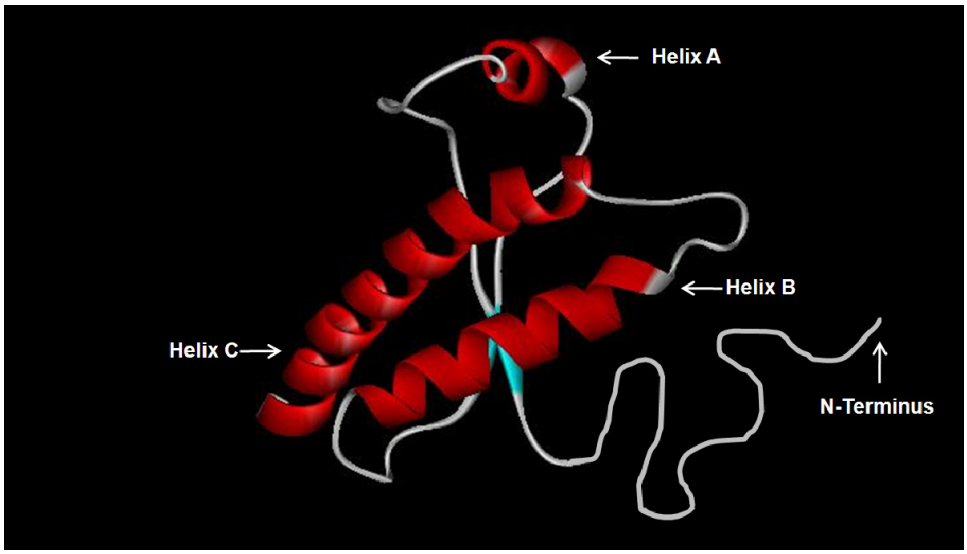

Figure 1-2. Structure of Syrian hamster PrP^{C} amino acids 125-228 from PDB 1B10, modified to include a representation of the unstructured N-terminal domain (amino acids 23-124, gray), the three α-helices A, B, C (red) and both β-strands (blue). Random coil secondary structure and turns are also in gray.

While the presence of PrP^{Sc} is diagnostic of prion disease, the exact mechanism of toxicity is unknown. Some propose that disease is caused by a gain of toxic function of

PrP^{Sc} whereby the misfolded prion is responsible for neuronal apoptosis and pathology of disease [6]. Others have speculated that the fibrils are formed to protect the cell from a smaller, intermediate species responsible for disease, as smaller oligomers have been shown to be more toxic to neurons [73, 74]. Discerning the location of conversion to PrP^{Sc} could illuminate the mechanisms of apoptosis. One hypothesis is that the low pH of the endosomal compartment destabilizes PrP^{C}, allowing for conversion and aggregation, as low pH was shown to trigger PrP misfolding *in vitro* [75, 76]. Other speculative locations of conversion include lipid raft domains on the cell surface, and the cytosol [77, 78]. Cells overexpressing PrP showed an accumulation of PrP^{Sc} in the cytosol due to retrograde transport to the ER when proteasome activity was dysfunctional. The direct mechanism of apoptosis is still controversial but the downstream pathways of both proteosome impairment and ER stress have been implicated [13].

Evidence exists that would argue the relationship between PrP^{Sc} and pathogenesis of disease. It is possible in some brain areas to show strong staining for PrP^{Sc} where there is no sign of neurodegeneration. Furthermore, transgenic animal models have shown that there can be high levels of brain degeneration in the absence of detectable PrP^{Sc} as well as high levels of PrP^{Sc} in animals with no neuropathologies (for review see [79]). Because of this and other data, some propose that a loss of function of PrP^{C} and not the buildup of PrP^{Sc} could be the cause of pathogenesis. What exact functions and mechanisms are involved, however, still remains to be seen.

Proposed Function of PrP^{C} Although highly studied, the role of prion protein in non-diseased organisms remains unknown. The creation of knockout mice devoid of

the prion gene produced minor defects in electrophysiology and circadian rhythms, but no major neurological or behavioral defects were evident. It was found that prion infectivity and propagation does not occur in PrP null mice, but no critical function could be assigned due to the lack of phenotypic abnormalities [59]. There have been many studies regarding the putative function of PrP^C in the brain (for reviews see [3, 6]). PrP^C localizes to lipid rafts, which are patches of plasma membrane often enriched in sphingolipids, GPI-linked proteins, and tyrosine kinases also thought to be points of signal transduction activity [67]. Because of this along with studies showing evidence of prion interacting with various signaling molecules, it has been postulated that PrP^C may play a role in signal transduction and neuroprotection [80-82]. Other potential ligands for PrP^C have included the anti-apoptotic molecule Bcl-2 [83]. Sequence homology of the octapeptide repeats with a domain common to the Bcl-2 anti-apoptotic family along with the ability of PrP^C to protect human neurons from Bax –induced apoptosis *in vitro* is evidence that PrP^C may belong in this family. This protective effect was not observed when PrP^C had mutations in the octapeptide repeats or mutations associated with inherited prion diseases in the C-terminal region [84]. However, the lack of evidence supporting PrP^C localization to the mitochondria, ER or cytoplasm where Bcl-2 proteins normally exist is an argument against this proposed role of PrP^C [13].

While numerous alternative functions are proposed [80-82, 85-90], a long held thought has been that PrP is involved in copper binding and neuronal protection from oxidative damage [91, 92]. The octapeptide repeat residues have been shown to bind Cu^{2+} ions at physiological concentrations at neutral pH and show less affinity at lower pH [93, 94]. Additionally, high concentrations of copper ions have been shown to rapidly

stimulate the reversible internalization of PrP^C [95]. These studies suggest a possible mechanism of copper binding, transport and release upon entering the more acidic endosomal compartments. Over-expression of PrP^C has been shown to increase copper uptake into cells and PrP null mice were shown to have lower copper content in brain membranes than WT mice [96]. Free Cu^{2+} is cytotoxic and the role of binding free copper ions could prevent oxidative damage throughout the brain. Although there is some controversy concerning the role of prion in copper binding and homeostasis, this hypothesis is still readily supported. Infected brain tissue was shown to contain heightened amounts of free radicals, oxidative damage of protein and disruption of metal ion levels [97]. Copper binding to PrP^C is shown to change its conformation and interfere with the folding of recombinant PrP^C. It is believed that the misfolding of PrP^C represents a loss of function of copper binding resulting in abnormal metal levels and neuronal damage [91].

Many other proposed functions of PrP^C including a role in sleep-awake cycles [89], memory and behavior [86], immune system activation [85], synaptic plasticity [87], neural stem cell biogenesis and development [88], and renewal of stem cells found in bone marrow [90]. Although there is much to learn, research shows PrP^C to be a multi-faceted protein able to interact with multiple ligands and cellular molecules, potentially producing wide-range consequences on physiology and behavior [6].

(B) Misfolded Isoforms

PrP^{Sc} PrP^C is monomeric, soluble, and is sensitive to proteinase K digestion. Through an unknown mechanism PrP^C misfolds into an isoform enriched in β-sheet structure and partially resistant to proteinase K digestion. This infectious isoform, PrP^{Sc},

is found in the brains of diseased mammals, is multimeric, insoluble, and aggregates, forming fibrils and plaques in the infected cells. PrP^{Sc} is stable at slightly acidic to neutral pH conditions and can be detected with the binding of several reporter molecules like Congo red, Thioflavine T (ThT), 8-Anilino-1- naphthalenesulfonic acid (ANS) and PrP^{Sc} specific antibodies. ThT and Congo red both bind to amyloid fibrils and ANS interacts with hydrophobic β-sheets [98-101].

PrP^{β} Prion can exist in another abnormal but stable isoform that is derived from recombinant PrP and is known as the β-oligomeric isoform [98], denoted as PrP^{β} by our laboratory. This isoform shares similarities with the PrP^{Sc} isoform as it is highly enriched in β-sheet secondary structure, binds ANS and some antibodies similarly to PrP^{Sc} (although with less affinity), and is slightly resistant to proteinase K digestion although much less so than PrP^{Sc} [98-100]. Antibody binding studies showed residues 90-120 are accessible in PrP^{β} but are part of the core of PrP^{Sc} amyloids and are not accessible in the infectious isoform [98].

In contrast to the insoluble, infectious PrP^{Sc}, the oligomeric forms of PrP are soluble, spherical aggregates that are stable at acidic pH [98, 101] and do not bind ThT or Congo red. Although various sizes of β-enriched oligomeric particles have been found or formed from *in vivo* and *in vitro* isolation techniques (varying in size from a few molecules to ~100 molecules depending on isolation techniques) [73, 102, 103], the soluble, recombinant PrP^{β} isoform produced using our laboratory techniques is an octamer [104]. It has been shown that recombinant PrP^{β} can form amyloid fibrils under certain experimental conditions, but is not infectious [98, 101]. However, small β-enriched aggregates isolated from brain tissue are found to be more infectious and toxic

to neuronal cells than the amyloid fibrils [73, 74]. It is under debate whether PrP^{β} is on pathway to the formation of mature fibrils, but because of its similarities to PrP^{Sc} and its solubility, PrP^{β} is ideal for study using spectroscopic techniques.

PrP^{F} The other β-sheet enriched isoform that is readily formed with recombinant PrP is the fibrillar isoform, PrP^{F} [99, 105]. This isoform is most similar to PrP^{Sc} in that it is insoluble, fibrillar, contains high β-sheet content and is stable at slightly acidic to neutral pH. Recombinant fibrils have been found to be mildly infectious in transgenic mice overexpressing PrP^{C} [98], but in most other cases they remain non-infectious when compared to fibrils isolated from brain tissue. PrP^{F} is structurally similar to PrP^{Sc} as viewed by infrared spectroscopy (IR) [99] and its binding to ANS, ThT, and Congo red along with PrP^{Sc} specific antibodies [98, 100]. Though PrP^{F} has enhanced resistance to proteinase K digestion, it has a smaller resistant core than PrP^{Sc}. While proteinase K digestion of the misfolded isoforms creates fragments of slightly variable sizes, the main proteinase K resistant core of PrP^{Sc} comprises residues 90-231 and is shown to maintain infectivity following digestion [11]. Because of the structural and physical similarities to PrP^{Sc}, PrP^{F} is used to support data collected from PrP^{β} and to represent the conformation of infectious PrP^{Sc}.

1-3. Structural Elucidation of PrP^{Sc}

The transition from PrP^{C} to PrP^{Sc} is accompanied by the slight decrease of α-helical secondary structure and a significant increase of β-sheet content. Based on IR and Circular Dischroism (CD) spectra, PrP^{Sc} has ~40% β–sheet secondary structure as compared to PrP^{C} having only ~3% [53, 106, 107]. The aggregated, multimeric nature of misfolded prion makes it difficult to use traditional methods for structure determination

such as NMR and x-ray crystallography. Although 2D crystal structures, x-ray diffraction and electron microscopy (EM) pictures can give overall structure characteristics that confirm the cross β-sheet spine and fibrillar nature of the misfolded forms, the atomic-level structural detail is lacking. Elucidating the structure of the misfolded prion isoform may allow for the development of drug therapies or early detection systems for prion diseases, or illuminate mechanistic details of conversion and disease pathology. Although the structure is not known, there are two predominate computational models of PrP^{Sc} predicting structural details. Along with computational models, several scientific techniques have been utilized to provide structural data. This section describes two theoretical models of PrP^{Sc} and then describes structural data obtained through various scientific approaches. For most of these studies and for the work described in this thesis, a truncated version of PrP (residues 90 – 232) was used, so unless specifically defined, all mention of the N-terminus refers to residue 90, not residue 23 (see Figure 1-1). This section concludes with my hypothesis and specific aims of my thesis as related to the two theoretical models of PrP^{Sc}.

(A) Models

β-Helix Model Traditional methods of detailed protein structure determination involved NMR and X-ray crystallography techniques. To use these methods, the protein sample generally must be soluble in solution, be pure and be concentrated without aggregation. Because of these requirements, detailed structural elucidation of PrP^{Sc} has been hampered. X-ray diffraction has shown that amyloid fibrils from prion and other amyloidogenic precursor peptides contain cross β-structures where the β-sheets are arranged parallel to the fibril long axis and the β-strands are perpendicular to this axis

[108]. Amyloid fibrils from a fungal HET prion was shown by NMR to form a solenoid with a triangular hydrophobic core containing cross β-sheet structure [109]. Microscopic techniques have given constraints of fibrillar size and morphology for mammalian PrP. One EM study observed the formation of fibrillar rods with 69 X 69 Å cross section dimensions [110]. Although these data provide a glimpse of the gross morphology of PrP^{Sc}, they lack the detail necessary for high resolution structural determination. Using these pieces of information as a guide, Govaerts et al published a model of PrP^{Sc} structure known as the β-helix model [111]. The model was created by searching a database of known protein structures for a model that would fit the constraints of the gathered data. Specifically, the search criteria for a structure included a cross β-architecture, a diameter of <50 Å, and exposed β-sheet edges to allow for the stacking of monomers. Once the potential candidates were identified, the PrP protein sequence was threaded through the structures to observe compliance. From these, a parallel, left-handed β-helical structure, where the β-strands turn inward and helically wind about an imaginary axis, seemed to best fit the data and constraints.

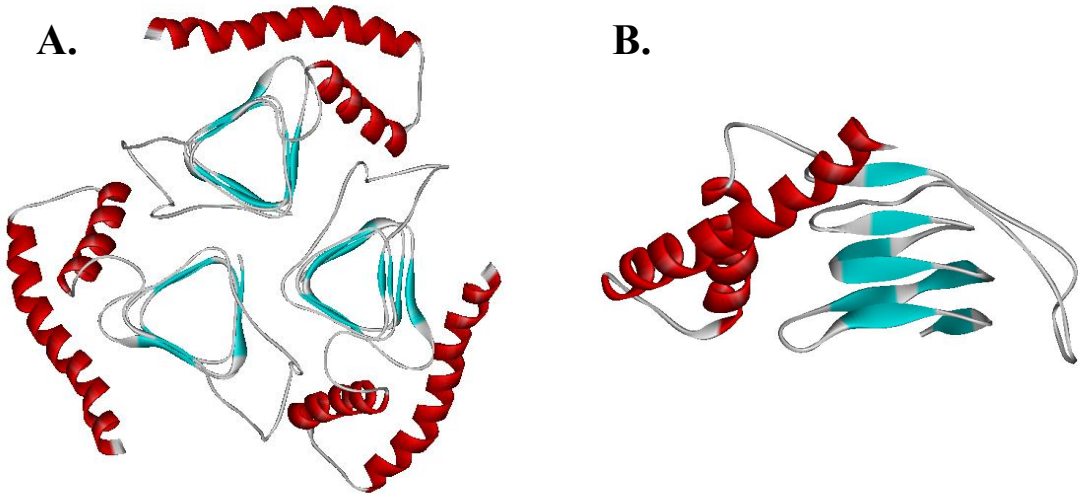

Figure 1-3. The Govaerts β-helix model of PrP^{Sc} colored by secondary structure where α-helices are red, β-strands are blue and random loops, coils in gray. Structure coordinates were kindly provided by Govaerts [111].

In this model, residues 90-175 form the β-helices while the C-terminal α-helices B and C remain mostly intact as does the disulfide bridge. The formation of this β-helical conformation allows for trimeric units that roughly fit the fibril dimensions. The trimers have the ability to stack and interact at the tops and bottoms of the β-helical interfaces to form a cross β-structure parallel to the long fibril axis [111]. This model agrees with data supporting conformational rearrangement in the N-terminus while the two C-terminal α-helices remain relatively unchanged [112].

β–Spiral Model Mari DeMarco and Valerie Daggett developed the β-spiral model for PrP^{Sc} structure by using molecular dynamics simulations with the sequence of human PrP^{C} (residues 90-231) under conditions of low pH (pH 3.2-4.7) at 25° C [107, 113, 114]. There is evidence that the misfolding of PrP^{C} may occur in the endosomal compartments where the pH is acidic [76, 115]. By mimicking these conditions and

using molecular mechanics, they were able to show disruption of salt bridges and tertiary structure in the C-terminus of PrP^C at low pH, which in turn triggered changes in the N-terminal region. In one of the low pH simulations, the N-terminus was seen to form some extended structure in the form of β-sheets. The formation of β-strands extending up to Helix A and the docking of the new strands to the already existing β-strands in PrP^C allowed for their packing and stability [114]. This region has been shown to be important in the conversion process [116].

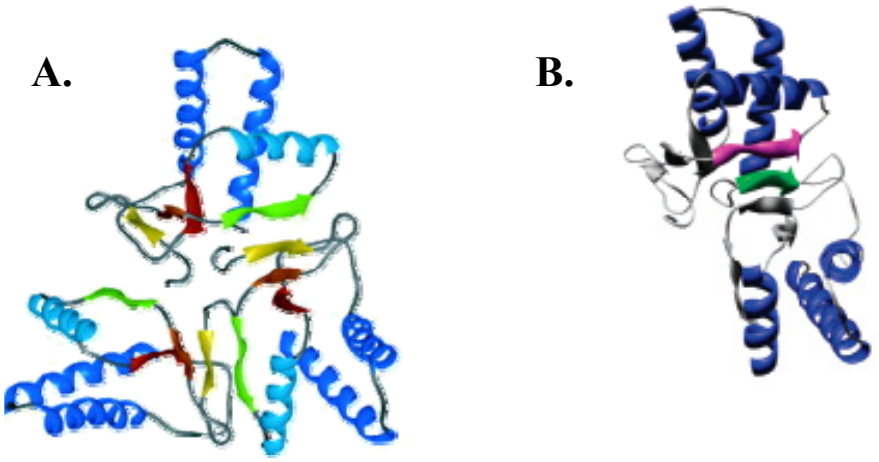

Figure 1-4. The Daggett and DeMarco β-Spiral model formed by N-terminal extended structure in the form of β-sheets. (A) shows a trimeric unit (for comparison with the β-helix model) and (B) shows the monomer-monomer interactions, with interfaces of aggregation colored purple and green. Figures are are taken from publications [107, 113] (used with permission; (A) copyright 2004 National Academy of Sciences, U.S.A.).

In the β-spiral model, the major structural changes occur in the N-terminus whereas all three of the α-helices remain fairly unchanged. Besides instability and increased flexibility caused by the low pH conditions and the loss of long-range salt bridges especially in Helix A, the α-helices did not unfold. This agrees with data showing that the C-terminus is not critical for conversion and the large structural changes

occur in the N-terminus [3, 114, 117-120]. For example, the formation of disease is seen to occur with truncated PrP that lacks Helices A, B, and C whereas the N-terminal and hydrophobic region (105-126) are seen to be necessary for conversion and are neurotoxic [117, 118, 120]. Another study exhibited the importance of N-terminal residues and the hydrophobic segment 113-128 as truncations of this segment did not propagate prions [3]. Furthermore, several mutations causing prion disease are found in the N-terminal region, and mutation containing a stop codon at 145 or 160 still propagate prion disease even though most of the the C-terminus is absent [114, 119].

Although contradicting evidence exists concerning the accessibility of the N-terminus in PrP^{Sc}, this region of PrP^{C} clearly undergoes conformational change upon conversion to PrP^{Sc}. Antibodies targeting epitopes in the C-terminal region (residues 225-231) were shown to bind both PrP^{C} and PrP^{Sc}, but when antibodies were targeted to the N-terminal region (residues 90-120), only epitopes in PrP^{C} and denatured PrP^{Sc} were reactive (epitopes were not accessible in folded PrP^{Sc}) [112]. Baskakov similarly reported that residues 90-120 were buried in PrP^{Sc}, but antibodies were found to bind these residues in PrP^{β} [98]. There also exist PrP^{Sc}-specific antibodies that recognize non-linear epitopes in the regions spanning 89-112 and 136-158, which do not bind to PrP^{C} [100]. Together, these findings implicate that the N-terminal region of PrP undergoes a conformational change and plays a role in the conversion process.

(B) Techniques to Elucidate Structure

H/D Exchange A hydrogen-deuterium exchange experiment conducted by the Surewicz group shows very strong protection of the amide hydrogens spanning residues 169-213 in human recombinant PrP^{F} [121]. This strong protection more than 25 hours

after exchange is highly demonstrative of cross β-structure. While residues 160-213 were highly protected, residues 90-160 showed only slightly slower deuterium incorporation than PrP^C, supporting the conclusion that any structure in these residues is not involved in the cross-β stacking interactions. The area of proposed cross β-structure in these fibrils corresponds to helix 2 most of helix 3 and the loop between the two helices in PrP^C [121].

EPR Spin Labeling In another paper by Surewicz, recombinant human PrP was used for site-directed spin labeling coupled with EPR spectroscopy to locate the regions involved in cross β–structure [122]. Upon fibril formation and the associated stacking of β-strands, the spin labels on each monomer interact in a distance-dependent manner. The EPR spectra provide information on contact sites and the distance and packing of monomers. In this study, the cross β-structure was shown to be in-register and stacked parallel to the fiber axis, and was mapped to the C-terminal half of PrP from residues 160 to 220. These studies contrast dramatically with both theoretical models of PrP^{Sc}, as the β-sheets form from Helices B and C of PrP^C, contrary to the β-helix and β-spiral models that show β-sheet structure formation at the N-terminus with most of the α-helices intact [122].

Antibody Binding Studies In another study, fibrils made from full-length recombinant mouse prion (23-230) were probed with multiple, specific antibodies recognizing different PrP epitopes and conformations. It was seen that under non-denaturing conditions, epitope 95-105 was solvent accessible whereas epitope 132-156 was predominantly buried but became partially exposed under slight denaturation [100]. Previous studies had shown a proteinase K resistant core of rPrP composed of residues

152/153-230 and 162-230 [123]. These residues were thought to compose the stable cross β-sheet structures. In this antibody study, epitopes 159-174 and 224-230 were completely buried in fibrillar form and full denaturation was required for their accessibility [100].

Antibody binding studies have been conducted to observe differences in structure between PrP^{C} and PrP^{Sc}. A difference in antibody binding of residues 90-113 was observed, binding to PrP^{C} but not to PrP^{Sc} [98]. Another antibody study showed that there was an increase in tyrosine accessibility in PrP^{Sc} and found a selective YYR epitope in PrP^{Sc} that is not accessible in PrP^{C} [124]. These YYR repeats are located at residues 149-151 and 162-164. and although that study did not identify the exact accessible epitope, later studies by Lennon demonstrated that there was a significant increase in tyrosine reactivity toward nitration at the 149-151 YYR repeat, pinpointing that segment as the accessible epitope [104]. Identifying other regions or residues that are accessible and thus specific for one isoform will provide structural clues about the changes that occur following conversion.

(C) Hypothesis and Goals of Research

There are still many unanswered questions surrounding the conversion of cellular protein into the infectious agent that causes disease. Where and how does the conversion process take place in the cell, what is the mechanism of apoptosis and disease pathology and what is the structure of the infectious isoform? The answers to these questions will speed the discovery of therapeutic or preventative agents able to combat prion disease. Specifically, determining the structure of PrP^{Sc} will enable the advancement of early detection systems and clinical screenings to prevent the spread of infectious prion. Although gross structural features of fibrils have been observed using microscopy and

diffraction techniques, the molecular details of the structure remain to be elucidated. The conversion from PrP^{C} to infectious PrP^{Sc} is accompanied by changes in conformation as seen through antibody binding, IR, CD, hydrogen deuterium exchange and EPR, and there are at least two computational models for the structure of PrP^{Sc}. Using structural data as it becomes available, it should be possible to validate or provide contrary evidence for one or both models. My research uses tryptophan fluorescence techniques with recombinant Syrian hamster PrP (residues 90-232) to quantify the solvent accessibility of specific residues in the various recombinant isoforms of prion: PrP^{C}, PrP^{F}, and PrP^{β}.

My hypothesis is that both the β-helix and β-spiral model are mutually exclusive and their differences will be distinguishable by tryptophan fluorescence techniques and measurements. Whether one model is able to entirely represent the data or if they both show discrepancies is to be determined. By using tryptophan fluorescence and quenching to measure accessibility changes between PrP^{C} and the misfolded isoforms PrP^{β} and PrP^{F}, it will be possible to ascertain if the models represent the data, and to compare the acquired tryptophan data with information gathered from other structural studies.

Aims The overall aim of my thesis is to probe various isoforms of the prion protein using tryptophan fluorescence quenching techniques. Specifically, I will:

- Measure the tryptophan fluorescence quenching rate constant (k_q) for the various isoforms (PrP^{C}, PrP^{β}, PrP^{F}) for several single tryptophan mutants. The positions for Trp placement via mutation are G123W, W145, Y150W, N159W, Y163W and Y218W. The bimolecular quenching rate constant k_q will be measured using steady-state and time-resolved techniques with acrylamide. Steady-state

quenching k_q's will be correlated with solvent accessible surface area (SASA) data and compared with the correlation of the SASA and kq's from other previously reported, naturally occurring, single tryptophan containing proteins [125].

- Estimate solvent accessibility based on k_q values for PrP^{β} and PrP^{F} mutants along with the correlation with SASA data.
- Compare collected fluorescence data with the theoretical models of PrP^{Sc} to provide support or evidence against one or both models. I will also compare the fluorescence data with other published spectroscopic data for further structural information.
- Identify a mutant that exhibits a significant isoform-specific change in solvent exposure and/or fluorescence parameters (lifetime). This will be useful for the potential development of drug assays or PrP^{Sc} detection.

By monitoring conformational changes between the α-helical rich and β-sheet rich isoforms, models of PrP^{Sc} can be tested, other structural information can be validated, and the information can be used to further develop assays that detect the conversion of PrP^{C} to PrP^{Sc}.

References

1. Leopoldt JG: **Nutzliche und auf die Erfahrung gegrundete Einleitung zu der Land-Wirthschafft**. In., vol. 5. Sorau; 1750: 348.
2. Schneider K, Fangerau H, Michaelsen B, Raab WH: **The early history of the transmissible spongiform encephalopathies exemplified by scrapie**. *Brain Res Bull* 2008, **77**(6):343-355.
3. Aguzzi A, Baumann F, Bremer J: **The prion's elusive reason for being**. *Annu Rev Neurosci* 2008, **31**:439-477.
4. Brown P, Bradley R: **1755 and all that: a historical primer of transmissible spongiform encephalopathy**. *Bmj* 1998, **317**(7174):1688-1692.

5. Chong-Suk R: **Prions and Prion Diseases: Fundamentals and Mechanistic Details**. *Journal of Microbiology and Biotechnology* 2007, **17**(7):1059-1070.
6. Linden R, Martins VR, Prado MA, Cammarota M, Izquierdo I, Brentani RR: **Physiology of the prion protein**. *Physiol Rev* 2008, **88**(2):673-728.
7. McKintosh E, Tabrizi SJ, Collinge J: **Prion diseases**. *J Neurovirol* 2003, **9**(2):183-193.
8. Onodera T, Sakudo A, Wu G, Saeki K: **Bovine spongiform encephalopathy in Japan: history and recent studies on oxidative stress in prion diseases**. *Microbiol Immunol* 2006, **50**(8):565-578.
9. Poser CM: **Notes on the history of the prion diseases. Part I**. *Clin Neurol Neurosurg* 2002, **104**(1):1-9.
10. Poser CM: **Notes on the history of the prion diseases. Part II**. *Clin Neurol Neurosurg* 2002, **104**(2):77-86.
11. Prusiner SB: **Prions**. *Proc Natl Acad Sci U S A* 1998, **95**(23):13363-13383.
12. Prusiner SB: **Shattuck lecture--neurodegenerative diseases and prions**. *N Engl J Med* 2001, **344**(20):1516-1526.
13. Soto C: **Prions The New Biology of Proteins**. Boca Raton, FL: CRC Press Taylor and Francis Group; 2006.
14. Pattison IH: **Scrapie--a personal view**. *J Clin Pathol Suppl (R Coll Pathol)* 1972, **6**:110-114.
15. Greig JR: **Scrapie**. *Transactions of the Highland and Agricultural Society of Scotland* 1940, **52**:71-79.
16. Cuille J, Chelle PL: **La Maladie Dite Tremblante du Mouton Est-Elle Inoculable?** *Les Comptes Rendus de l'Academie des Sciences* 1936, **203**:1552-1554.
17. Cuille J, Chelle PL: **Experimental Transmission of Trembling to the Goat**. *Les Comptes Rendus des Seances de l'Academie des Sciences* 1939, **208**:1058-1060.
18. Gordon WS: **Louping Ill, Tick-Borne Fever and Scrapie**. *The Veterinary Record* 1946, **58**:516-525.
19. Hadlow WJ: **Scrapie and Kuru**. *Lancet* 1959, **2**:289-290.
20. Sigurdsson B: **Rida, a Chronic Encephalitis of Sheep with General Remarks on Infections which Develop Slowly and Some of Their Special Characteristics**. *British Veterinary Journal* 1954, **110**:341-354.
21. Pattison IH, Gordon WS, Millson GC: **Experimental production of scrapie in goats**. *J Comp Pathol* 1959, **69**:300-312.
22. Chandler RL: **Encephalopathy in mice produced by inoculation with scrapie brain material**. *Lancet* 1961, **1**(7191):1378-1379.
23. Collinge J, Whitfield J, McKintosh E, Beck J, Mead S, Thomas DJ, Alpers MP: **Kuru in the 21st century--an acquired human prion disease with very long incubation periods**. *Lancet* 2006, **367**(9528):2068-2074.
24. Gajdusek DC, Zigas V: **Degenerative disease of the central nervous system in New Guinea; the endemic occurrence of kuru in the native population**. *N Engl J Med* 1957, **257**(20):974-978.
25. Klatzo I, Gajdusek DC, Zigas V: **Pathology of Kuru**. *Lab Invest* 1959, **8**(4):799-847.

26. Bedino J: **Creutzfeldt-Jakob Disease and Related Disorders**. In: *Champion Expanding Encyclopedia of Mortuary Practices.* vol. 625. Springfield, Ohio: The Champion Company; 1995: 2514-2517.
27. Gajdusek DC, Gibbs CJ, Alpers M: **Experimental transmission of a Kuru-like syndrome to chimpanzees**. *Nature* 1966, **209**(5025):794-796.
28. Gibbs CJ, Jr., Gajdusek DC, Asher DM, Alpers MP, Beck E, Daniel PM, Matthews WB: **Creutzfeldt-Jakob disease (spongiform encephalopathy): transmission to the chimpanzee**. *Science* 1968, **161**(839):388-389.
29. Gajdusek DC: **D. Carleton Gajdusek; The Nobel Prize in Physiology or Medicine 1976 Autobiography**. In: *Les Prix Nobel en 1976.* Edited by Odelberg W. Stockholm: Nobel Foundation; 1977.
30. Institute K: **The Nobel Prize in Physiology or Medicine. Press Release**. In.; 1976.
31. Gerstmann J: **Uber eine noch nicht beschriebenes Reflexphanomen bei einer Erkrankung des zerebellaren Systems**. *Wiener Medizinische Wochenschrift* 1928, **78**:906-908.
32. Gerstmann J, Straussler E, Scheinker I: **Uber eine eigenartige hereditar-familiare Erkrankung des Zentralnervensystem; zugleich ein Beitrag zur Frage des vorzeitigen lokalen Alterns**. *Zeitschrift fur Neurologie* 1936, **154**:736-762.
33. Masters CL, Gajdusek DC, Gibbs CJ, Jr.: **Creutzfeldt-Jakob disease virus isolations from the Gerstmann-Straussler syndrome with an analysis of the various forms of amyloid plaque deposition in the virus-induced spongiform encephalopathies**. *Brain* 1981, **104**(3):559-588.
34. Hsiao K, Baker HF, Crow TJ, Poulter M, Owen F, Terwilliger JD, Westaway D, Ott J, Prusiner SB: **Linkage of a prion protein missense variant to Gerstmann-Straussler syndrome**. *Nature* 1989, **338**(6213):342-345.
35. Lugaresi E, Medori R, Montagna P, Baruzzi A, Cortelli P, Lugaresi A, Tinuper P, Zucconi M, Gambetti P: **Fatal familial insomnia and dysautonomia with selective degeneration of thalamic nuclei**. *N Engl J Med* 1986, **315**(16):997-1003.
36. Collinge J, Palmer MS, Sidle KC, Gowland I, Medori R, Ironside J, Lantos P: **Transmission of fatal familial insomnia to laboratory animals**. *Lancet* 1995, **346**(8974):569-570.
37. Tateishi J, Brown P, Kitamoto T, Hoque ZM, Roos R, Wollman R, Cervenakova L, Gajdusek DC: **First experimental transmission of fatal familial insomnia**. *Nature* 1995, **376**(6539):434-435.
38. Medori R, Tritschler HJ, LeBlanc A, Villare F, Manetto V, Chen HY, Xue R, Leal S, Montagna P, Cortelli P *et al*: **Fatal familial insomnia, a prion disease with a mutation at codon 178 of the prion protein gene**. *N Engl J Med* 1992, **326**(7):444-449.
39. Will RG, Ironside JW, Zeidler M, Cousens SN, Estibeiro K, Alperovitch A, Poser S, Pocchiari M, Hofman A, Smith PG: **A new variant of Creutzfeldt-Jakob disease in the UK**. *Lancet* 1996, **347**(9006):921-925.
40. Sigurdson CJ: **A prion disease of cervids: chronic wasting disease**. *Vet Res* 2008, **39**(4):41.

41. Pattison IH: **Resistance Of The Scrapie Agent To Formalin**. *J Comp Pathol* 1965, **75**:159-164.
42. Alper T: **The scrapie enigma: insights from radiation experiments**. *Radiat Res* 1993, **135**(3):283-292.
43. Alper T, Haig DA, Clarke MC: **The exceptionally small size of the scrapie agent**. *Biochem Biophys Res Commun* 1966, **22**(3):278-284.
44. Alper T, Cramp WA, Haig DA, Clarke MC: **Does the agent of scrapie replicate without nucleic acid?** *Nature* 1967, **214**(5090):764-766.
45. Prusiner SB: **Stanley B. Prusiner; The Nobel Prize in Physiology or Medicine 1997 Autobiography**. In: *Les Prix Nobel The Nobel Prizes 1997.* Edited by Frangsmyr T. Stockholm: Nobel Foundation; 1998.
46. Bolton DC, McKinley MP, Prusiner SB: **Identification of a protein that purifies with the scrapie prion**. *Science* 1982, **218**(4579):1309-1311.
47. Marsh RF, Kimberlin RH: **Comparison of scrapie and transmissible mink encephalopathy in hamsters. II. Clinical signs, pathology, and pathogenesis**. *J Infect Dis* 1975, **131**(2):104-110.
48. Prusiner SB: **Prion Biology and Diseases 2^{cd} Edition**, 2^{cd} Edition edn: Cold Spring Harbor Laboratory Press; 2004.
49. Griffith JS: **Self-replication and scrapie**. *Nature* 1967, **215**(5105):1043-1044.
50. Soto C, Castilla J: **The controversial protein-only hypothesis of prion propagation**. *Nat Med* 2004, **10 Suppl**:S63-67.
51. Institute K: **The Nobel Prize in Physiology or Medicine 1997. Press Release**. In.; 1997.
52. Gasset M, Baldwin MA, Fletterick RJ, Prusiner SB: **Perturbation of the secondary structure of the scrapie prion protein under conditions that alter infectivity**. *Proc Natl Acad Sci U S A* 1993, **90**(1):1-5.
53. Pan KM, Baldwin M, Nguyen J, Gasset M, Serban A, Groth D, Mehlhorn I, Huang Z, Fletterick RJ, Cohen FE *et al*: **Conversion of alpha-helices into beta-sheets features in the formation of the scrapie prion proteins**. *Proc Natl Acad Sci U S A* 1993, **90**(23):10962-10966.
54. Prusiner SB: **An approach to the isolation of biological particles using sedimentation analysis**. *J Biol Chem* 1978, **253**(3):916-921.
55. Prusiner SB, Garfin DE, Baringer JR, Cochran SP, Hadlow WJ, Race R, Eklund CM. In: *Persistent Viruses.* Edited by Stevens J, Todaro G, Fox CF. New York: Academic Press; 1978: 591-613.
56. Kaneko K, Zulianello L, Scott M, Cooper CM, Wallace AC, James TL, Cohen FE, Prusiner SB: **Evidence for protein X binding to a discontinuous epitope on the cellular prion protein during scrapie prion propagation**. *Proc Natl Acad Sci U S A* 1997, **94**(19):10069-10074.
57. Telling GC, Scott M, Mastrianni J, Gabizon R, Torchia M, Cohen FE, DeArmond SJ, Prusiner SB: **Prion propagation in mice expressing human and chimeric PrP transgenes implicates the interaction of cellular PrP with another protein**. *Cell* 1995, **83**(1):79-90.
58. Gabizon R, McKinley MP, Groth D, Prusiner SB: **Immunoaffinity purification and neutralization of scrapie prion infectivity**. *Proc Natl Acad Sci U S A* 1988, **85**(18):6617-6621.

59. Bueler H, Aguzzi A, Sailer A, Greiner RA, Autenried P, Aguet M, Weissmann C: **Mice devoid of PrP are resistant to scrapie**. *Cell* 1993, **73**(7):1339-1347.
60. Meyer-Luehmann M, Coomaraswamy J, Bolmont T, Kaeser S, Schaefer C, Kilger E, Neuenschwander A, Abramowski D, Frey P, Jaton AL *et al*: **Exogenous induction of cerebral beta-amyloidogenesis is governed by agent and host**. *Science* 2006, **313**(5794):1781-1784.
61. Scott M, Peretz D, Ridley RM, Baker HF, DeArmond SJ, Prusiner SB. In: *Prion Biology and Diseases, 2nd Edition.* Edited by Prusiner SB. Cold Spring Harbor, New York: Cold Spring Harbor Laboratory Press; 2004: 435-482.
62. Legname G, Baskakov IV, Nguyen HO, Riesner D, Cohen FE, DeArmond SJ, Prusiner SB: **Synthetic mammalian prions**. *Science* 2004, **305**(5684):673-676.
63. Kocisko DA, Come JH, Priola SA, Chesebro B, Raymond GJ, Lansbury PT, Caughey B: **Cell-free formation of protease-resistant prion protein**. *Nature* 1994, **370**(6489):471-474.
64. Saborio GP, Permanne B, Soto C: **Sensitive detection of pathological prion protein by cyclic amplification of protein misfolding**. *Nature* 2001, **411**(6839):810-813.
65. Castilla J, Saa P, Hetz C, Soto C: **In vitro generation of infectious scrapie prions**. *Cell* 2005, **121**(2):195-206.
66. Caughey B, Baron GS: **Prions and their partners in crime**. *Nature* 2006, **443**(7113):803-810.
67. Harris DA: **Trafficking, turnover and membrane topology of PrP**. *Br Med Bull* 2003, **66**:71-85.
68. Cohen FE, Prusiner SB: **Pathologic conformations of prion proteins**. *Annu Rev Biochem* 1998, **67**:793-819.
69. DeArmond SJ, Qiu Y, Sanchez H, Spilman PR, Ninchak-Casey A, Alonso D, Daggett V: **PrPc glycoform heterogeneity as a function of brain region: implications for selective targeting of neurons by prion strains**. *J Neuropathol Exp Neurol* 1999, **58**(9):1000-1009.
70. Liu H, Farr-Jones S, Ulyanov NB, Llinas M, Marqusee S, Groth D, Cohen FE, Prusiner SB, James TL: **Solution structure of Syrian hamster prion protein rPrP(90-231)**. *Biochemistry* 1999, **38**(17):5362-5377.
71. Knaus KJ, Morillas M, Swietnicki W, Malone M, Surewicz WK, Yee VC: **Crystal structure of the human prion protein reveals a mechanism for oligomerization**. *Nat Struct Biol* 2001, **8**(9):770-774.
72. Kaimann T, Metzger S, Kuhlmann K, Brandt B, Birkmann E, Holtje HD, Riesner D: **Molecular model of an alpha-helical prion protein dimer and its monomeric subunits as derived from chemical cross-linking and molecular modeling calculations**. *J Mol Biol* 2008, **376**(2):582-596.
73. Silveira JR, Raymond GJ, Hughson AG, Race RE, Sim VL, Hayes SF, Caughey B: **The most infectious prion protein particles**. *Nature* 2005, **437**(7056):257-261.
74. Simoneau S, Rezaei H, Sales N, Kaiser-Schulz G, Lefebvre-Roque M, Vidal C, Fournier JG, Comte J, Wopfner F, Grosclaude J *et al*: **In vitro and in vivo neurotoxicity of prion protein oligomers**. *PLoS Pathog* 2007, **3**(8):e125.

75. Borchelt DR, Taraboulos A, Prusiner SB: **Evidence for synthesis of scrapie prion proteins in the endocytic pathway**. *J Biol Chem* 1992, **267**(23):16188-16199.
76. Swietnicki W, Petersen R, Gambetti P, Surewicz WK: **pH-dependent stability and conformation of the recombinant human prion protein PrP(90-231)**. *J Biol Chem* 1997, **272**(44):27517-27520.
77. Ma J, Lindquist S: **Conversion of PrP to a self-perpetuating PrPSc-like conformation in the cytosol**. *Science* 2002, **298**(5599):1785-1788.
78. Ma J, Wollmann R, Lindquist S: **Neurotoxicity and neurodegeneration when PrP accumulates in the cytosol**. *Science* 2002, **298**(5599):1781-1785.
79. Chiesa R, Harris DA: **Prion diseases: what is the neurotoxic molecule?** *Neurobiol Dis* 2001, **8**(5):743-763.
80. Mouillet-Richard S, Ermonval M, Chebassier C, Laplanche JL, Lehmann S, Launay JM, Kellermann O: **Signal transduction through prion protein**. *Science* 2000, **289**(5486):1925-1928.
81. Spielhaupter C, Schatzl HM: **PrPC directly interacts with proteins involved in signaling pathways**. *J Biol Chem* 2001, **276**(48):44604-44612.
82. Zanata SM, Lopes MH, Mercadante AF, Hajj GN, Chiarini LB, Nomizo R, Freitas AR, Cabral AL, Lee KS, Juliano MA *et al*: **Stress-inducible protein 1 is a cell surface ligand for cellular prion that triggers neuroprotection**. *Embo J* 2002, **21**(13):3307-3316.
83. Kurschner C, Morgan JI: **Analysis of interaction sites in homo- and heteromeric complexes containing Bcl-2 family members and the cellular prion protein**. *Brain Res Mol Brain Res* 1996, **37**(1-2):249-258.
84. Bounhar Y, Zhang Y, Goodyer CG, LeBlanc A: **Prion protein protects human neurons against Bax-mediated apoptosis**. *J Biol Chem* 2001, **276**(42):39145-39149.
85. Cashman NR, Loertscher R, Nalbantoglu J, Shaw I, Kascsak RJ, Bolton DC, Bendheim PE: **Cellular isoform of the scrapie agent protein participates in lymphocyte activation**. *Cell* 1990, **61**(1):185-192.
86. Criado JR, Sanchez-Alavez M, Conti B, Giacchino JL, Wills DN, Henriksen SJ, Race R, Manson JC, Chesebro B, Oldstone MB: **Mice devoid of prion protein have cognitive deficits that are rescued by reconstitution of PrP in neurons**. *Neurobiol Dis* 2005, **19**(1-2):255-265.
87. Maglio LE, Perez MF, Martins VR, Brentani RR, Ramirez OA: **Hippocampal synaptic plasticity in mice devoid of cellular prion protein**. *Brain Res Mol Brain Res* 2004, **131**(1-2):58-64.
88. Steele AD, Emsley JG, Ozdinler PH, Lindquist S, Macklis JD: **Prion protein (PrPc) positively regulates neural precursor proliferation during developmental and adult mammalian neurogenesis**. *Proc Natl Acad Sci U S A* 2006, **103**(9):3416-3421.
89. Tobler I, Gaus SE, Deboer T, Achermann P, Fischer M, Rulicke T, Moser M, Oesch B, McBride PA, Manson JC: **Altered circadian activity rhythms and sleep in mice devoid of prion protein**. *Nature* 1996, **380**(6575):639-642.

90. Zhang CC, Steele AD, Lindquist S, Lodish HF: **Prion protein is expressed on long-term repopulating hematopoietic stem cells and is important for their self-renewal**. *Proc Natl Acad Sci U S A* 2006, **103**(7):2184-2189.
91. Brown DR: **Copper and prion disease**. *Brain Res Bull* 2001, **55**(2):165-173.
92. Pattison IH, Jebbett JN: **Clinical and histological recovery from the scrapie-like spongiform encephalopathy produced in mice by feeding them with cuprizone**. *J Pathol* 1973, **109**(3):245-250.
93. Miura T, Sasaki S, Toyama A, Takeuchi H: **Copper reduction by the octapeptide repeat region of prion protein: pH dependence and implications in cellular copper uptake**. *Biochemistry* 2005, **44**(24):8712-8720.
94. Wells MA, Jackson GS, Jones S, Hosszu LL, Craven CJ, Clarke AR, Collinge J, Waltho JP: **A reassessment of copper(II) binding in the full-length prion protein**. *Biochem J* 2006, **399**(3):435-444.
95. Pauly PC, Harris DA: **Copper stimulates endocytosis of the prion protein**. *J Biol Chem* 1998, **273**(50):33107-33110.
96. Brown DR, Qin K, Herms JW, Madlung A, Manson J, Strome R, Fraser PE, Kruck T, von Bohlen A, Schulz-Schaeffer W *et al*: **The cellular prion protein binds copper in vivo**. *Nature* 1997, **390**(6661):684-687.
97. Wong BS, Brown DR, Pan T, Whiteman M, Liu T, Bu X, Li R, Gambetti P, Olesik J, Rubenstein R *et al*: **Oxidative impairment in scrapie-infected mice is associated with brain metals perturbations and altered antioxidant activities**. *J Neurochem* 2001, **79**(3):689-698.
98. Baskakov IV, Legname G, Baldwin MA, Prusiner SB, Cohen FE: **Pathway complexity of prion protein assembly into amyloid**. *J Biol Chem* 2002, **277**(24):21140-21148.
99. Bocharova OV, Breydo L, Parfenov AS, Salnikov VV, Baskakov IV: **In vitro conversion of full-length mammalian prion protein produces amyloid form with physical properties of PrP(Sc)**. *J Mol Biol* 2005, **346**(2):645-659.
100. Novitskaya V, Makarava N, Bellon A, Bocharova OV, Bronstein IB, Williamson RA, Baskakov IV: **Probing the conformation of the prion protein within a single amyloid fibril using a novel immunoconformational assay**. *J Biol Chem* 2006, **281**(22):15536-15545.
101. Tattum MH, Cohen-Krausz S, Thumanu K, Wharton CW, Khalili-Shirazi A, Jackson GS, Orlova EV, Collinge J, Clarke AR, Saibil HR: **Elongated oligomers assemble into mammalian PrP amyloid fibrils**. *J Mol Biol* 2006, **357**(3):975-985.
102. Redecke L, von Bergen M, Clos J, Konarev PV, Svergun DI, Fittschen UE, Broekaert JA, Bruns O, Georgieva D, Mandelkow E *et al*: **Structural characterization of beta-sheeted oligomers formed on the pathway of oxidative prion protein aggregation in vitro**. *J Struct Biol* 2007, **157**(2):308-320.
103. Tzaban S, Friedlander G, Schonberger O, Horonchik L, Yedidia Y, Shaked G, Gabizon R, Taraboulos A: **Protease-sensitive scrapie prion protein in aggregates of heterogeneous sizes**. *Biochemistry* 2002, **41**(42):12868-12875.

104. Lennon CW, Cox HD, Hennelly SP, Chelmo SJ, McGuirl MA: **Probing structural differences in prion protein isoforms by tyrosine nitration**. *Biochemistry* 2007, **46**(16):4850-4860.
105. Vendrely C, Valadie H, Bednarova L, Cardin L, Pasdeloup M, Cappadoro J, Bednar J, Rinaudo M, Jamin M: **Assembly of the full-length recombinant mouse prion protein I. Formation of soluble oligomers**. *Biochim Biophys Acta* 2005, **1724**(3):355-366.
106. Caughey BW, Dong A, Bhat KS, Ernst D, Hayes SF, Caughey WS: **Secondary structure analysis of the scrapie-associated protein PrP 27-30 in water by infrared spectroscopy**. *Biochemistry* 1991, **30**(31):7672-7680.
107. DeMarco ML, Silveira J, Caughey B, Daggett V: **Structural properties of prion protein protofibrils and fibrils: an experimental assessment of atomic models**. *Biochemistry* 2006, **45**(51):15573-15582.
108. Sunde M, Serpell LC, Bartlam M, Fraser PE, Pepys MB, Blake CC: **Common core structure of amyloid fibrils by synchrotron X-ray diffraction**. *J Mol Biol* 1997, **273**(3):729-739.
109. Wasmer C, Lange A, Van Melckebeke H, Siemer AB, Riek R, Meier BH: **Amyloid fibrils of the HET-s(218-289) prion form a beta solenoid with a triangular hydrophobic core**. *Science* 2008, **319**(5869):1523-1526.
110. Wille H, Michelitsch MD, Guenebaut V, Supattapone S, Serban A, Cohen FE, Agard DA, Prusiner SB: **Structural studies of the scrapie prion protein by electron crystallography**. *Proc Natl Acad Sci U S A* 2002, **99**(6):3563-3568.
111. Govaerts C, Wille H, Prusiner SB, Cohen FE: **Evidence for assembly of prions with left-handed beta-helices into trimers**. *Proc Natl Acad Sci U S A* 2004, **101**(22):8342-8347.
112. Peretz D, Williamson RA, Matsunaga Y, Serban H, Pinilla C, Bastidas RB, Rozenshteyn R, James TL, Houghten RA, Cohen FE *et al*: **A conformational transition at the N terminus of the prion protein features in formation of the scrapie isoform**. *J Mol Biol* 1997, **273**(3):614-622.
113. DeMarco ML, Daggett V: **From conversion to aggregation: protofibril formation of the prion protein**. *Proc Natl Acad Sci U S A* 2004, **101**(8):2293-2298.
114. DeMarco ML, Daggett V: **Molecular mechanism for low pH triggered misfolding of the human prion protein**. *Biochemistry* 2007, **46**(11):3045-3054.
115. Arnold JE, Tipler C, Laszlo L, Hope J, Landon M, Mayer RJ: **The abnormal isoform of the prion protein accumulates in late-endosome-like organelles in scrapie-infected mouse brain**. *J Pathol* 1995, **176**(4):403-411.
116. Salmona M, Malesani P, De Gioia L, Gorla S, Bruschi M, Molinari A, Della Vedova F, Pedrotti B, Marrari MA, Awan T *et al*: **Molecular determinants of the physicochemical properties of a critical prion protein region comprising residues 106-126**. *Biochem J* 1999, **342 (Pt 1)**:207-214.
117. Forloni G, Angeretti N, Chiesa R, Monzani E, Salmona M, Bugiani O, Tagliavini F: **Neurotoxicity of a prion protein fragment**. *Nature* 1993, **362**(6420):543-546.
118. Kitamoto T, Iizuka R, Tateishi J: **An amber mutation of prion protein in Gerstmann-Straussler syndrome with mutant PrP plaques**. *Biochem Biophys Res Commun* 1993, **192**(2):525-531.

119. Mead S: **Prion disease genetics**. *Eur J Hum Genet* 2006, **14**(3):273-281.
120. Supattapone S, Bouzamondo E, Ball HL, Wille H, Nguyen HO, Cohen FE, DeArmond SJ, Prusiner SB, Scott M: **A protease-resistant 61-residue prion peptide causes neurodegeneration in transgenic mice**. *Mol Cell Biol* 2001, **21**(7):2608-2616.
121. Lu X, Wintrode PL, Surewicz WK: **Beta-sheet core of human prion protein amyloid fibrils as determined by hydrogen/deuterium exchange**. *Proc Natl Acad Sci U S A* 2007, **104**(5):1510-1515.
122. Cobb NJ, Sonnichsen FD, McHaourab H, Surewicz WK: **Molecular architecture of human prion protein amyloid: a parallel, in-register beta-structure**. *Proc Natl Acad Sci U S A* 2007, **104**(48):18946-18951.
123. Bocharova OV, Breydo L, Salnikov VV, Gill AC, Baskakov IV: **Synthetic prions generated in vitro are similar to a newly identified subpopulation of PrPSc from sporadic Creutzfeldt-Jakob Disease**. *Protein Sci* 2005, **14**(5):1222-1232.
124. Paramithiotis E, Pinard M, Lawton T, LaBoissiere S, Leathers VL, Zou WQ, Estey LA, Lamontagne J, Lehto MT, Kondejewski LH *et al*: **A prion protein epitope selective for the pathologically misfolded conformation**. *Nat Med* 2003, **9**(7):893-899.
125. Eftink MR, Ghiron CA: **Exposure of tryptophanyl residues in proteins. Quantitative determination by fluorescence quenching studies**. *Biochemistry* 1976, **15**(3):672-680.

CHAPTER 2: METHODS

2-1. Mutants

(A) Choosing mutants

Single tryptophan mutants were made to observe changes in solvent accessibility at specific residues in PrP^{C} as compared to PrP^{β} or PrP^{F}. Ideally, positions that exhibited the greatest change in solvent accessibility between PrP^{C} and the misfolded isoforms were desired.

The mutants Y163W and Y150W are part of two YYR motifs found in PrP. Work done by Cashman and colleagues [1] found that there is increased accessibility of one or both of the YYR motifs in PrP isolated from brain homogenates of infected mice compared to brain homogenates of non-infected mice. Specifically, it was reported that antibody binding for the YYR epitope occurs in PrP^{Sc} but not in PrP^{C} suggesting that at least one of these repeats becomes more exposed in the misfolded state. Since both Y163W and Y150W are part of the two YYR motifs, they are of particular interest for positions implicated in significant conformational change following conversion to the misfolded isoforms. Also, the YYR (residues 149 – 151) motif containing Y150W was found to become more sensitive to tyrosine nitration following conversion to PrP^{β} [2].

Position 218 is a buried residue when looking at the structure of PrP^{C}, but based on nitration work previously done in our lab [2], it looks to be more exposed than predicted based on visible and calculated solvent accessibility. One hypothesis was that nitration of a neighboring YYD sequence (residues 225-227) slightly changed the conformation of PrP and allowed Y218 to become more accessible for nitration. To look

at this position more closely with respect to accessibility and past data from nitration work, this mutant was chosen for tryptophan fluorescence quenching studies.

Some mutants were chosen based on residues where large differences in solvent accessibility were calculated among theoretical models of misfolded prion protein. Such was the case for mutants G123W and N159W. According to calculations from Valerie Daggett and Mari DeMarco [3], G123W and N159W were positions that differed greatly in accessibility between two proposed models of misfolded PrP, the β-helix and the β-spiral model. This would allow for clear distinction between the models when relating solvent accessibility results from tryptophan fluorescence quenching measurements in the misfolded isoforms. As seen in Table 2-1, there are clear differences in calculated solvent accessibility between the two models for N159W and G123W.

Summary		Solvent Exposure		
		PrP^C	Spiral	Beta-helix
GLY	123	exposed	Exposed (76)	buried (6)
TRP	145	exposed	Exposed (89)	buried (15)
ASN	159	buried	buried (12)	exposed (120)

Table 2-1. Positions and their corresponding calculated solvent accessible surface area data (SASA) in the β-spiral model and the β-helix model of misfolded PrP are shown. Calculated SASA was provided by Mari DeMarco and Valerie Daggett [3].

W145 is a naturally occurring Trp residue that shows calculated differences in solvent accessibility between the two models of misfolded PrP. Thus, it was a clear choice for tryptophan quenching studies.

(B) Making Mutations

The recombinant prion protein construct used in these experiments contained the codons for residues 90-231 from golden Syrian hamster prion [4]; this construct lacks most of the unstructured N-terminus as well as the C-terminal GPI anchor, and since it is expressed in *E. coli*, the protein product will lack the glycosylation present in eukaryotic PrP. The truncated sequence was used as residues 90-231 have been shown to comprise the proteinase K resistant core in PrP^{Sc} and are sufficient for fibril formation and infectivity [5].

As described in a previous publication from the McGuirl group [2], the codons for residues 90-231 were subcloned from Syrian hamster prion plasmid pHaPrP into pET24a+, creating the expression plasmid pET24PrP90. Mutagenesis was performed as described below to form the pET24PrP90/W99F template for producing the W145 variant, and for making pET24PrP90/W99F/W145Y template plasmid containing no intrinsic tryptophan residues. Using the template plasmid, single tryptophan mutants were made at selected positions via site-directed mutagenesis using a QuikChange kit from Stratagene. Following mutagenesis steps and *Dpn*I digestion to rid the sample of methylated parental DNA, the amplified mutant plasmid was transformed into E. *coli* XL-1 blue cells. The plasmid DNA was isolated from E. *coli* cells using a QIAprep miniprep kit from QIAGEN and submitted to the UM Murdock Sequencing Facility for analysis. The pET24PrP90 mutant plasmids with the desired mutation were transformed into E. *coli* BL21(DE3)-Rosetta cells (Novagen, Inc.) for protein expression. Rosetta strains carry the pRARE plasmid that is used to supply tRNAs for mammalian codons rarely occurring in E. *coli* to allow for increased protein expression [6]. The original

cloning and some of the mutants were made previously by others in the lab. Specifically, the original cloning and the template pET24PrP90W99F/W145Y, the pET24PrP90W99F single mutant plasmid and the pET24PrP90W99F/W145Y/Y218W double mutant plasmid were made by Sam J. Chelmo, the pET24PrP90W99F/W145Y/Y163W mutant plasmid and the pET24PrP90W99F/W145Y/Y150W plasmid were made by Dr. Hui-Chun Yeh. During this project I made the two mutants pET24PrP90W99F/W145Y/G123W and pET24PrP90W99F/W145Y/N159W. Mutagenesis was performed with a Stratagene QuikChange kit using 20 ng of the pET24PrP90W99F/W145Y plasmid template and 50 ng of each primer (N159W or G123W forward and reverse primers) with DNA Polymerase and dNTP's. The N159W primer sequences are as followed:
5'-GAAAACATGAACCGCTACCCTTGGCAAGTGTATTACCGGCCAG for the forward primer and
5'-CTGGCCGGTAATACACTTGCCAAGGGTAGCGGTTCATGTTTTC for the reverse primer. The G123W primer sequences are as followed: forward primer sequence is 5'-GCGGCAGGGGCCGTGGTGTGGGGCCTTGGTGGCTACATG and the reverse sequence is
5'-CATGTAGCCACCAAGGCCCCACACCACGGCCCCTGCCGC. After an initial denaturation step of 3.5 minutes at 95 °C, PCR cycles were conducted with a denaturing temperature of 95 °C for 0.5 minutes, an annealing temperature of 55 °C for 1 minute and an extension temperature of 68 °C for 6 min or 1-2 min per kb.

2-2. Expression and Purification

(A) Expression

BL21(DE3)-Rosetta E.*coli* cells were transformed with the desired pET24PrP90 mutant plasmid, selected on LB Kan/Cm plates containing 50 μg/ml kanamycin (Kan) and 34 μg/ml chloramphenicol (Cm). Liquid cultures were grown from a single colony at 37 °C in 2xYT media containing 50 ug/ml kanamycin and 34 ug/ml chloramphenicol antibiotics. Cell growth was monitored by optical density readings measured with an HP8453A UV-visible spectrophotometer or a Molecular Devices SpectraMax M2^e and were grown to an OD_{600} of 1-2 before expression was induced. To induce expression of the prion protein, a lactose analog, isopropyl-β-D-thiogalactoside (IPTG) was added to a final concentration of 0.5 mM by adding 1 mL of 0.5 M IPTG per liter of cell culture. Cells were grown for an additional 4-5 hours following induction, were spun down and were frozen at –20 °C overnight. Typically 3 liters were grown at a time and cell pellets were collected by centrifugation in an F7S rotor using a Sorvall RC 5B Plus centrifuge at 5,000 rpm for 20 min. The resulting cell pellets containing prion protein inclusion bodies were frozen to induce cell lysis.

(B) Purification

PrP was purified using modifications to published procedures [2, 4]. Frozen cells were suspended in lysis buffer (50 mM Tris-HCl buffer at pH 7.5 containing 100 μg/mL lysozyme) and were shaken at 37 °C for up to 6 hours before being frozen at –20 °C once more. After thawing the cells, DNase I was added (10 μg/ml), and the mixture was incubated at room temperature for 1.5 hrs before adding 1% Triton X-100 and stirring for an additional 10 min. The cells were then placed on ice for 10 min and were centrifuged;

the supernatant was discarded and the inclusion bodies containing the prion protein were collected.

The inclusion bodies containing PrP were purified by repeated resuspension in 50 mM Tris-HCl pH 7.5 containing 1% Triton X-100 (some purifications used 10 mM CHAPS or BugBuster along with Triton X-100) followed by centrifugation. The inclusions bodies were then solubilized in buffer A (8 M urea, 0.1 M potassium phosphate pH 8.0) with 50 mg/mL Sigma protease inhibitor cocktail for 1-2 hours. The sample was then centrifuged to remove insoluble protein prior to use.

The supernatant, now containing the solubilized PrP, was collected and subjected to ammonium sulfate precipitation by the addition of buffer B (0.1 M potassium phosphate pH 8.0) along with NH_4SO_4 (for a final concentration of 4 M urea 0.1 M potassium phosphate, 1 M NH_4SO_4, 25 % ammonium sulfate saturation) while gently stirring. After being placed on ice for 30 min, the suspension was centrifuged and the precipitated protein was suspended in buffer A while the supernatant was saved for further NH_4SO_4 additions and precipitations. Further additions to 35 % or 70 % NH_4SO_4 saturation resulted in a sample with less protein contamination (more pure pellets of PrP) although the nucleic acid component increased (as judged by SDS/PAGE and the A_{280}/A_{260} ratios). The suspended protein pellet, now unfolded in buffer A, was further purified using a nickel ion affinity column. The protein was batch bound to 50 ml Ni (II)-Chelating Sepharose resin (GE Healthcare) prepared in buffer A, was poured into a 5cm diameter column and was then washed with buffer A until the A_{280} reached < 0.03. A 2 L linear gradient from buffer A to buffer B was run to refold the protein on the column, and the protein was then eluted with 60 mM imidazole in buffer B. Some

mutants were particularly difficult to elute with imidazole and had to be eluted using buffer A and then refolded by another process.

The purity of the eluted protein was tested using SDS/PAGE analysis on a Pharmacia PhastSystem (GE Healthcare) using 8-25 % polyacrylamide gels and Coomassie Blue staining. The protein sample was mixed with a 2XTB buffer containing 20 mM Tris-HCl, 2 mM EDTA, 5% SDS, 10% β-mercaptoethanol and bromophenyl blue at pH 8 buffer and boiled at 99 °C for at least 5 min before adding the samples to the gel. BioRad broad range standards were used for mass determination.

If the samples contained any contaminant protein as seen in the acrylamide gel, further purification was necessary and HIC (hydrophobic interaction chromatography) was utilized on an AKTA FPLC (Amersham Biosciences). About 10 mg of protein was loaded onto a HI-Prep Phenyl Sepharose 16/10 column (GE Healthcare) in 4 M urea, 1 M NH_4SO_4, 0.1 M potassium phosphate at pH 8.0 and a gradient was run from 1 M to 0 M NH_4SO_4 in 25 mM Tris-HCl, 4 M urea at pH 8.0. Protein usually eluted from the column between 0.4 to 0.5 M NH_4SO_4. If the protein was sufficiently pure (as judged by SDS/PAGE), it was then concentrated in 6 M guanidine hydrochloride for refolding and isoform conversion.

(C) Alternate Purification Techniques

While some of the purification was achieved using the protocol outlined above, a few mutants were more difficult to purify than others, and the procedure was adjusted for a greater and timelier yield. For some of the mutants, elution off the nickel column could not be achieved using 60 mM imidazole and buffer B, so buffer A + imidazole had to be used to unfold the protein and elute it. The refolding process on the column seemed to be

problematic for some mutants, so the procedure was adjusted: before the nickel column, solublized samples were refolded by dialysis into buffer B, any insoluble protein was removed by centrifugation, and the supernatant was then batch bound to the Ni (II)-Chelating Sepharose resin. The column was washed with buffer B until the A_{280} was <0.03 and the protein could be eluted with 60 mM imidazole in buffer B.

If the protein had could not be purified by HIC or still had contamination following HIC purification, the protein was concentrated into 6 M guanidine hydrochloride, 10 mM potassium phosphate at pH 8.0 and passed through a 30 kDa MWCO membrane in an Amicon stirred cell. To achieve this, the volume was reduced to a few milliliters, more 6 M guanidine solution was added and this process was repeated 3-4 times to ensure that the majority of PrP (MW ~16 kDa) had passed through the membrane. Following concentration of the flowthrough fraction, the sample was dialyzed into 10 mM Na Acetate (NaOAc) at pH 5.5 and then the purity was determined via SDS/PAGE analysis.

2-3. Conversion/Refolding to the Three Isoforms

Pure protein was stored at a concentration of 120 μM in 6 M guanidine hydrochloride, 10 mM potassium phosphate at pH 8.0 at 4 °C or –20 °C until being refolded into PrP^C or converted to PrP^β or PrP^F. Refolding of denatured protein into PrP^C was achieved by dialysis into 10 mM NaOAcbuffer at pH 5.5 and samples were centrifuged before proceeding with data collection.

Conversion to PrP^β was achieved by altering a method published by Baskakov et al [5]. Using purified protein in the storage conditions above, a 6-fold dilution was performed using 1 part protein and 5 parts beta conversion buffer (3.6 M urea, 160 mM

NaCl, 60 mM NaOAc at pH 3.7). The conversion solution was stored at 37 °C overnight and was dialyzed the next morning into 10 mM NaOAc buffer at pH 5.5 before being centrifuged and used in data collection.

Conversion to PrP^F started with refolding protein into PrP^C by dialyzing into 15 mM potassium phosphate buffer at pH 6.5. The refolded sample was then centrifuged and the supernatant mixed with fibril conversion buffer (4.8 M urea, 2 M guanidine hydrochloride, 60 mM potassium phosphate at pH 6.5). One part conversion buffer was added to three parts protein and the sample was then concentrated in an Amicon stirred cell to a concentration of 1.5 mg/mL. The concentrated protein was then placed in a Lab-Line Instruments Titer Plate shaker at a shaking setting of 5 for 16-24 hours at 37 °C. The insoluble fibrils were then twice centrifuged at 7000-10,000 rpm for 10 min in a microcentrifuge and washed with 15 mM potassium phosphate buffer at pH 6.5. The precipitate was pipetted gently to form a suspension; flicking of the eppendorf tube was allowed, but vortexing destroyed the fibrils, so harsh treatment was avoided during handling.

2-4. Verification

Following purification procedures, the final purity of the protein sample was assessed using SDS/PAGE as described in the purification section above. Protein preparations yielded 10-20 mg of highly pure protein as seen in Figure 2-1.

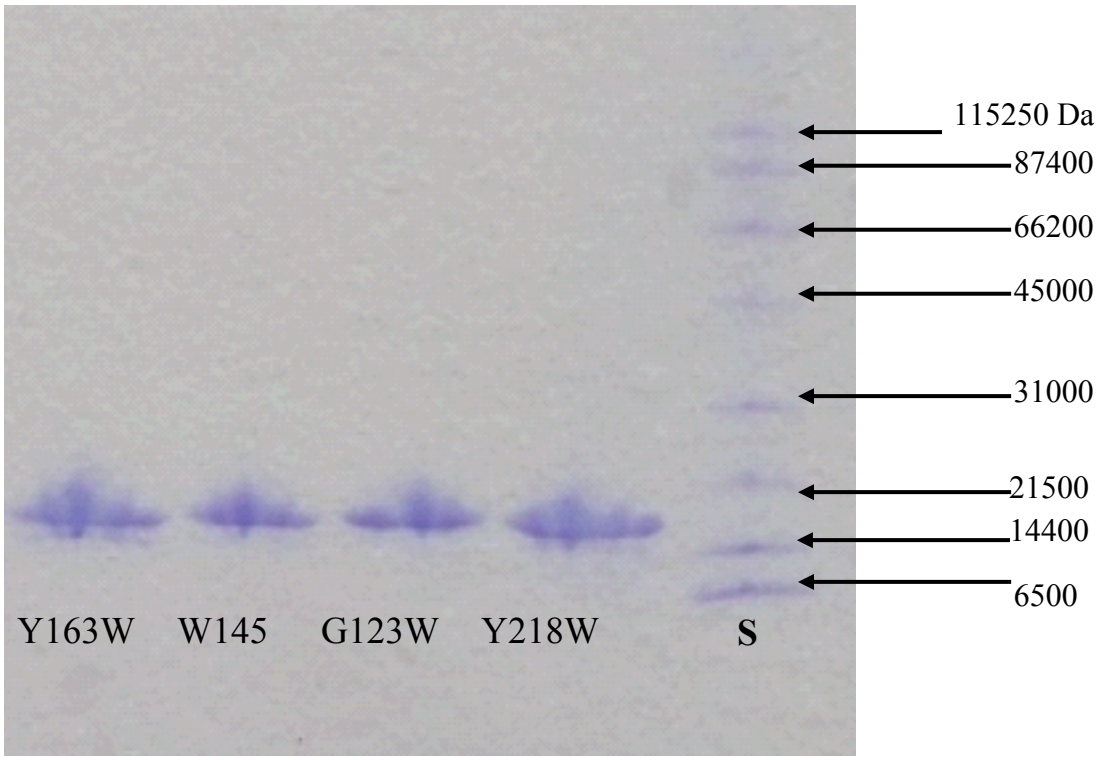

Figure 2-1. SDS/PAGE of different mutant protein samples for purity determination along with a BioRad broad range standard (S). PrP90 is ~16,000 Da.

Proper conversion to PrP^C and PrP^β was verified by using circular dichroism (CD), a technique that reports on protein secondary structure. Measurements were taken in a 0.1 cm path cuvette with 8-20 μM PrP^C or PrP^β scanning from 190-300 nm at 200 nm/min using a Jasco 810 spectrophotometer. Measurements were recorded using 5-10 accumulations at 20-25 ºC using a bandwidth of 2 nm, a response time of 1 second and a data pitch of 1 nm.

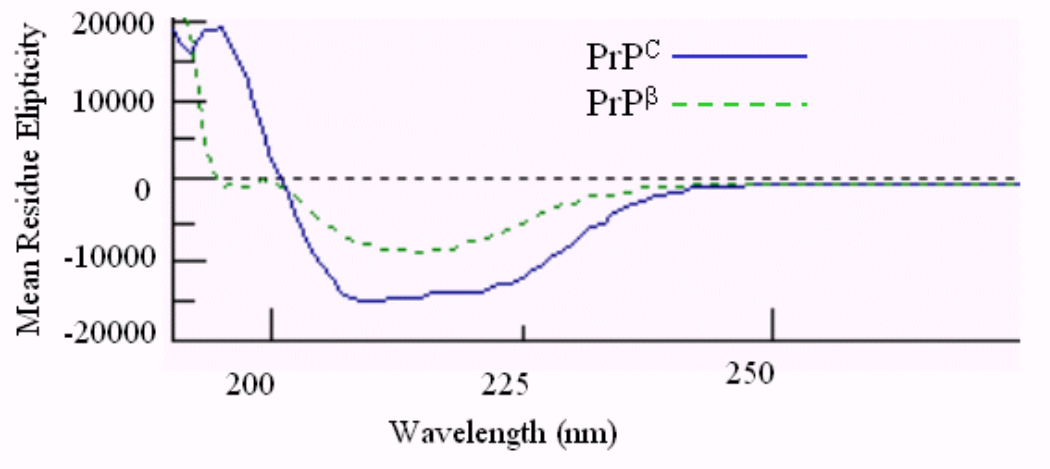

Figure 2-2. Representative CD spectra of N159W PrP^C and PrP^β data exhibiting typical α-helical or β-sheet spectral characteristics [7]. PrP^C is composed mostly of α-helical secondary structure and exhibits two minima around 209 and 222 nm while PrP^β is composed mainly of β-sheets and has one minimum around 216 nm.

CD spectral data was converted to mean residue elipticity (MRE) on the y-axis for each sample. Mean residue elipticity [θ] is calculated and then applied to the spectra by the equation below.

$$[\theta] = 1/(10npc) \qquad \text{Equation 2-1}$$

giving units in degrees cm^2 $dmol^{-1}$ residue $^{-1}$, where n is # of residues in the protein, p is the pathlength of the cuvette in centimeters and c is concentration of the protein sample in μM.

To determine the MRE, the concentration of converted PrP was needed. Samples were unfolded by dilution with a 6.7 M guanidine hydrochloride stock to achieve a final concentration of 6.0 M guanidine hydrochloride 0.01 M potassium phosphate pH 7.4. The protein concentrations were determined using their absorbance at 280 nm. Extinction

coefficients were determined using the ProtParam tool on the Expasy website (expasy.org) which calculates protein extinction coefficients using the Edelhoch method based on the number of tryptophan, tyrosine, and cysteine residues and their corresponding exctinction coefficients determined by Pace et al. [8]. The extinction coefficient for single Trp prion protein mutants were similar and were calculated as ~22,000 $M^{-1}cm^{-1}$ at 280 nm measured in water. To determine the concentration of the fibrillar samples, the protein was diluted into the same guanidine hydrochloride stock solution to a final concentration of 6 M guanidine hydrochloride and the fibrils were allowed to denature and dissolve for ~30 min before measurements were taken. The UV spectra were taken in a 1 cm pathlength UV cuvette using a UV-visible HP8453A photodiode array spectrophotometer.

To verify that the mutations introduced in the prion protein did not disrupt the conformational stability of PrP^C, thermal denaturation profiless were measured via CD. The T_m (temperature at which 50% of the secondary structure has disappeared) values were obtained and compared with that of WT PrP90. The T_m values for all the mutant PrPs were close to WTPrP90 and the unfolding curves appeared similar in shape and were consistent with simple two state folding.

Proper conversion to PrP^F was verified using a ThT (thioflavin T) assay [9] and electron microscopy imaging techniques. For the ThT assay, fibrils were diluted into a 5 mM NaOAc buffer at pH 5.5 containing 10 μM ThT to a final concentration of ~0.3-0.5 μM protein. The fluorescence emission spectrum (450 – 600 nm) of the resulting suspension was measured using an excitation wavelength of 445 nm using a Jasco 810 CD spectrophotometer equipped with a scanning fluorescence detector. ThT binds to

amyloid fibrils, which enhances and shifts its fluorescence emission spectrum (see Figure 2-3). In contrast, ThT does not bind to PrP^C or PrP^β and so the ThT fluorescence spectrum does not change from that of the dye alone.

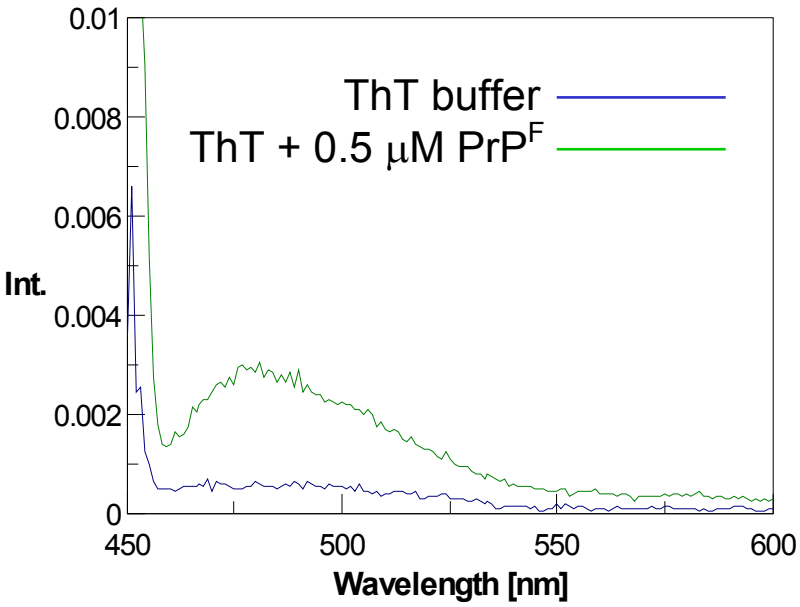

Figure 2-3. The fluorescence emission spectra of 10 μM ThT in 5 mM NaOAc buffer pH 5.5 with and without fibrillar protein. The emission of ThT is much enhanced by the presence of 0.5 μM fibrils.

Electron microscope images were taken at the UM EMtrix facility using the following protocol: 5 μl of fibrils suspended in buffer to a final concentration of 20-100 μM monomer were bound to Formvar carbon coated specimen grids for 1 hour and then washed with water and dyed with uranyl acetate for 30 seconds before being washed again with water and dried. Following binding of the protein on the grids, the images were viewed and magnified using a Hitachi H-7100 TEM (transmission electron microscopy) instrument and pictures and grids were saved for later usage or viewing. The

samples were viewed and proper fibril formation was verified by distinguishing between fibrillar structures and globs of precipitate (see Figure 2-4).

Figure 2-4. PrP N159W fibrils at 70,000X magnification (Bar =100 nm).

2-5. Tryptophan Fluorescence Data Collection and Experimentation

Steady state data were collected at 20 °C on a Jasco 810 CD spectrophotometer equipped with a scanning fluorescence detector using 8-20 μM protein in 10 mM NaOAc buffer pH 5.5. Measurements were taken in either a 1 cm or 0.4 cm far-UV quartz cuvette (Nova biotech). The sample was excited at 295 nm and the emission was recorded from 300-500 nm**.** Steady state quenching was accomplished by adding aliquots of buffered 5 M acrylamide to the sample so that each addition increased the quencher concentration by ~0.05 M, up to a final acrylamide concentration of 0.5 M. Fluorescence measurements were performed with a response time of 0.25 sec, a sensitivity of 500 V, a data pitch of 1 nm, an excitation bandwidth of 5 nm and an emission bandwidth of 10 nm.

The majority of the lifetime measurements were taken at Fluorescence Innovations Inc., in Bozeman, MT using a prototype ultraviolet fluorescence lifetime spectrometer. Florescence measurements were recorded at 20° C and the sample temperature was controlled with a four-cuvette turret from Quantum Northwest (Spokane, WA). The sample concentration was 8-20 μM, was held in either a 1 cm or 0.4 cm far-UV quartz cuvette (Nova biotech) and was excited at 292-294 nm using a compact frequency-doubled dye laser having 200 μJ energy per pulse, 1000 Hz pulse repetition frequency, and 0.5 ns pulse duration. The fluorescence was detected using a Varian Cary Eclipse spectrofluorimeter modified with a Hamamatsu R-7400 photomultiplier tube (PMT). The PMT was biased at 400-500 V for the various experiments.

Time-domain fluorescence data were recorded using a proprietary transient digitizer that generates a decay curve for each laser pulse, employs an analog memory

and samples at 1 gigasample/sec. The effective sampling rate is increased to every 200 ps via 5X interleaving. Each fluorescence decay spectra was averaged over 1000 laster shots. Fluoresence data were recorded between 300 and 400 nm for every quencher concentration. As with steady-state measurements, a buffered solution of 5 M acrylamide was titrated into the sample at 0.05 M increments to a final concentration of 0.5 M acrylamide. Lifetimes of N-acetyl-tryptophanamide (NATA) and p-terphenyl (PTP) were measured to derive the instrument response function (IRF) for later data analysis (see following section).

One trial of lifetime measurements was also performed at UM in The laboratory of Dr. JB Alexander (Sandy) Ross using time-correlated single-photon counting (TCSPC) with a FLASC 1000 sample chamber (Quantum Northwest, Liberty Lake, WA). Samples were excited at 295 nm using a frequency-doubled ps Mira 900 Ti:Sapphire laser (Coherent, Santa Clara, CA) and magic angle polarization. The emission was recorded at 350 nm using the TimeHarp 200 PCI board (PicoQuant, Berlin) until at least 8 X 10^3 counts were obtained at the maximum of the decay curve. Acrylamide was added in 0.1 M increments up to 0.4 M acrylamide total. The fluorescence decay spectra were recorded at 20 °C.

2-6. Data Analysis and Modification

Steady-state fluorescence spectra were analyzed using Origin software or Jasco 800 windows spectral analysis. Baselines were corrected through editing options and volume increases were accounted by normalizing the fluorescence intensities to the initial concentrations of protein. The intensity and λ_{max} (wavelength at maximum fluorescence intensity) were extracted and used for further analysis.

The data from lifetime measurements were fit using the following process.

$$I(t)= \sum \alpha_i \exp(-t/\tau_i), \qquad \text{Equation 2-2}$$

Equation 2-2, where α_i is the amplitude of the exponential with lifetime τ_i, was convoluted with the instrument response function (IRF) and the resulting function was compared with the data [10]. The α_i and τ_i values were varied using Excel's Solver program and the fit to the data was evaluated using a least-squared analysis. Unless a sufficient improvement in χ^2 values was obtained by adding another lifetime component (χ^2 decrease by half), the simplest model was assumed to be the best analysis and the τ values (lifetimes or decay times) were then determined. In the cases where more than one lifetime was observed, a weighted τ value was calculated using Equation 2-3.

$$\langle\tau\rangle = (\alpha_1\tau_1^2 + \alpha_2\tau_2^2)/(\alpha_1\tau_1+\alpha_2\tau_2). \qquad \text{Equation 2-3}$$

Fluorescence intensity or lifetime quenching (taken at the λ_{max} of the corresponding steady-state spectrum) was plotted using the Stern-Volmer equation.

$$F_0/F = \tau_0/\tau = k_q(\tau_0)[Q] + 1 \qquad \text{Equation 2-4}$$

(where F_0 is fluorescence in the absence of quencher and F is fluorescence with the given quencher concentration, [Q] is quencher concentration and τ_0 is the fluorescence lifetime of the protein in the absence of quencher). From the Stern-Volmer plot and the lifetime value τ_0, the k_q or the bi-molecular quenching constant was determined [10]. To correct for the presence of static quenching in steady-state measurements and to compare our steady-state k_q values to published k_q values [11] of other single tryptophan-containing proteins, the curves were fit, when applicable, to a modified Stern-Volmer equation taking into account the static component.

$$F_0/F\, e^{V[Q]} = 1 + K_{SV}[Q] \qquad \text{Equation 2-5}$$

where $K_{SV} = k_q \tau_0$ is the dynamic quenching component and V is the static quenching component defined by some as the sphere of action [10]. By plotting $F_0/F \exp(V[Q])$ vs [Q] and varying V until the best fit line is achieved, it is possible to derive a more accurate diffusion-limited rate constant in the presence of static quenching. It is important to note that not all steady-state quenching curves could be fit to the above equation as the fit to a straight line could not be improved by adding the static component (V).

To further check the correlation between solvent accessibility and k_q values, the NMR structure of PrP^C obtained from the protein data bank (ID# 1B10, structure no. 4, containing residues 109-219) [12, 13] were modified to reflect the sequence of the single-tryptophan mutants; these were then energy-minimized using Sybyl_7.3 or 8.0. Energy minimizations were performed using the Powell Method Gradient at 0.05 kcal/Å mol. The solvent accessible surface area (SASA) of the tryptophan was measured using MOLMOL calculations and the exposure of the entire residue (including backbone) was recorded and could be compared to the k_q results obtained for PrP^C.

References

1. Paramithiotis E, Pinard M, Lawton T, LaBoissiere S, Leathers VL, Zou WQ, Estey LA, Lamontagne J, Lehto MT, Kondejewski LH *et al*: **A prion protein epitope selective for the pathologically misfolded conformation**. *Nat Med* 2003, **9**(7):893-899.
2. Lennon CW, Cox HD, Hennelly SP, Chelmo SJ, McGuirl MA: **Probing structural differences in prion protein isoforms by tyrosine nitration**. *Biochemistry* 2007, **46**(16):4850-4860.
3. Daggett V, DeMarco ML. In. Edited by McGuirl MA; 2005.
4. Speare JO, Rush TS, 3rd, Bloom ME, Caughey B: **The role of helix 1 aspartates and salt bridges in the stability and conversion of prion protein**. *J Biol Chem* 2003, **278**(14):12522-12529.
5. Baskakov IV, Legname G, Baldwin MA, Prusiner SB, Cohen FE: **Pathway complexity of prion protein assembly into amyloid**. *J Biol Chem* 2002, **277**(24):21140-21148.

6. Novy R, Drott D, Yaeger K, Mierendorf R: **Overcoming the codon bias of E. coli for enhanced protein expression**. In: *in**Nova**tions.* vol. 12; 2001: 1-3.
7. Lobley A, Whitmore L, Wallace BA: **DICHROWEB: an interactive website for the analysis of protein secondary structure from circular dichroism spectra**. *Bioinformatics* 2002, **18**(1):211-212.
8. Gasteiger E, Hoogland C, Gattiker A, Duvaud S, Wilkins MR, Appel RD, Bairoch A: **Protein Identification and Analysis Tools on the ExPASy Server**. In: *The Proteomics Protocols Handbook.* Edited by Walker JM, Third Edition edn: Humana Press; 2005: 571-607.
9. Naiki H, Higuchi K, Hosokawa M, Takeda T: **Fluorometric determination of amyloid fibrils in vitro using the fluorescent dye, thioflavin T1**. *Anal Biochem* 1989, **177**(2):244-249.
10. Lakowicz JR: **Principles of Fluorescence Spectroscopy Third Edition**: Springer; 2006.
11. Eftink MR, Ghiron CA: **Exposure of tryptophanyl residues in proteins. Quantitative determination by fluorescence quenching studies**. *Biochemistry* 1976, **15**(3):672-680.
12. DeMarco ML, Daggett V: **From conversion to aggregation: protofibril formation of the prion protein**. *Proc Natl Acad Sci U S A* 2004, **101**(8):2293-2298.
13. Liu H, Farr-Jones S, Ulyanov NB, Llinas M, Marqusee S, Groth D, Cohen FE, Prusiner SB, James TL: **Solution structure of Syrian hamster prion protein rPrP(90-231)**. *Biochemistry* 1999, **38**(17):5362-5377.

CHAPTER 3: FLUORESCENCE MEASUREMENTS AND RESULTS

The purpose of this project is to probe changes in conformation among the various isoforms (PrP^C, PrP^β and PrP^F) using tryptophan fluorescence measurements. Both steady-state and time-resolved fluorescence measurements were used and the reasons for using both are outlined here. Steady-state spectrum measurements require simple instrumentation and analysis, providing an accessible method for measuring tryptophan fluorescence changes. To quantify the accessibility of the tryptophan in each of the isoforms, steady-state measurements were coupled with fluorescence quenching using acrylamide and the k_q value (quenching rate constant) was determined. Steady-state quenching measurements can be complicated by the presence of static quenching and determination of the diffusion-controlled k_q can prove difficult. Besides supplying the lifetime (τ_0) necessary for k_q determination, time-resolved measurements were taken and coupled with acrylamide quenching to directly provide a diffusion-controlled k_q for each sample, as these measurements are not influenced by static quenching mechanisms.

The purpose of this chapter is to introduce each type of fluorescence measurement and show the results. This chapter ends with a section on k_q determination and a brief discussion of the results.

3-1. Steady-State Measurements

(A) Introduction to Steady-State Measurements

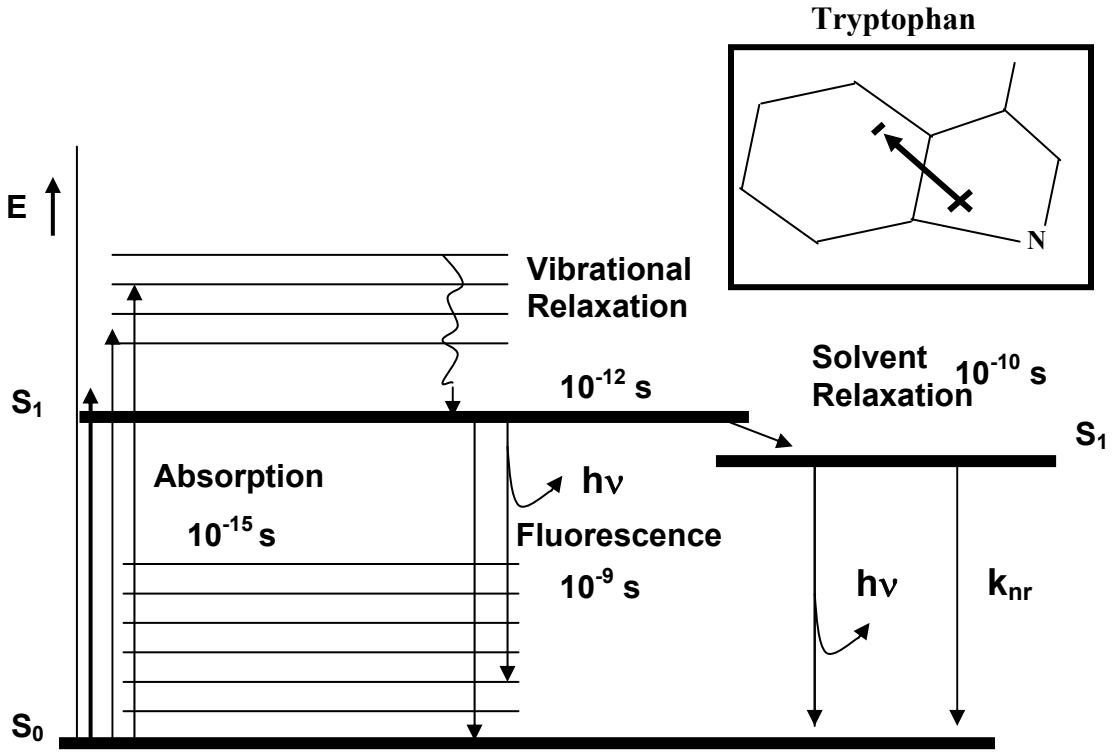

Figure 3-1. Jablonksi diagram showing energy states of a molecule. If a molecule in the ground state (S_0) absorbs a photon with energy equal to the energy difference between the ground state and excited state (S_1), it will transition to the excited state. The molecule comes to rest within the lowest energy level of the excited state. An electron's return to ground state can be accompanied by an emission of a photon whose energy is equal to hν (Planck's constant times frequency). Right corner inset showing tryptophan molecule with an arrow representing the dominant dipole in the excited state.

The relationship between the absorption and emission of photons can be depicted using a Jablonski diagram (Figure 3-1). When a molecule in its ground state (S_0) absorbs light of a particular energy, a transition occurs to the first excited electronic state (S_1) where the molecule rapidly relaxes to the lowest vibrational level of S_1. During the return to the ground state, the molecule can lose energy in the form of vibration or heat or emit a photon (energy equal to hν) in a process known as fluorescence. While some

information regarding the environment of a fluorophore can be derived from the absorption spectrum of a molecule, the fluorescence spectrum is generally a much more sensitive probe for understanding molecular interaction and conformations.

For steady-state fluorescence measurements, the sample is excited with a continuous beam of light and the emission spectrum is recorded [1]. Steady-state fluorescence can be used to derive the quantum yield--the number of photons emitted vs. the number of photons absorbed, which is given in Equation 3-1.

$$\Phi = k_r/(k_r + k_{nr}) \qquad \text{Equation 3-1.}$$

In Equation 3-1 k_r is the rate of radiative decay processes (fluorescence) and k_{nr} is the rate of all the other processes that contribute to non-radiative decay (nonfluorescence due to nearby quenching molecules; solvent, nearby polar residues or the amide backbone etc…[1, 2]. Due to the ability of the indole ring to transfer electrons in the excited state, tryptophan fluorescence is highly sensitive to changes in the surrounding environment and is commonly used to report changes in conformation or binding events in proteins [1]. Tryptophan has a larger dipole moment in the excited state than the ground state (Figure 3-1); this causes water molecules to orient themselves around the dipole, stabilize the excited state and produce a lower energy of emission. This phenomenon is referred to as solvent relaxation and occurs at timescales near 10^{-10} s, whereas the lifetime of tryptophan fluorescence lasts for 10^{-9} s, so the emission spectrum reflects the solvent relaxed state (See Figure 3-1) [1]. The more exposed a tryptophan is to solvent, the more solvent relaxation occurs, which causes a lower energy (longer wavelength) of emission. Fully exposed tryptophan emits at a λ_{max} (wavelength at intensity maximum) around 350 nm in aqueous solution. A blue shift in emission along with an increase in intensity

(discussed in more detail in the next section) can indicate a decrease in solvent exposure, which in a protein correlates with a more buried residue. It has been shown that there is a strong correlation between the λ_{max} of tryptophan emission and its accessibility to exogenous quenchers as determined by k_q value [1, 3].

(B) Steady-State Results

As seen in Figures 3-2 and 3-3, the spectra of mutants in the 3 different isoforms exhibit shifts in intensity and/or wavelength.

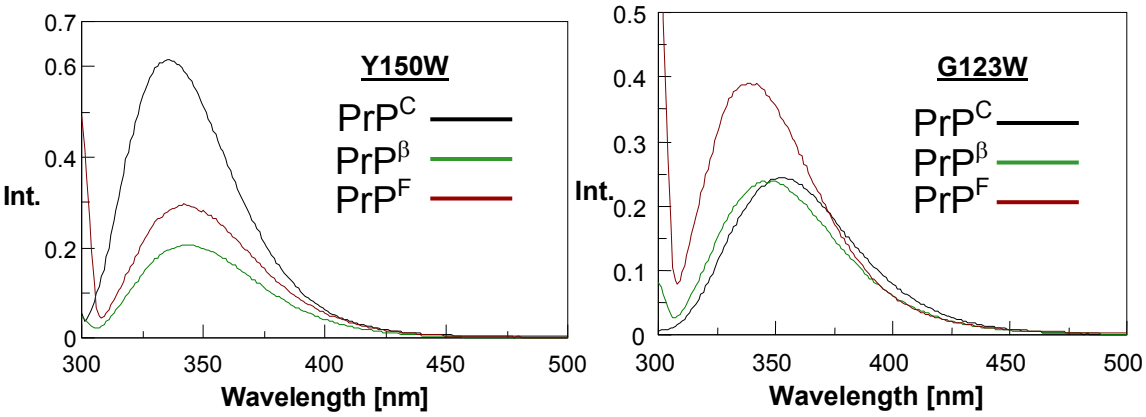

Figure 3-2. Representative steady-state spectra for Y150W and G123W mutants showing intensity vs. wavelength for the three different isoforms PrP^C, PrP^β, and PrP^F. All spectra normalized to 20 μM concentration. Spectral overlays for the other mutants can be found in the Appendix (Figure A-1).

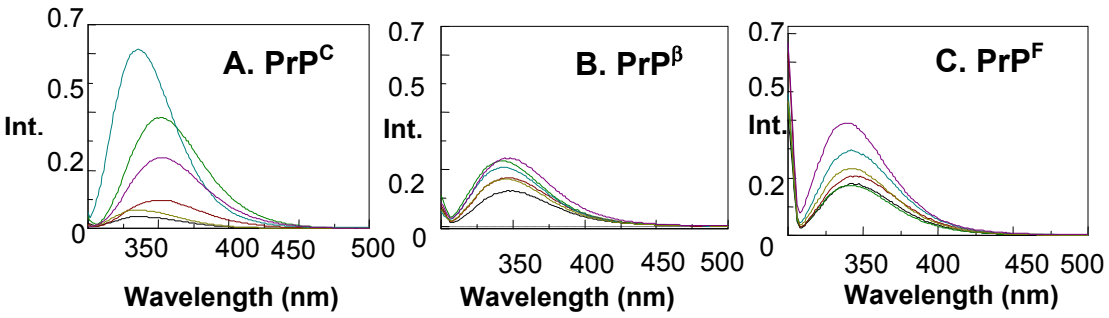

Figure 3-3 (A-C). Representative steady-state spectra overlayed for all the mutants of a particular isoform at 20 μM concentration (A) PrP^C; (B) PrP^β; (C) PrP^F. Y150W — N159W— G123W — W145 — Y163W — Y218W —

While mutants in the PrP^C isoform exhibit a wide range of λ_{max} values (Figure 3-3A), mutants in the PrP^β and PrP^F isoforms similarly show more consistency in their λ_{max} values (Figure 3-3, B and C). Table 3-1 shows all the λ_{max} and intensity values for the mutants in the three isoforms for direct comparison.

	PrP^C		PrP^β		PrP^F	
Mutants	**λ_{max} (nm)**	**Intensity**	**λ_{max} (nm)**	**Intensity**	**λ_{max} (nm)**	**Intensity**
G123W	353	0.28	347	0.27	339	0.4
W145	351	0.10	347	0.17	344	0.21
Y150W	336	0.62	344	0.21	343	0.29
N159W	352	0.38	344	0.23	343	0.18
Y163W	336	0.06	345	0.17	343	0.22
Y218W	334	0.04	348	0.12	343	0.18

Table 3-1. Representative λ_{max} and intensity values from the steady-state spectra of the six mutants in the three isoforms. All intensities are normalized to 20 μM concentration.

For the PrP^C isoform, G123W, W145 and N159W show λ_{max} values between 351 and 353 nm, indicating exposed tryptophan, while Y150W, Y163W and Y218W all show

significant blue shifts in emission with λ_{max} around 334-336 nm, which indicates the tryptophan is more buried than in the first three mutants. These results are supported by MOLMOL [4] calculated solvent accessible surface areas (SASA) for tryptophan residues in the PrP^C structure, which predicts that mutants Y150W, Y163W, and Y218W have ~3%, 5%, and 10% tryptophan exposure, respectively. In contrast, mutants G123W and W145 have ~69% and 50% exposure, respectively. N159W has 23% accessibility as determined by MOLMOL calculations, but has a λ_{max} at 352 nm, which would correspond to a much more exposed residue. Thus, λ_{max} values alone may be insufficient to accurately assign solvent exposure to a tryptophan molecule within a protein.

As seen for PrP^β and PrP^F, shifts in intensity and λ_{max} can be observed and used to predict changes in accessibility of the Trp compared to PrP^C. For G123W, there is a blue shift in λ_{max} for PrP^β and PrP^F and the intensity significantly increases in PrP^F, indicating the Trp becomes more buried upon conversion. This pattern can also be seen for W145. In Y150W, there is a red shift in λ_{max} and a decrease in intensity indicating a more exposed residue in PrP^β and PrP^F. For the other mutants, however, there are some seemingly conflicting observations. For Y163W and Y218W, there is an increase in intensity for PrP^β and PrP^F indicating a more buried Trp, but the wavelength of emission shifts to the red indicating a more exposed residue. For N159W, there is a decrease in intensity indicating more exposure, but the blue shift in λ_{max} indicates a more buried residue. Because observations in spectral shifts and intensities are influenced by factors besides solvent exposure, another approach is needed to measure changes in tryptophan exposure among the three isoforms.

3-2. Steady-State Quenching Measurements

(A) Introduction to Steady-State Quenching

Although it would be convenient to directly correlate shifts in intensity and emission to changes in solvent exposure, other environmental factors influence tryptophan fluorescence emission as well. Due to the ability of indole to transfer electrons in the excited state, factors such as nearby histidine, phenylalanine, or tyrosine residues along with amino acids having ionic side chains, polar residues, the peptide backbone, or disulfide bonds can influence the fluorescence emission [1]. Anything that acts upon the dipole moment of the excited tryptophan including solvent molecules can cause shifts in λ_{max} and intensity. Thus, to more accurately quantify the accessibility of tryptophan to solvent, a molecule that diffuses to the fluorophore and quenches the fluorescence emission is titrated and changes in fluorescence are measured. By measuring the fluorescence as a function of quencher concentration, one can determine the accessibility of the quencher to the fluorophore and by analysis determine the solvent accessibility/surface exposure of the fluorophore. A Stern-Volmer plot is then determined, given by the equation below.

$$F_0/F = 1 + K_{SV}[Q] = 1 + k_q\tau_0[Q] \qquad \text{Equation 3-2}$$

K_{SV} is the Stern-Volmer constant, k_q is the bimolecular quenching rate constant, and F_0 and τ_0 are the fluorescence intensity at λ_{max} and the lifetime in the absence of quencher, respectively. The Stern-Volmer constant can indicate exposure to quencher, since the larger the slope, the more quenching has occurred. However, to fully quantify the efficiency of quenching and thus the accessibility of the fluorophore to solvent, k_q values are calculated and compared. The bimolecular quenching rate constant defines the

diffusion-controlled or dynamic rate of quenching over the lifetime of the fluorophore. The faster and more efficient the rate of quenching, the more access the quencher (and thus the solvent) has to the tryptophan. By measuring the k_q, it is possible to quantify the efficiency of quenching and thus the amount of exposure of the tryptophan to solvent for direct comparisons between the various isoforms of the protein mutants.

The purpose of quencher studies is to derive the rate that the quencher encounters the fluorophore due to dynamic quenching mechanisms. Acrylamide is the quencher we selected (Figure 3-4D) since it is a polar, non-ionic, electron-deficient molecule that can quench fluorophores in pockets or clefts of the protein matrix. Unlike ionic quenchers that may be hindered by electrostatics, acrylamide may be a better choice for fibrillar samples where the tryptophan may not be completely accessible at the surface.

A problem frequently encountered while using acrylamide in determining the dynamic quenching rate constant in steady-state measurements is static quenching. Static quenching occurs when the quencher forms a ground state complex with the fluorophore, causing a decrease in fluorescence as the excited-state electron immediately returns to the ground state without the emission of a photon [1]. This increases the observed Stern-Volmer constant, but the data do not represent diffusion-controlled quenching mechanisms, which make it difficult to derive the true dynamic rate of quenching. Stern-Volmer plots representing both dynamic and static quenching mechanisms generally deviate from a straight line and display upward curvature as quencher concentration is increased.

Multiple mathematical models have been derived to help give physical explanations to observations amidst the wide variation of tryptophan fluorescence data.

Specifically for steady-state data, equations have been derived to try and separate the effects of static quenching from dynamic mechanisms [1, 5]. In a simple model, Eftink and Ghiron have reported a modified Stern-Volmer equation that tries to distinguish between static and dynamic quenching contributions in a Stern-Volmer plot displaying upward curvature [3]. This modified plot is represented by Equation 3-3.

$$F_0/(F\exp(V[Q])) = 1 + K_{SV}[Q] \qquad \text{Equation 3-3}$$

K_{SV} is the dynamic quenching component and V is the static quenching component or the quenching "sphere of action" [3]. V has been described as representing the volume around the fluorophore where at the time of excitation, a quencher molecule is found and forms an encounter complex [5]. According to Eftink, V is related to the probability that the acrylamide is found close enough to the tryptophan as to quench it immediately or statically [3].

It is important to note that although this modified Stern-Volmer equation gives a simple equation that attempts to distinguish between the contributions of static and dynamic quenching, and indeed can give some idea about the sphere of action of the tryptophan, it is ultimately applying a correction factor to the data to allow a fit to a straight line in plots displaying curvature in the slope. It may not be a sufficient model when multiple or heterogenous populations of tryptophan molecules are present and each displays a unique static component.

(B) Steady-State Quenching Results

As seen in Figure 3-4(A-C), steady-state fluorescence was measured at increasing acrylamide additions. For N159W, PrP^C fluorescence is quenched at lower acrylamide concentrations than the PrP^β or PrP^F isoforms.

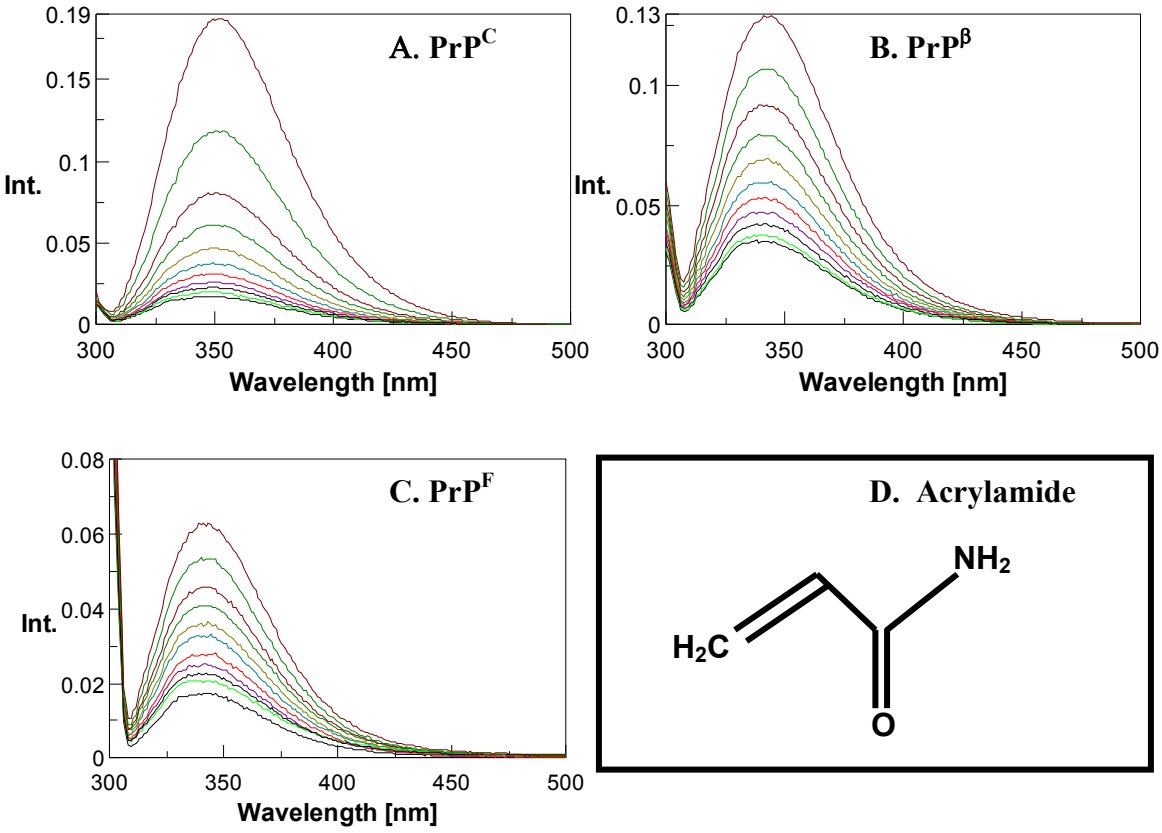

Figure 3-4 (A-C). Representative steady-state quenching spectra for N159W in PrP^{C}, PrP^{β}, and PrP^{F} isoforms showing intensity vs. wavelength. Acrylamide was added at 0.05 M increments up to 0.5 M concentration total. Overlayed quenching spectra for the other mutants in the three isoforms can be found in the Appendix (Figure A-2). (D) The structure of acrylamide.

As seen in Figure 3-5, there is an upward curvature in the unmodified Stern-Volmer plots (Equation 3-2), indicating combined static and dynamic quenching mechanisms. By plotting the data according to the modified Stern-Volmer equation (Equation 3-3), the contribution of the static component (represented by V) can be accounted for and the dynamic quenching rate constant estimated.

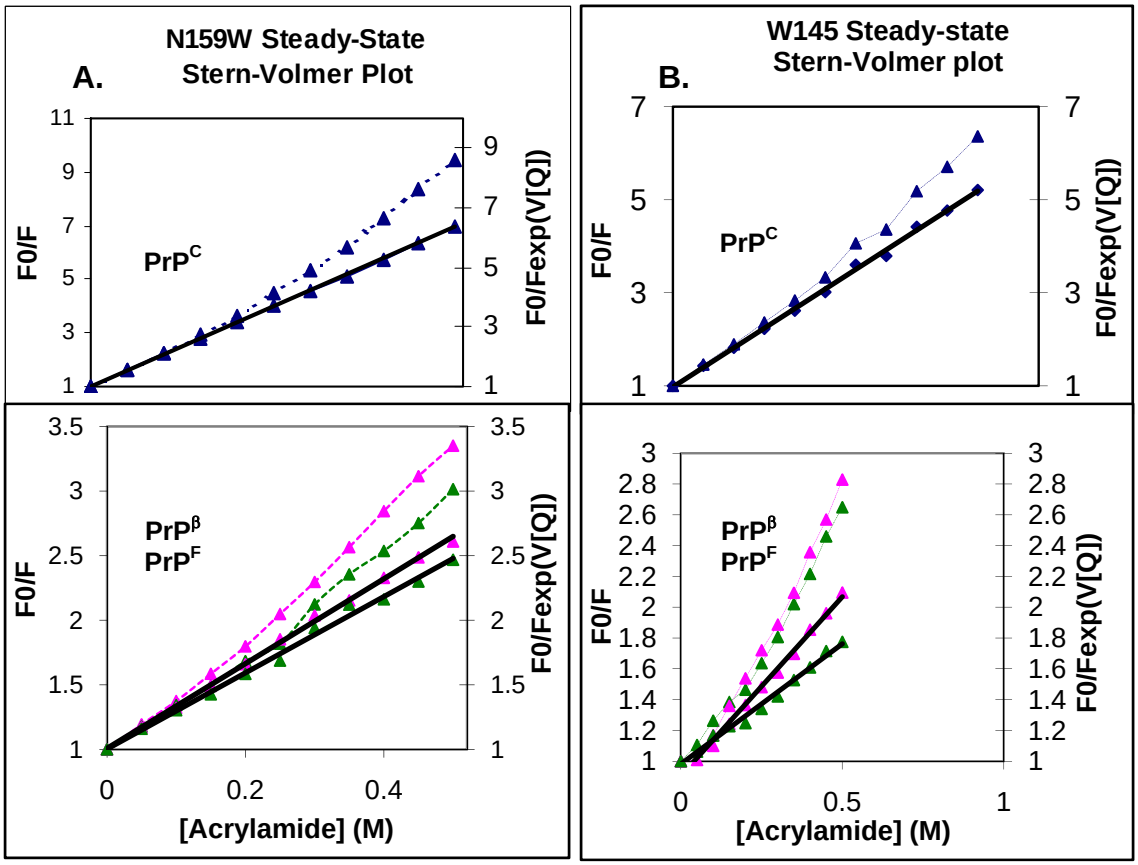
A.
N159W Steady-State
Stern-Volmer Plot
F0/F
F0/Fexp(V[Q])
PrP^C
PrP^β
PrP^F
[Acrylamide] (M)
B.
W145 Steady-state
Stern-Volmer plot

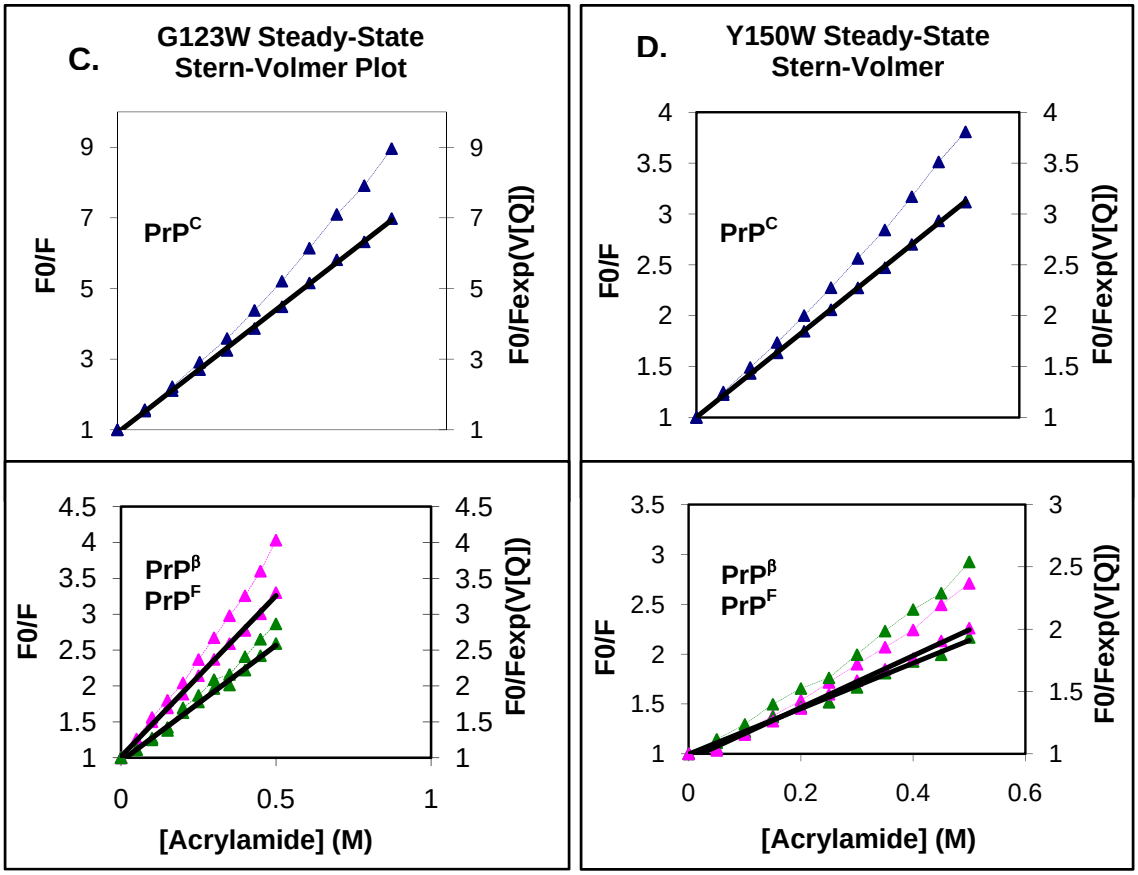
C.
G123W Steady-State Stern-Volmer Plot
PrP^C
F0/F
F0/Fexp(V[Q])
PrP^β
PrP^F
[Acrylamide] (M)
D.
Y150W Steady-State Stern-Volmer

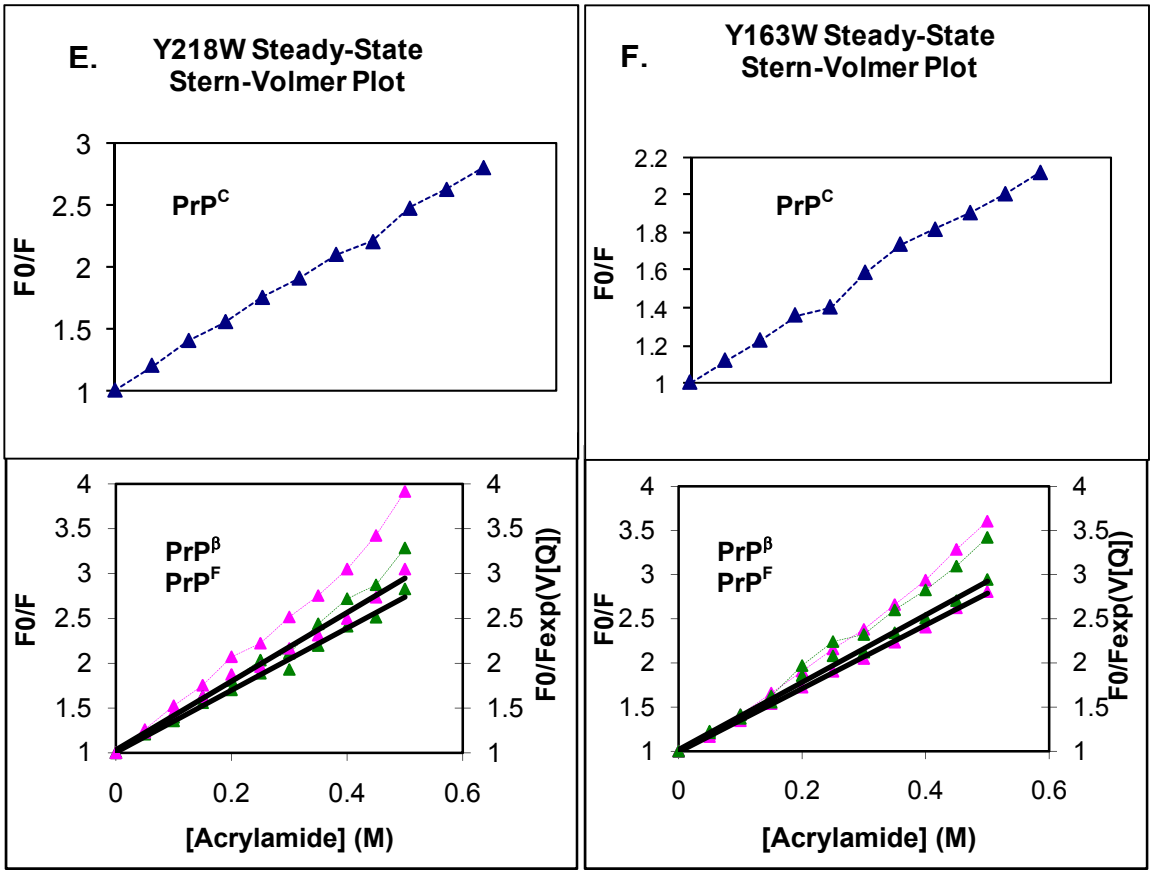

Figure 3-5 (A-F). Steady-state Stern-Volmer plots for Prp^{β} ▲, PrP^{F} ▲, and PrP^{C} ▲ plotted according to modified and unmodified equations. When plotting the data to the unmodified Stern-Volmer equation (dotted lines) the left y-axis is used and when the data is plotted to the modified Stern-Volmer equation (solid lines) the right y-axis is used.

With the exception of Y218W and Y163W PrP^{C}, all the mutants in the various isoforms exhibit some amount of upward curvature and using the modified equation at least modestly improves the R^2 values for the slopes. Table 3-2 summarizes the slopes or K_{SV} values using both unmodified and modified Stern-Volmer equations. When using the

modified Stern-Volmer equation, K_{SV} represents the dynamic quenching constant and V represents the static quenching constant as determined by plotting the data to the modified Stern-Volmer equation and varying V until an optimum R^2 value was achieved. In the case where V=0, no fit improvement could be attained and the data were left unmodified.

	Unmodified		Modified		
Mutant & Isoform	**K_{SV} (M^{-1})**	**R^2**	**K_{SV} (M^{-1})**	**V (M^{-1})**	**R^2**
G123W					
PrP^C	14.5 ± 2.0	0.9947	11.9 ± 0.7	0.35	0.9979
PrP^β	4.7 ± 1.7	0.9845	4.1 ± 0.7	0.2	0.9989
PrP^F	4.9 ± 1.5	0.9912	3.5 ± 0.4	0.1	0.9946
W145					
PrP^C	10.8 ± 1.6	0.9914	8.4 ± 0.8	0.4	0.9966
PrP^β	4.5 ± 0.7	0.9909	3.1 ± 0.8	0.5	0.9958
PrP^F	3.3 ± 0.1	0.9881	2.4 ± 1.2	0.4	0.9904
Y150W					
PrP^C	5.2 ± 0.6	0.9975	4.1 ± 0.3	0.35	0.9999
PrP^β	3.7 ± 0.3	0.9928	2.2 ± 0.2	0.6	0.9977
PrP^F	4.1 ± 0.2	0.9909	3.2 ± 0.9	0.3	0.9930
N159W					
PrP^C	17.4 ± 0.5	0.9898	11.3 ± 0.7	0.8	0.9993
PrP^β	4.4 ± 0.6	0.9946	3.4 ± 0.1	0.35	0.9968
PrP^F	3.7 ± 0.5	0.9953	2.6 ± 0.1	0.4	0.9977
Y163W					
PrP^C	2.3 ± 0.1	0.9964	--------	0	-------
PrP^β	5.1 ± 0.1	0.9962	3.6 ± 0.1	0.5	0.9994
PrP^F	5.7 ± 0.8	0.9833	3.4 ± 0.2	0.7	0.9913
Y218W					
PrP^C	3.1 ± 0.7	0.9978	-------	0	-------
PrP^β	5.1 ± 0.2	0.9964	4.1 ± 0.6	0.3	0.9982
PrP^F	4.4 ± 0.1	0.9895	3.5 ± 0.1	0.3	0.9918

Table 3-2. The K_{SV} values, V values, and fits to a straight line given by R^2 for both modified and unmodified Stern-Volmer equations for the six mutants in the three isoforms. For the modified equation, K_{SV} and V correspond to the Stern-Volmer constant for the dynamic component and the static quenching component, respectively.

When representing dynamic quenching, K_{SV}^{-1} is the quencher concentration at which 50% of the intensity is quenched. For PrP^C isoforms of mutants N159W, G123W, and W145, half the fluorescence is quenched below 0.15 M acrylamide whereas isoforms of the rest of the mutants require at least 0.25 M acrylamide to quench 50% of the fluorescence.

The static quenching constant is sometimes used to gain information on the exposure and surroundings of the tryptophan. It was shown that in most single-Trp proteins there is a general agreement between V values and accessibility as determined by k_q values [3]. Because the structure for PrP^C is known and solvent accessible surface area (SASA) data can be calculated, it is interesting to examine the data more closely for this isoform. It is seen from Table 3-2 that N159W exhibits the largest V value while G123W, W145 and Y150W display lower yet significant V values and Y218W and Y163W do not improve with the fitting of any V component. The presence of a static component indicates that the quencher molecule can exist close enough to the indole ring to form a complex and statically quench the fluorescence. While most of the V values for the various positions make sense in considering their corresponding SASA (Table 3-3), a couple exceptions exist.

Y163W, Y218W and Y150W all exhibit low K_{sv} values, have blue-shifted steady-state intensity emissions (Table 3-1) and are predicted to have a low degree of solvent exposure from MOLMOL calculations (Table 3-3). As these positions are found within secondary structural elements of PrP^C (see chapter 4) these data make sense. In the case of Y150W, however, the V value would argue that there is a significant amount of quencher accommodation at this position, even though it is part of α-helix 1, to allow for

complex formation with the quencher. Similar discrepancies are observed for N159W. From Table 3-3, it can be seen that SASA for N159W is calculated to be 23% exposure, but the K_{sv} and the large V values along with the red shifted λ_{max} (Table 3-1) are indicative of a much more exposed residue. Together, these data show that the probability of finding an acrylamide molecule adjacent to the tryptophan at position 159 is very favorable. The greater-than-expected solvent exposure may be due to intrinsic protein breathability at this position or to the presence and orientation of the tryptophan molecule, which could lead to quencher accommodation unpredicted by MOLMOL calculations.

Mutant PrP^C	MOLMOL % exposure
G123W	68
W145	46
Y150W	4
N159W	22
Y163W	5
Y218W	10

Table 3-3. SASA data for all six positions in PrP^C calculated using the structure of PrP109-219 [PDB 1B10 [6] structure # 4 [7]] and MOLMOL software [4] by residue (see Methods, Chapter 2).

For PrP^{β} and PrP^F isoforms, it is seen that every position exhibits at least some amount of static quenching. While the K_{SV} values show decreased exposure upon conversion, the existence of static quenching means that acrylamide can at least partially penetrate the multimeric complexes and exist adjacent to the fluorophore. For G123W, there is little static component compared to the other positions, so this N-terminal residue is not as free to complex with acrylamide in the β-rich isoforms. For Y163W PrP^F and

Y150W PrP^{β} slightly larger values for V are observed, indicating that acrylamide might readily bind within the active volume of the fluorophore.

3-3. Time-Resolved Measurements

(A) Introduction to Time-Resolved Measurements

While steady-state data can provide useful information on the environment of a fluorophore, much more sensitive information can be gained by the use of time-resolved fluorescence measurements. Time-resolved measurements are taken by exciting a sample with a pulse of light shorter than the decay time (lifetime) of the sample. Lifetime is defined as the average time the molecules remain in the excited state following excitation [1] and is related to the rates of radiative decay (fluorescence) and non-radiative decay (nonfluorescence due to nearby quenching molecules: solvent, nearby polar residues, etc…[2]) given by Equation 3 – 4.

$$\tau = 1/(k_r + k_{nr}) \qquad \text{Equation 3-4}$$

The lifetime is calculated by fitting the emission spectra to

$$I(t) = I_0 e^{-t/\tau} \qquad \text{Equation 3-5}$$

for a single lifetime decay or

$$I(t) = \sum \alpha_i \exp(-t/\tau_i) \qquad \text{Equation 3-6}$$

for multiple lifetime decays. α is the amplitude and represents the fraction of the molecules in each conformation, i, at t=0 [1]. Whereas the α values represent the amplitudes of the corresponding lifetimes to the intensity of the time-resolved data, the fractional contribution of each lifetime to the steady-state intensity is represented by Equation 3-7.

$$f = \alpha_i \tau_i / \sum \alpha_i \tau_i \qquad \text{Equation 3-7}$$

Average lifetimes are often used in data interpretation and are represented by weighted (wtd) τ_0, which gives the weighted average of all the lifetime components by Equation 3-8.

$$<\tau> = \sum \alpha_i \tau_i^2 / \sum \alpha_i \tau_I \qquad \text{Equation 3-8}$$

It has been proposed that single tryptophan proteins exhibit complex decays due to the presence of individual rotamers (rotation of the tryptophan moiety) within the protein. If a single tryptophan can adopt slightly different rotamer configurations within the protein, then the indole ring will be exposed to slightly differing environments and interactions with nearby substituents or solvent, leading to different decay times for each rotamer [2, 8]. Movements or flexibility within the protein itself may also cause different microenvironments for the trytophan to encounter. In the fibrils and perhaps the β-oligomer, multiple decay times could be indicative of either multiple rotamers within a monomer or of heterogenous populations within multi-subunit complexes.

Fluorescence kinetics are complex and fitting is not always straight-forward. Because of the high complexity and variability of protein fluorescence, some suggest that the kinetics should not be described by discrete lifetime components, but should be represented by a distribution of lifetimes or a nonexponential decay [1, 8]. This requires fitting to additional models like Gaussian or Lorentzian distributions. Although these fittings were not conducted for these data, the various methods of data analysis and potential mathematical models to describe physical phenomena should be considered when interpreting the data.

Besides providing a more sensitive indicator of tryptophan environment, the emission lifetime (τ_0) is needed to calculate the k_q. The emission decay or lifetime is

proportional to the steady-state intensity. The steady-state intensity at a given wavelength is the integral of the intensity decay at that wavelength;

$$I_{SS} = \int I_0 e^{-t/\tau} dt = I_0 \tau \qquad \text{Equation 3 -9}$$

The steady-state spectrum is then the sum of all the photons emitted during the lifetime decay over all the wavelengths of emission. Figure 3-6 shows fluorescence emission decay as a function of time and wavelength to visibly demonstrate the connection between lifetime and steady-state emission.

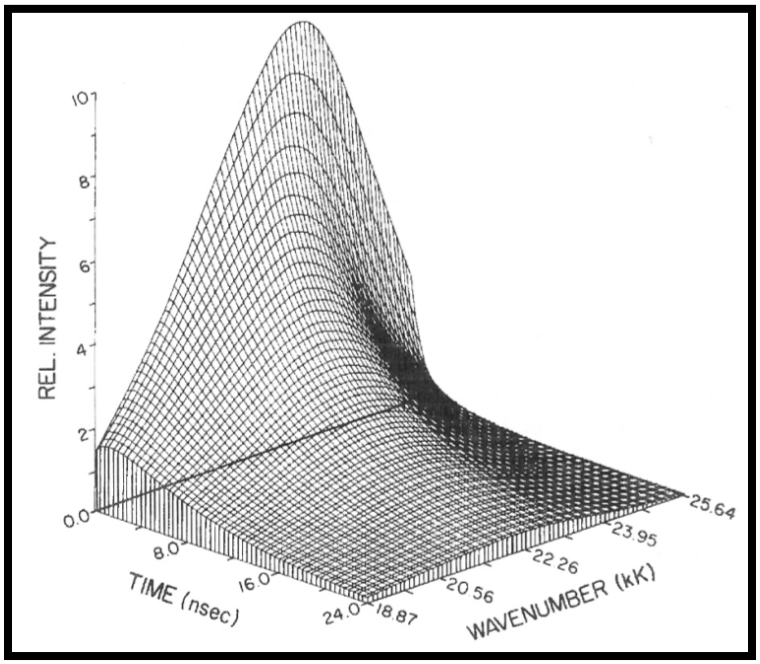

Figure 3-6. 3-D graph showing fluorescence intensity as a function of time and energy for 2,6-p-toluidinonapththalene adsorbed to egg L-α-lecithin vesicles. The steady-state spectrum is represented by the intensities at time=0 ns across all the wavelengths multiplied by τ (given by Equation 3-9). From Badea and Brand [9], used with permission.

(B) Lifetime Results

As described in the methods, the lifetime was measured for all the mutants in the three isoforms; Equation 3-6 was convoluted with the instrument response function (IRF) and the resulting function was fit to the data using χ^2 and least square analysis. Weighted residuals were also obtained to observe the quality of fit. Values giving the lowest χ^2 value and random weighted residuals were desired, but unless a significant improvement in χ^2 (reduction by half) was shown, the simplest fit was used. An example of fit and weighted residuals is shown for Y218W PrP^{β} in Figure 3-7.

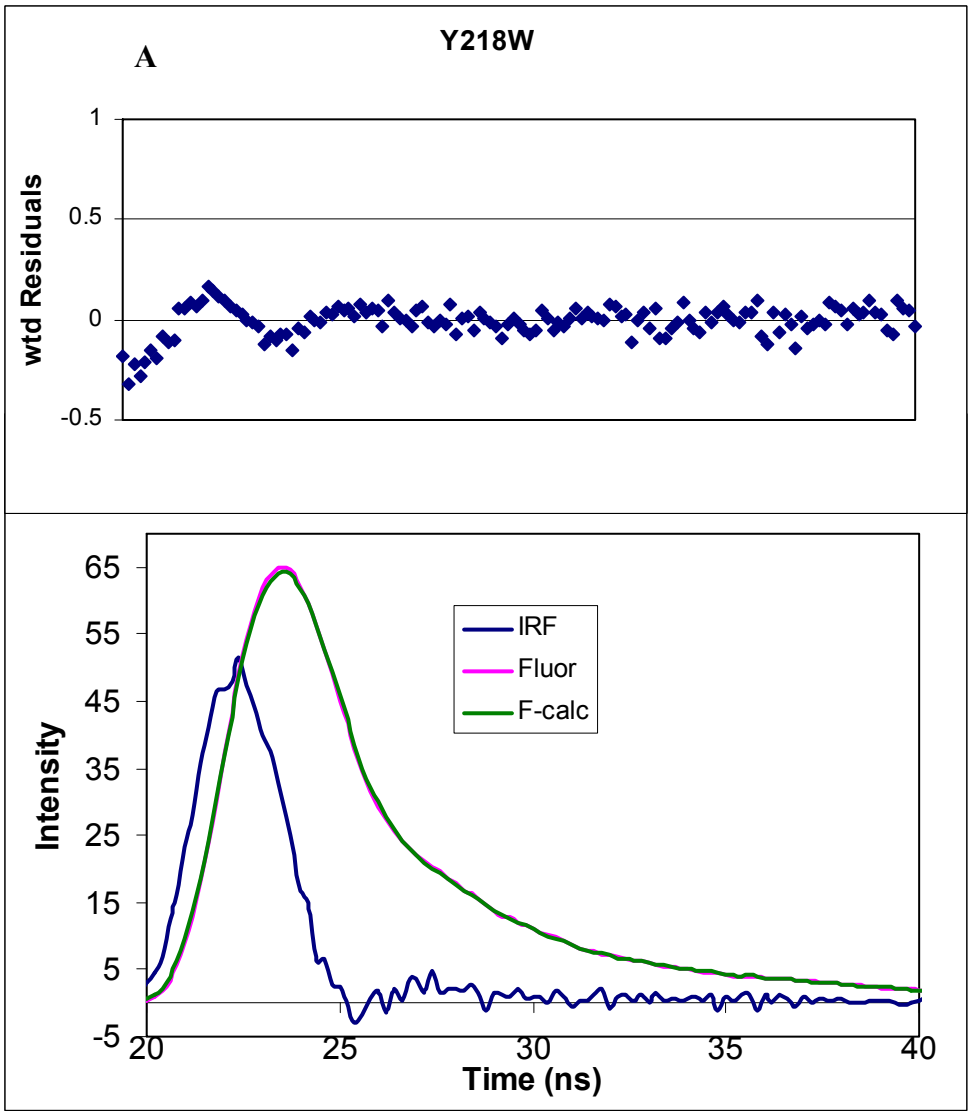

Figure 3-7. The fluorescence intensity decay fit to two lifetimes for Y218W PrP^{β}. (A) shows the weighted residuals for the calculated fit.

Table 3-4 summarizes the fluorescence decay parameters obtained for the mutants in the three isoforms. Most of the mutants in the various isoforms fit to multi-exponential decays with the short lifetime exhibiting the larger α values (normalized to unity). Whereas the short lifetime populations contribute more to the lifetime intensity as

indicated by the dominant amplitude value (Table 3-4), the contributions of each lifetime component/population to the steady-state fluorescence intensity are almost evenly weighted (50/50 or 60/40) for the long and the short lifetime components as seen by the f-values.

Mutant & Isoform	α_1	τ_1	α_2	τ_2	$\langle\tau\rangle$	f_1	f_2
G123W							
PrP^C	0.41 ± 0.04	5.5 ± 0.1	0.59 ± 0.04	2.4 ± 0.1	4.3 ± 0.1	0.64	0.36
PrP^β	0.26 ± 0.10	6.0 ± 0.4	0.74 ± 0.10	2.3 ± 0.1	4.2 ± 0.2	0.48	0.52
PrP^F	0.27 ± 0.03	4.6 ± 0.3	0.73 ± 0.03	1.3 ± 0.2	3.2 ± 0.3	0.56	0.44
W145							
PrP^C	0.20 ± 0.20	4.4 ± 0.1	0.8 ± 0.02	1.1 ± 0.1	2.7 ± 0.1	0.49	0.51
PrP^β	0.22 ± 0.20	5.1 ± 0.4	0.78 ± 0.02	1.4 ± 0.2	3.3 ± 0.3	0.48	0.52
PrP^F	0.22 ± 0.02	4.8 ± 0.1	0.78 ± 0.02	1.2 ± 0.1	3.2 ± 0.2	0.55	0.45
Y150W							
PrP^C	1	4.4	----------	---------	--------	-------	---------
PrP^β	0.2	6.5	0.8	2.6	4.1	0.4	0.6
PrP^F	0.31	5.5	0.69	1.7	3.9	0.58	0.42
N159W							
PrP^C	0.48 ± 0.23	6.6 ± 1.0	0.52 ± 0.02	2.7 ± 0.7	5.3 ± 0.2	0.65	0.35
PrP^β	0.26 ± 0.02	5.3 ± 0.5	0.74 ± 0.02	1.7 ± 0.5	3.5 ± 0.4	0.51	0.49
PrP^F	0.26 ± 0.02	5.5 ± 0.1	0.74 ± 0.02	1.7 ± 0.1	3.7 ± 0.1	0.53	0.47
Y163W							
PrP^C	0.13	3.9	0.87	1.1	2.1	0.34	0.66
PrP^β	0.29	5.0	0.71	1.4	3.6	0.6	0.4
PrP^F	0.29 ± 0.01	5.0 ± 0.1	0.71 ± 0.01	1.3 ± 0.1	3.6 ± 0.1	0.61	0.39
Y218W							
PrP^C	0.11 ± 0.03	3.8 ± 0.1	0.89 ± 0.03	0.98 ± 0.01	1.9 ± 0.2	0.32	0.68
PrP^β	0.21 ± 0.01	5.1 ± 0.1	0.79 ± 0.01	1.7 ± 0.1	3.2 ± 0.1	0.45	0.55
PrP^F	0.18 ± 0.03	4.4 ± 0.3	0.82 ± 0.03	1.2 ± 0.1	2.6 ± 0.2	0.44	0.56

Table 3-4. Fluorescence decay parameters for the mutants in the different isoforms. f= fractional contribution and α= amplitude of the corresponding lifetimes normalized to unity. $\langle\tau\rangle$= weighted lifetime. Standard deviations represent replicated data.

If considering the data according to the rotamer model of tryptophan lifetimes, one population of tryptophan may be near a quenching moiety such as a charged amino acid or solvent molecule giving it a shorter lifetime and another rotamer with a larger lifetime could indicate partial shielding or rotation away from the quenching moiety. It is seen that these populations generally contribute similarly to the steady-state intensity while the shorter lifetime population contributes more to the lifetime intensity as seen from the f and α values, respectively.

3-4. Time-Resolved Quenching Measurements

(A) Introduction to Time-Resolved Quenching Measurements

As described in the steady-state sections, combined static and dynamic quenching can contribute significantly to the derivation of a diffusion-controlled quenching rate constant (k_q). Knowing which mathematical model represents the physical behavior of the system is also not straightforward. Because time-resolved measurements take into account only the emitting lifetime and not the statically quenched complexes, it is possible to derive a purely dynamic rate constant from a Stern-Volmer plot of time-resolved quenching data. This bypasses the necessity of additional fitting procedures to separate mixtures of dynamic and static quenching components from steady-state quenching curves.

Just as τ_0 can be fit to a distribution of lifetimes (exhibit non-exponential decay), it has been shown that the addition of quencher can produce a transient effect in diffusional quenching for some systems, contributing significantly to the decay data. This transient effect complicates the decay order by making an initially exponential decay a nonexponential decay as quencher concentration is increased. In the presence of

quencher, a fluorophore population can give a non-exponential decay due to rapid quenching of closely spaced fluorophore and quencher molecules [1]. This deviates from the simple Stern-Volmer relationship, and while this transient term may or may not be involved in this particular system, the influence of acrylamide on the fluorescence properties of a protein is something to consider, as our data were only fit to discrete lifetimes and not a distribution.

(B) Time-Resolved Quenching Results

Time-resolved measurements were taken as acrylamide was added in 0.05 M increments to a final concentration of 0.5 M, as for steady-state quenching. α values were allowed to vary in the fitting procedures. Stern-Volmer plots for the long, short and weighted lifetimes were plotted along with the amplitudes normalized to unity; Figure 3-8(A-C) represents lifetime Stern-Volmer plots. Additional plots are shown in the appendix (Figure A-3).

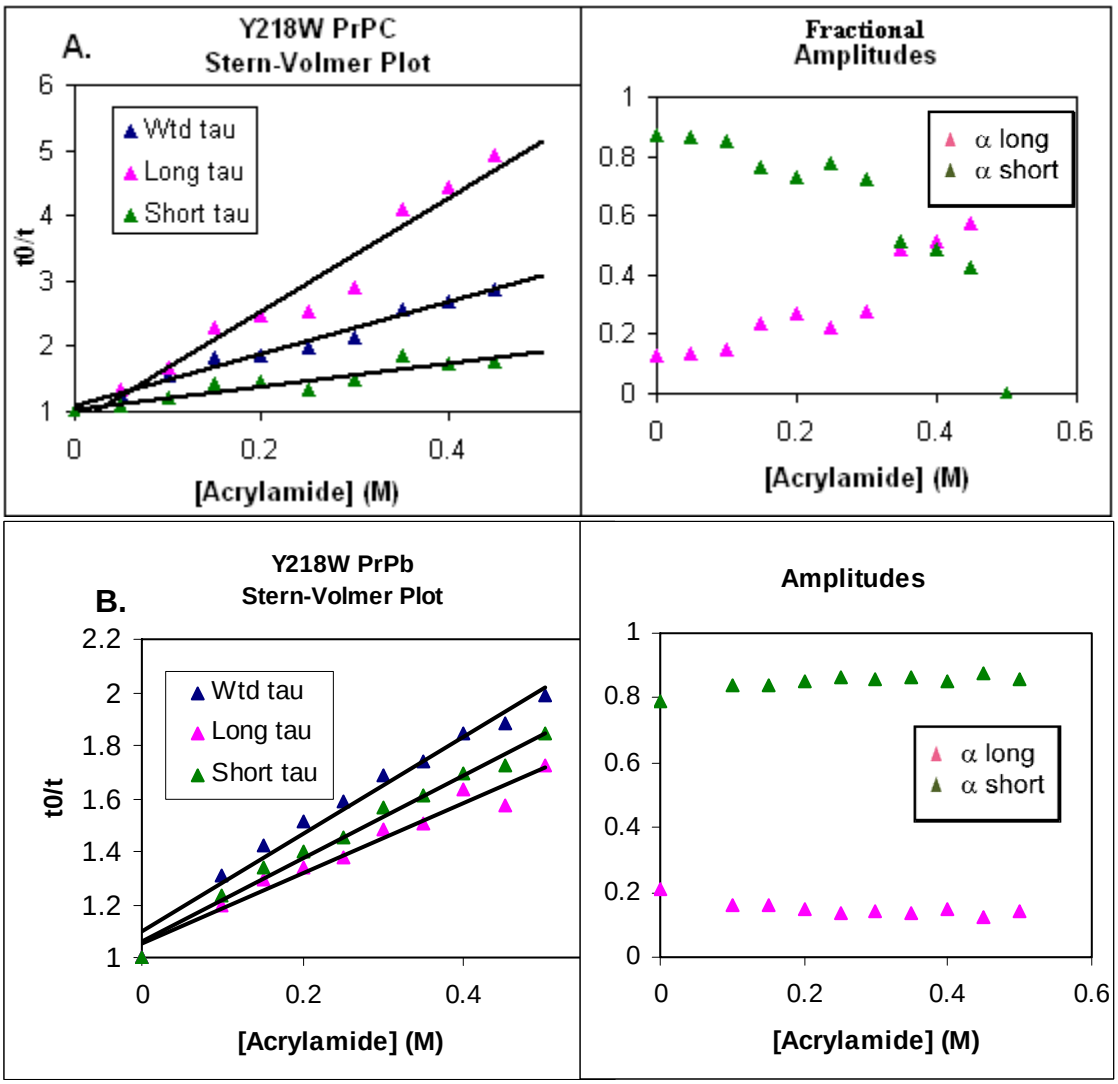
A.
Y218W PrPC
Stern-Volmer Plot
Wtd tau
Long tau
Short tau
t0/t
[Acrylamide] (M)
Fractional
Amplitudes
α long
α short
[Acrylamide] (M)
B.
Y218W PrPb
Stern-Volmer Plot
Wtd tau
Long tau
Short tau
t0/t
[Acrylamide] (M)
Amplitudes
α long
α short
[Acrylamide] (M)

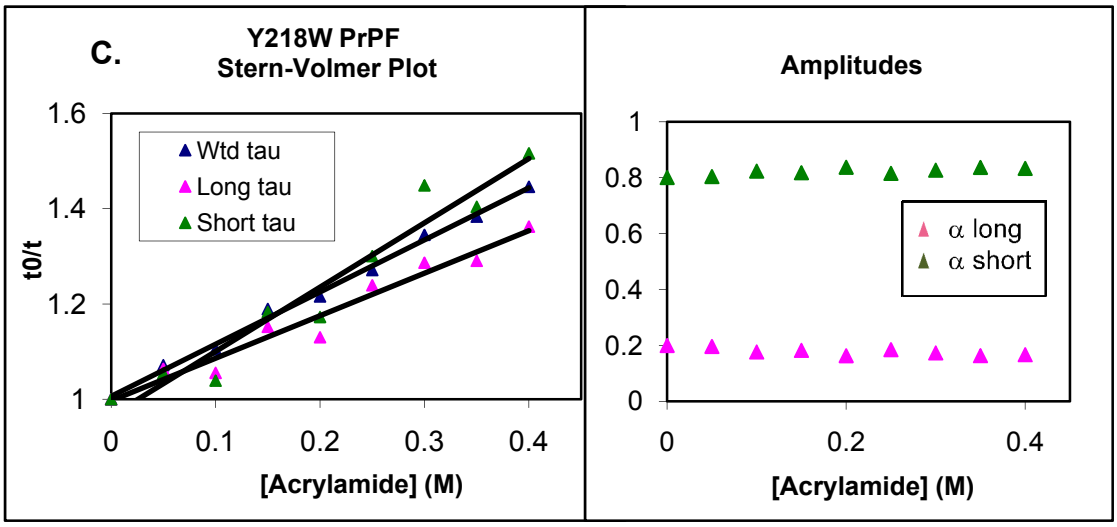

Figure 3-8 (A-C). Time-resolved quenching Stern-Volmer plots and α values for Y218W PrP^{C}, PrP^{β}, and $PrP^{F.}$

In PrP^{C}, it was observed that for the mutants Y163W and W145 the lifetime Stern-Volmer plots have an unreasonable non-linear appearance for both the short and the long lifetime components as quencher is increased (see Appendix). In the others, the long component is preferentially quenched, as judged by the significantly steeper K_{SV} values and the disappearance of the long lifetime component. Moreover, the ratio of amplitudes for each component varies as a function of acrylamide concentration. This indicates that independent dynamic quenching of each component is not occurring as should be expected. This behavior has been suggested as being due to selective, static quenching of the long lifetime component [10]. For the PrP^{β} and PrP^{F} samples the amplitudes remained constant and the long and short components display independent quenching behavior.

Because the ratio of the amplitudes varied for PrP^{C} as quencher was increased, data were plotted up to acrylamide concentrations where little amplitude deviation had

started to occur and K_{SV} values were determined from these concentrations only. Table 3-5 shows Stern-Volmer constants and R^2 values for weighted τ_0 Stern-Volmer plots along with the highest concentration of acrylamide used for each plot before the α ratio values significantly varied.

Mutant/Isoform	K_{sv}	Highest [Acrylamide] (M)	R^2
G123W PrP^C	9.6	0.2	0.999
PrP^β	1.7	0.3	0.971
PrP^F	0.9	0.3	0.958
W145 PrP^C	9.7	0.15	0.981
PrP^β	1.3	0.3	0.987
PrP^F	1.2	0.3	0.931
Y150W PrP^C	3.1	0.3	0.998
PrP^β	1.7	0.3	0.989
PrP^F	1.0	0.3	0.993
N159W PrP^C	9.8	0.15	0.999
PrP^β	1.5	0.2	0.987
PrP^F	1.1	0.3	0.991
Y163W PrP^C	2.4	0.3	0.972
PrP^β	1.7	0.3	0.992
PrP^F	1.2	0.25	0.994
Y218W PrP^C	3.4	0.3	.969
PrP^β	2.3	0.3	0.986
PrP^F	1.2	0.3	0.985

Table 3-5. Stern-Volmer constants along with R^2 values for the weighted τ_0 plots to the acrylamide concentration indicated for each mutant and isoform.

For N159W and W145 in the PrP^C isoform, the long lifetime component was entirely quenched by 0.2 M quencher concentration and only one lifetime was then

observed. For some of the other samples, deviation of the α ratios occurred at higher quencher concentrations, so the Stern-Volmer constants could be determined usinghigher quencher concentrations. For PrP^F and PrP^β where the α ratios did not significantly deviate even out to 0.5 M acrylamide, K_{SV} values were only taken to 0.3 M acrylamide for consistency.

3-5. Solvent Accessibility (k_q) Determination

(A) Introduction

The final step in determining the solvent accessibility of the tryptophan residue is to use the K_{SV} values from the time-resolved and steady-state Stern-Volmer plots and calculate the k_q's. As mentioned earlier, the bimolecular quenching rate constant defines the dynamic rate of quenching over the lifetime of the fluorophore. Whereas time-resolved quenching measurements report only the dynamic quenching component, steady-state quenching can become complicated with the mechanism of static quenching and may require mathematical modeling to acquire the dynamic component.

(B) Results/Discussion

The k_q values for lifetime quenching (including the individual lifetime components) as well as steady-state quenching are summarized in Table 3-6.

Mutant & Isoform	k_q values ($X 10^9 M^{-1}s^{-1}$) <τ> Wtd	τ_1 Long	τ_2 Short	Steady-State
G123W PrP^C	2.23 ± 0.23	2.06±0.68	3.06 ±1.72	2.58 ± 0.11
PrP^β	0.37 ± 0.03	0.15 ± 0.01	0.89 ± 0.01	1.1 ± 0.10
PrP^F	0.29 ± 0.04	0.13 ± 0.01	0.43 ± 0.6	1.07 ± 0.16
W145 PrP^C	3.52 ± 0.75	1.68 ± 1.26	1.77 ± 0.62	3.17 ± 0.17
PrP^β	0.42 ± 0.06	0.15 ± 0.01	0.61 ± 0.10	1.10 ± 0.22
PrP^F	0.39 ± 0.04	0.17 ± 0.02	0.66 ± 0.07	0.95 ± 0.10
Y150W PrP^C	0.7	---------	----------	0.90 ± 0.10
PrP^β	0.42	0.17	0.58	0.60 ± 0.03
PrP^F	0.25	0.13	0.63	0.95 ± 0.13
N159W PrP^C	1.85 ± 0.09	1.88 ± 0.55	2.6 ± 2.3	2.06 ± 0.07
PrP^β	0.41 ± 0.11	0.21 ± 0.09	0.68 ± 0.26	0.86 ± 0.08
PrP^F	0.29	0.15	0.75	0.83 ± 0.04
Y163W PrP^C	1.15	0.25	0.97	1.12 ± 0.05
PrP^β	0.48	0.2	0.63	1.12 ± 0.01
PrP^F	0.35 ± 0.09	0.18 ±0.04	0.71 ±0.34	1.28 ± 0.01
Y218W PrP^C	1.83 ± 0.04	1.56 ± 0.14	1.32 ± 0.37	1.68 ± 0.15
PrP^β	0.71 ± 0.03	0.29 ± 0.01	0.95 ± 0.11	1.42 ± 0.19
PrP^F	0.47 ±0.08	0.23 ± 0.04	1.34 ± 0.23	1.37

Table 3-6. Rate constants for each lifetime component (weighted, long and short) along with steady-state k_q values. Steady-state k_q values were calculated using the modified Stern-Volmer plot while taking the lifetime determined for the sample used for steady-state measurements. Standard deviations represent replicated data. Stern-Volmer constants (steady-state and time-resolved) were determined from the slopes plotted out to the same quencher concentration for each mutant and isoform. See Table 3-5 for appropriate acrylamide concentrations used in K_{SV} determination for each mutant and isoform.

It can be seen from Table 3-6 that for all mutants, the PrP^{β} and PrP^{F} isoforms have weighted k_q values that fall in between the k_q values for the long and short lifetime components, while most all of the mutants in the PrP^{C} isoform do not follow that pattern. This is explained mathematically by the changing α ratios in PrP^{C} when fitting the data to a multiexponential decay at increasing quencher concentrations. Although the individual components do not behave in a manner consistent with independent dynamic quenching as observed from the changing amplitude ratios, the weighted lifetime Stern-Volmer plot does follow expected, linear behavior and the k_q's obtained from the weighted lifetime $<\tau_0>$ are similar to the k_q's derived from the modified steady-state Stern-Volmer plot.

In contrast to PrP^{C}, the misfolded isoforms are similar and maintain relatively constant α ratios. This indicates that each lifetime behaves as an independent component expressing individual Stern-Volmer constants. While weighted lifetime k_q's do fall between the k_q's for the short and long lifetime components, they are not similar nor do they directly correlate with the k_q's derived from steady-state quenching, unlike the PrP^{C} isoform. This suggests that the modified Stern-Volmer equation used to correct for the static quenching does not sufficiently explain the physical behavior of the tryptophan steady-state quenching for these two isoforms. Because these two forms are made of multiple subunits, the tryptophan could be in heterogeneous (different monomers having different environments) and/or pocketed environments and other models may be necessary to explain the differences observed between steady-state and lifetime quenching k_q's [1, 5]. More complex mathematical models of quenching exist [5] and further fitting could potentially separate the components of static from dynamic quenching or perhaps supply a better physical interpretation of the steady-state data.

Normally they accomplish the goal of quantifying the accessibility of a tryptophan by determining the k_q value representing diffusion-controlled quenching mechanisms, but they could be difficult to assess in the absence of a known structure. With the use of the time-resolved measurements, the requirement for more complex mathematical fitting for steady-state data becomes unnecessary.

Using the k_q determined from the weighted τ_0 as representative of the overall tryptophan accessibility, it can be seen that the tryptophan becomes less accessible in the PrP^{β} and PrP^{F} isoforms for all the mutants and that the G123W, W145 and N159W mutants show the greatest change in k_q values between PrP^{C} and the misfolded isoforms.

As seen in the steady-state section, k_q values show a strong correlation to λ_{max} values. Just as the λ_{max} values become more homogenous in PrP^{β} and PrP^{F} isoforms, the weighted-τ_0 k_q values exhibit a similar, smaller range of values compared to the variation observed in PrP^{C}.

It has also been seen throughout all the sections that PrP^{β} and PrP^{F} exhibit similar fluorescence characteristics from steady-state spectra to lifetimes, K_{SV} values and k_q's. This lends support for using PrP^{β} as a model for the PrP^{F} isoform.

References

1. Lakowicz JR: **Principles of Fluorescence Spectroscopy Third Edition**: Springer; 2006.
2. Dahms TE, Szabo AG: **Conformational heterogeneity in crystalline proteins: time-resolved fluorescence studies**. *Methods Enzymol* 1997, **278**:202-221.
3. Eftink MR, Ghiron CA: **Exposure of tryptophanyl residues in proteins. Quantitative determination by fluorescence quenching studies**. *Biochemistry* 1976, **15**(3):672-680.
4. Koradi R, Billeter M, Wuthrich K: **MOLMOL: a program for display and analysis of macromolecular structures**. *J Mol Graph* 1996, **14**(1):51-55, 29-32.
5. Matyus L, Szollosi J, Jenei A: **Steady-state fluorescence quenching applications for studying protein structure and dynamics**. *J Photochem Photobiol B* 2006, **83**(3):223-236.

6. James TL, Liu H, Ulyanov NB, Farr-Jones S, Zhang H, Donne DG, Kaneko K, Groth D, Mehlhorn I, Prusiner SB *et al*: **Solution structure of a 142-residue recombinant prion protein corresponding to the infectious fragment of the scrapie isoform**. *Proc Natl Acad Sci U S A* 1997, **94**(19):10086-10091.
7. Alonso DO, DeArmond SJ, Cohen FE, Daggett V: **Mapping the early steps in the pH-induced conformational conversion of the prion protein**. *Proc Natl Acad Sci U S A* 2001, **98**(6):2985-2989.
8. Ross JB, Wyssbrod HR, Porter RA, Schwartz GP, Michaels CA, Laws WR: **Correlation of tryptophan fluorescence intensity decay parameters with 1H NMR-determined rotamer conformations: [tryptophan2]oxytocin**. *Biochemistry* 1992, **31**(6):1585-1594.
9. Badea MG, Brand L: **Time-resolved fluorescence measurements**. *Methods Enzymol* 1979, **61**:378-425.
10. Eftink MR, Ghiron CA: **Fluorescence quenching studies with proteins**. *Anal Biochem* 1981, **114**(2):199-227.

CHAPTER 4: DISCUSSION/CONCLUSIONS

The goal of my research was to observe changes in accessibility of tryptophan residues at specific positions that occur upon misfolding of the prion protein. By determining tryptophan accessibility changes among isoforms, positions exhibiting significant conformational changes can be identified, theoretical models of PrP^{Sc} can be assessed, and gathered data can be compared with structural data obtained from other reported techniques. Accessibility was determined by tryptophan fluorescence quenching measurements whereby the rate of dynamic quenching (k_q) and thus the solvent accessibility of the tryptophan could be measured and quantified. This chapter starts with a discussion of the data obtained from the results section and explains why particular k_q values are used to represent accessibility in each isoform. The k_q values are then used in conjunction with MOLMOL data to correlate k_q's with solvent accessible surface area in PrP^{C} and provide an estimate of tryptophan accessibilities in the misfolded isoforms. The accessibility data are then examined in context of structural information and are related to the computational models of PrP^{Sc} along with data from other techniques as discussed in the introduction. This chapter concludes with future directions.

4-1. k_q Determination from Dynamic Quenching

As seen in the results chapter, the k_q derived from steady-state measurements can be strongly influenced by static quenching mechanisms. Most mutants in the various isoforms exhibited at least some upward curvature in the steady-state Stern-Volmer plots, indicating static quenching was occurring, particularly at high quencher concentrations. While a modified Stern-Volmer equation may attempt to mathematically separate static and dynamic quenching components, the use of time-resolved quenching measurements

circumvents this need, as statically quenched complexes do not emit. In addition, using the modified Stern-Volmer equation appropriately accounts for the static quenching components in the PrP^C isoforms as the weighted time-resolved k_q values are comparable to k_q values acquired with the steady-state modified Stern-Volmer equation as seen in Table 3-6. For PrP^β and PrP^F, however, the k_q's derived from weighted time-resolved measurements are much lower than the k_q values acquired from the steady-state modified Stern-Volmer equation. This may indicate that the simple modified Stern-Volmer equation does not sufficiently separate the static and dynamic quenching components. Because the misfolded isoforms are multimeric complexes, there will be multiple tryptophan residues and environments per complex and each may exhibit both unique dynamic and static quenching components. Different environments in the misfolded monomers, especially significant at the ends versus the center of the fibril, can lead to unique static (V) and dynamic (K_{SV}) values for each tryptophan complicating the estimation of the overall static component in a simple modified Stern-Volmer fit of steady-state data. Although it may be possible to further use complex fitting methods and find an appropriate mathematical model to separate these components, the use of time-resolved quenching bypasses all static components and allows for the derivation of purely dynamic quenching rate constants.

Lifetime measurements can exhibit multi-exponential decay rates suggesting the presence of either different tryptophan rotational conformations (rotamers) of the same Trp or different populations. In the case of the misfolded, multimeric isoforms, it is logical to assume there may be more than one population of tryptophan in the multimeric molecule. While the analysis of lifetime measurements still prove very difficult in

distinguishing the individual accessibilities of each tryptophan population in the protein (due to numerous possibilities of local environment effects and self quenching), weighted lifetimes, however, provide an average accessibility of the tryptophans in the molecule, giving an overall depiction of the average accessibility of the tryptophan. Using k_q's that represent the dynamic rate constant of the overall population of the tryptophan (derived from the weighted lifetime Stern-Volmer plots), it is possible to compare accessibilities and overall changes of each tryptophan mutant upon conversion to a different isoform. For the following sections of data discussion, k_q values for PrP^C will be taken from the steady-state modified Stern-Volmer plots to compare with other steady-state data from literature. Since the steady-state and lifetime k_q values for PrP^C are within experimental error, the k_q values for PrP^β and PrP^F will be taken from the weighted lifetime Stern-Volmer plots since the steady-state measurements cannot be modified to acquire a true dynamic component.

4-2. Correlating k_q's with Tryptophan Solvent Accessible Surface Area (SASA)

As k_q is a measurement of the solvent accessibility of the fluorescing molecule, it should be possible to correlate k_q with the exposure of the tryptophan in a known structure. One program used by our lab to determine solvent accessible surface area (SASA) is MOLMOL [1]. Although this program was used to calculate the percent exposure of the entire residue (including backbone) and not just the side chain, it can give information on the tryptophan accessibility to solvent. In a paper published by Eftink and Ghiron, steady-state quenching measurements were conducted with proteins containing single tryptophan residues and the k_q values were reported [2]. At the time of the study, structures for all the proteins were not available. However, structures of many of these

proteins are now deposited in the protein data bank. I therefore determined the SASA of the tryptophan residues in the proteins using MOLMOL. For these proteins, the experimentally determined k_q values were plotted vs. the percent exposure of the tryptophans, and a linear correlation was observed (Figure 4-1). This correlation could be compared to the data obtained from the k_q's and SASA of tryptophan in PrP^C, as the NMR structure of PrP^C has been determined. Using the NMR structure of PrP^C, a particular residue was mutated to tryptophan using Sybyl (see Methods), and each individual mutated structure was energy minimized. These structural representations of PrP^C containing single tryptophan residues were used for SASA determination. The correlation of tryptophan SASA and k_q values can be further used to theoretically estimate the percent accessibility of the tryptophan in the misfolded isoforms of PrP^{β} and PrP^F.

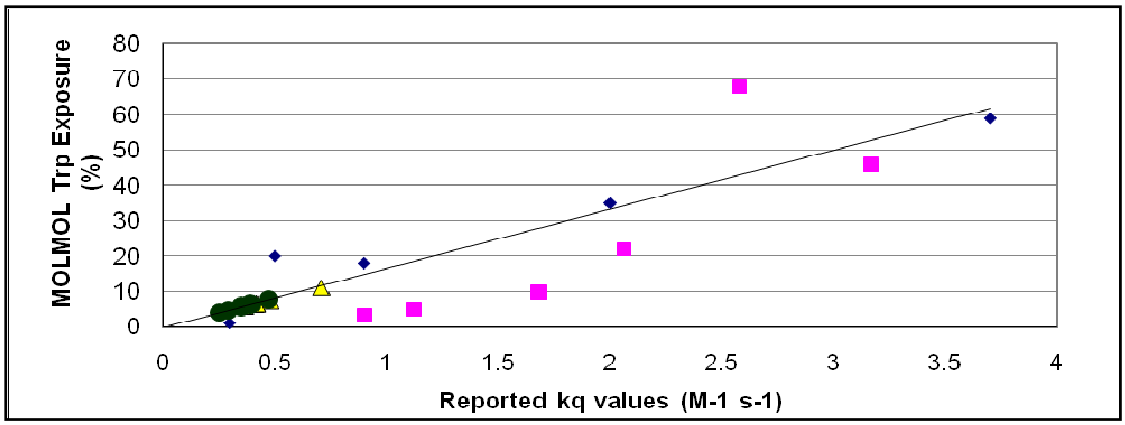

Figure 4-1. Graph fitting correlation of SASA and k_q values for single-tryptophan containing proteins with previously measured k_q values (blue diamonds) comparing fit with PrP^C mutants (pink squares) along with the theoretical values of SASA of PrP^{β} (yellow triangles) and PrP^F (green circles). Eftink proteins represented are glucagon (59% exposed, PDB file 1GCN), monellin (35%, PDB file 1IV9), Human Serum Albumin (HSA) (20%, PDB file 2BXG), S. Nuclease (18%, PDB file 1EY0), and Rnase T1 (1%, PDB file 1IYY)

Mutant	PrP^C k_q ($x10^9 M^{-1}s^{-1}$)	MOLMOL % exposure	PrP^β k_q ($x10^9 M^{-1}s^{-1}$)	Theoretical % exposure	PrP^F k_q ($x10^9 M^{-1}s^{-1}$)	Theoretical % exposure
G123W	2.58 ± 0.11	68	0.37	6	0.29	5
W145	3.17 ± 0.17	46	0.42	7	0.39	7
Y150W	0.90 ± 0.10	4	0.42	7	0.25	4
N159W	2.06 ± 0.07	22	0.41	7	0.29	5
Y163W	1.12 ± 0.05	5	0.48	8	0.35	6
Y218W	1.68 ± 0.15	10	0.71	12	0.47	8

Table 4-1. Measured k_q values of tryptophan in the various mutants and isoforms. The percent exposures of the tryptophan in PrP^C was determined by MOLMOL calculations from the NMR structure of ShaPrP109-228 [PDB 1B10 [3] structure # 4 [4]] whereas the percent exposures of PrP^β and PrP^F were calculated using slope of Figure 4-1.

	PrP^C		PrP^β		PrP^F	
Mutants	λ_{max} (nm)	**Intensity**	λ_{max} (nm)	**Intensity**	λ_{max} (nm)	**Intensity**
G123W	353	0.28	347	0.27	339	0.4
W145	351	0.10	347	0.17	344	0.21
Y150W	336	0.62	344	0.21	343	0.29
N159W	352	0.38	344	0.23	343	0.18
Y163W	336	0.06	345	0.17	343	0.22
Y218W	334	0.04	348	0.12	343	0.18

Table 4-2. (same as Table 3-1) Representative λ_{max} and intensity values from the steady-state spectra of the six mutants in the three isoforms. All intensities are normalized to 20 μM concentration.

(A) PrP^C

The percent solvent accessible surface area (SASA) of tryptophan residues in single-Trp proteins were graphed as a function of their k_q values (Figure 4-1) determined by Eftink [2]. While small indole derivatives and free Trp in solution approach the diffusion limit and have k_q values between 7-10 x 10^9 $M^{-1}s^{-1}$, the maximum values

expected for exposed residues in a randomly coiled or unstructured dynamic peptide attached to a backbone will be smaller and are represented by glucagon (Figure 4-1) and ACTH (not shown) as measured by Eftink, having k_q values of 3.7 and 4.2 x 10^9 $M^{-1}s^{-1}$, respectively. Since glucagon is an intrinsically dynamic peptide, NMR and X-ray structures have been elucidated only when the molecule is interacting with a lipid or receptor. So, the calculated SASA is based on a structure of glucagon that may not maximally represent the exposure of this residue in a completely unstructured peptide. However, even when exhibiting secondary structure in the form of an α-helix, glucagon's Trp is highly exposed (~60%) and shows good correlation with the rest of the data in Figure 4-1. Table 4-1 shows the k_q values for positions in PrP^C calculated using steady-state data and modified Stern-Volmer plots. It is noteworthy to add that the steady-state and weighted lifetime k_q values of PrP^C did not give significantly different results, and the steady-state values were used to compare to the k_q values of other proteins given in literature by steady-state data. The tryptophan positions in PrP^C exhibit a wide range of SASA, from highly exposed in W145 to significantly buried in Y150W. It is also seen from the results (Table 4-2 replicating Table 3-1) that the measured λ_{max} values of the steady-state spectra of PrP^C mutants correlate well with the range and extent of solvent accessibility. The residues in PrP^C exhibiting the greatest accessibility as seen from SASA and k_q values are W145 and G123W; these have the most red-shifted spectra.

The slight correlative deviation of PrP^C mutants from Eftink proteins could also be explained by different experimental conditions. It can be seen in Figure 4-1 that PrP^C k_q's, taken apart from the other single-Trp proteins, demonstrate a close correlation with predicted SASA. The k_q values for other single-Trp proteins studied by Eftink were all

measured by the same laboratory, just as PrP^C mutant k_q values were all measured under similar experimental conditions. While showing some deviation from the correlation of other single-Trp proteins, the correlations among PrP^C mutants would make sense if experimental conditions were a factor.

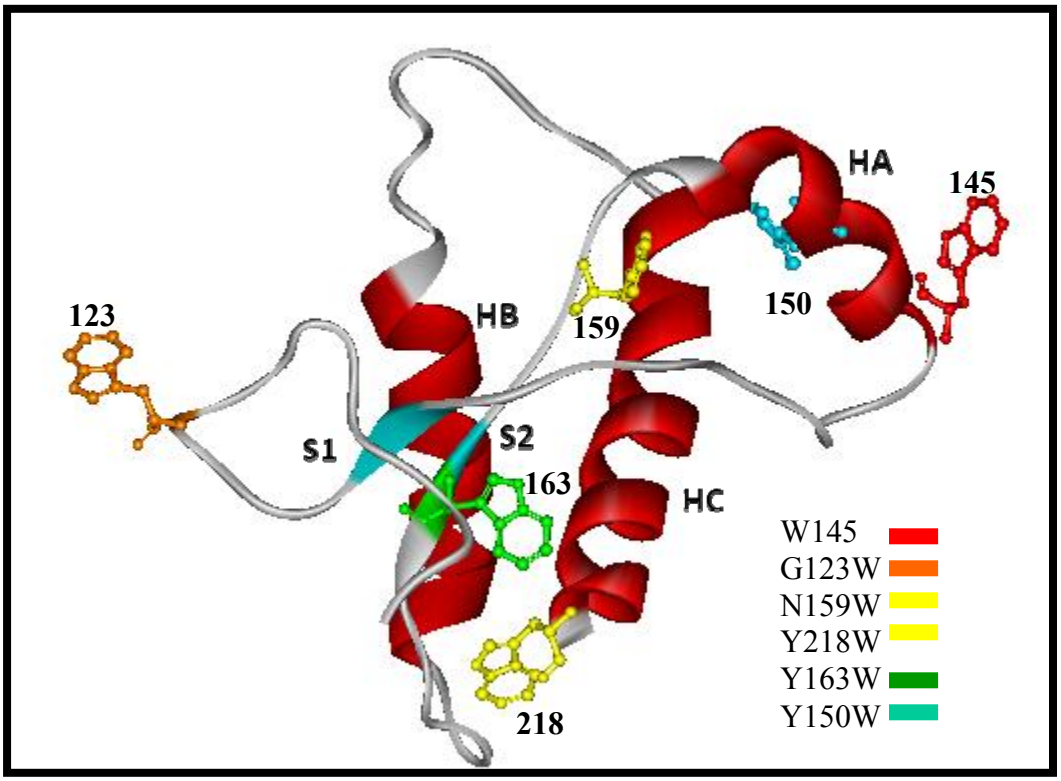

Figure 4-2. Showing PrP109-219. For visualization purposes, all six tryptophan mutations were inserted together and the resulting structure was energy minimized. This differs from the method used to calculate individual tryptophan SASA values listed in Table 4-1. Accessibility based on k_q values is represented by color from red (most accessible) to blue (least accessible); **red>orange>yellow>green>blue.**

While the solvent accessibility calculations for G123W and W145 indicate fully exposed residues (compare to glucagon), G123W has a much lower k_q value than expected for a fully exposed residue. At first glance (Figure 4-2) it appears peculiar that G123W reports less accessibility in k_q values than W145, as it is located in such a floppy

segment of protein and appears to have more solvent accessibility according to MOLMOL calculations. One explanation for this behavior is that G123W is located in the hydrophobic segment of prion known to exhibit transient structure in wild type PrP^C [5]. It is postulated that this hydrophobic segment is slightly stabilized by interaction with Helix B or the first β-strand (S1) as has been suggested from NMR data [5]. The formation of this transient interaction would only be furthered favored and stabilized by the presence of a hydrophobic tryptophan residue. This propensity could account for the lower-than-expected k_q value for G123W.

In contrast to G123W, all the rest of the positions (except W145) exhibit higher k_q values than the SASA data would indicate (Figure 4-1; note that this structure is truncated missing the last 12 residues of Helix C). This discrepancy may be due to some flexibility of PrP^C in solution. The protein in the monomeric form is flexible, especially in the unstructured N-terminus (residues 90-119). In fact it is seen that all tryptophan positions with the exception of Y150W display multiple decay components (Table 3-3), which is indicative of single tryptophan residues sampling multiple environments, different local quenching effects, and thus multiple lifetime decays. From our data, it can be argued that there exists some flexibility at the positions tested allowing for rotational conformations. Also, the existence of a static quenching component for every position except Y218W and Y163W (Table 3-2) would indicate that the structure is accommodating enough even in buried areas of well-defined secondary structure (Y150 in Helix A) to allow for complex formation between the tryptophan and the quencher. N159W shows a very large static quenching component in contrast to its relatively low SASA. This may indicate a favorable accommodation of the quencher, either through intrinsic flexibility of the

protein, or due to the presence and orientation of the Trp residue having greater exposure than predicted by MOLMOL.

In the case of Y218W, the residue appears to be much more exposed than predicted from its structure. This phenomenon was also observed in tyrosine nitration studies where Y218 was more reactive to nitration than predicted based on the MOLMOL solvent accessibility calculations [6]. A potential explanation in the tyrosine nitration study was that conformational changes induced by nitration of other nearby residues (Tyr 225 and Tyr 226) allowed for increased accessibility of Tyr 218. In addition, there are other factors that influence tyrosine nitration besides solvent accessibility (see YYR epitope section starting on page 18). The introduction of a tryptophan residue could have potentially caused a local change in structure that was not well accounted for in the energy-minimized Y218W model used for SASA determination, causing it to be more accessible than predicted by MOLMOL. However, taken together, the tyrosine nitration and tryptophan fluorescence data could indicate the presence of a solvent accessible pocket or flexibility within the globular domain, which remains unobserved in the NMR data.

(B) PrP^{β}

Eftink reported k_q values of single-Trp proteins based on steady-state fluorescence quenching and the calculated SASA was used to create Figure 4-1. It was shown that k_q's measured for PrP^C using steady-state fluorescence quenching coupled with SASA correlate well with the plot. Table 3-6 shows that steady-state and time-resolved k_q values for PrP^C provide very comparable data. Therefore, time-resolved k_q data for PrP^{β} and PrP^F can be used to predict the theoretical solvent accessibility of the overall tryptophan

molecules. This k_q data would indicate that all six residues become more buried upon conversion to PrP^{β} and have solvent accessibilities in a narrow range of ~6-11%.

For PrP^{β}, we used the weighted lifetime Stern-Volmer plot to determine k_q, and the SASA/k_q correlation plot (Figure 4-1) to determine the overall accessibility of the tryptophan residues in PrP^{β}. Overall, it is seen that there is a decrease in solvent accessibility at every tryptophan position after conversion to the misfolded isoform. While it may not be possible with a very large aggregated molecule to determine whether these decreases in solvent accessibility are due to conformational change within monomers or inter-subunit packing events, PrP^{β} is only an octamer [6, 7]. Therefore, if a conformational change occurs that increases the accessibility of a Trp molecule, it should be possible to detect using quenching techniques. It was seen through intrinsic fluorescence in alpha-synuclein peptide that while the exposed Trp residue became buried upon conversion to the fibril, it stayed exposed in the oligomeric intermediate forms [8]. This provides evidence that tryptophan fluorescence quenching can be used to evaluate exposure in multimeric complexes, especially in oligomers. Therefore, our data suggest that all six positions in PrP are more buried in PrP^{β} than in PrP^{C}. However, the largest changes in SASA are noted for W145 and G123W.

Also seen from the Table 4-1 and Figure 4-1, the k_q values for all the mutants in the PrP^{β} isoform cluster and are around 0.4-0.5 x 10^9 $M^{-1}s^{-1}$. These similar values are supported by consistent λ_{max} values from steady-state spectra within PrP^{β} indicating similar solvent exposures (Table 4-2).

(C) PrP^F

Much like the PrP^β isoform, PrP fibrils exhibit a clustering of k_q values in the range 0.3-0.4 x 10^9 $M^{-1}s^{-1}$, and this observation is also supported by the narrow range of blue shifted λ_{max} values in the steady-state spectra (Table 4-2). Again, while the discrimination between conformational change or packing effects may not be straight-forward, it can be seen that the k_q values of PrP^β are always slightly greater than the k_q values of PrP^F, and this could be plausibly attributed to the greater packing (less solvent exposure) in fibrils than in the octameric β-oligomer.

The range in theoretical solvent accessibilities, as predicted using k_q values, is similar to that of PrP^β and spans from ~4-8% with Y218W being the most accessible. For a relative comparison concerning the accessibility of the residues in the misfolded conformations, the accessibility of Y150W can be examined. The exposure of position Y150W in PrP^C is very similar to the accessibility of positions in PrP^β and PrP^F as it exhibits a k_q value of 0.7 x 10^9 $M^{-1}s^{-1}$ (weighted τ), 0.9 x 10^9 $M^{-1}s^{-1}$ (steady-state) and a solvent exposure of 4%. This can be compared to the k_q values in the misfolded isoforms ranging from ~0.3-0.7 x 10^9 $M^{-1}s^{-1}$. Thus, position 150 does not appear to undergo any large change in solvent exposure upon conversion to a β-enriched isoform.

Although there is an observable trend toward hydrophobic and buried environments in PrP^β and PrP^F, when positions are considered individually as a function of conformation, a clearer picture emerges. G123W and W145 both exhibit a very large change from highly exposed to significantly buried in both misfolded conformations (Table 3-6). Also, the static quenching component (V) decreases in G123W upon conversion (Table 3-2). These observed changes imply that the N-terminus (at least

residues 90-145) takes on alternative structure and that the residues become highly buried and may be part of the hydrophobic core. This is also seen in N159W, although to a lesser extent. N159W in PrP^{C} is on the cusp of the second β-strand (161-163) and while it is seen to be fairly exposed based on k_q calculations (Table 3-6), it may form at least some transient extended β-structure [5]. Upon conversion to PrP^{Sc}, N159W is seen to significantly decrease its solvent accessibility, potentially becoming part of the hydrophobic β-sheet core. The residues at positions 150, 163 and 218 are all included in well defined α-helical (150, 218) or β-strand (163) secondary structure. Upon conversion, their solvent accessibilities decrease, but the changes in exposure are small compared with the other three mutants. While structural changes could be occurring at these positions, it is not possible from this data to distinguish between structural changes in the monomer and inter-subunit packing causing the decrease in accessibility.

Our laboratory as well as others have used PrP^{β} as a representative isoform of PrP^{Sc} due to its solubility for spectroscopic analysis. Because of this, it is noteworthy to add that data from both PrP^{F} and PrP^{β} were very comparable and exhibited commonalities throughout the results. Similar patterns and ranges in steady-state spectra, lifetimes, quenching profiles and k_q values all provide significant support for the suitability of the β-oligomer for depicting the structures of the fibrillar samples.

4-3. Computational Models of PrP^{Sc}

A hypothesis of my thesis was that both the β-helix and β-spiral model are mutually exclusive and by probing conformational differences among the isoforms using Trp fluorescence and quenching, these models could be distinguished, supported or challenged. This section examines the two computational models of PrP^{Sc}, the predictions

of accessibility of residues based on these structures, along with the quenching data and its implications.

(A) β–Helix Model

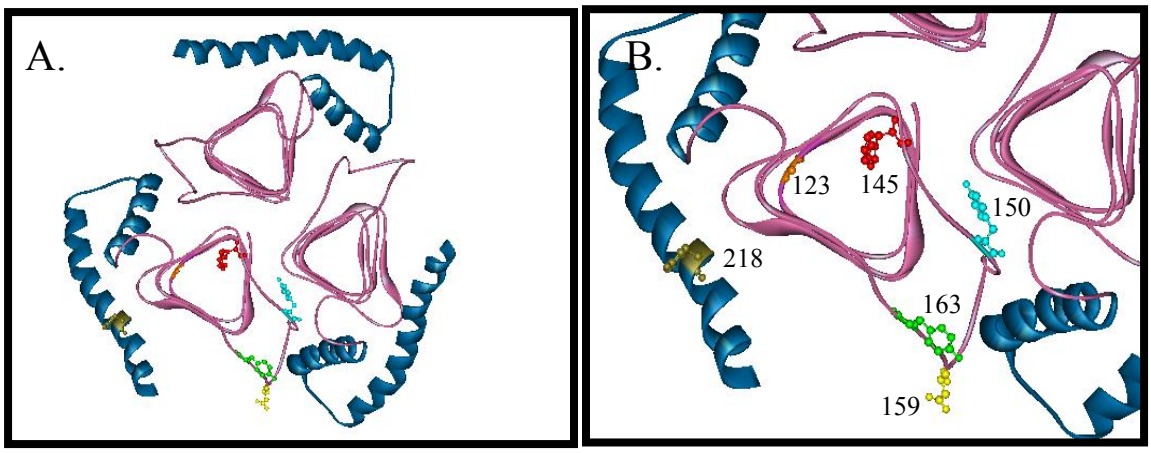

Figure 4-3. Showing Govaerts model for PrP^{Sc} [9]. (A) shows a trimer of misfolded residues comprising the fibillar core. (B) shows a close-up of a single monomer and the six mutant positions used in this study. Residues are colored similarly to Figure 4.2: (From most to least exposed in PrP^{C} based on k_q calculations): W145 ■ G123 ■ N159 ■ Y218 ■ Y163 ■ Y150 ■. Structure coordinates kindly provided by Govaerts.

In the β-helix model by Govaerts [9], residues 89-175 form β-helices while the C-terminal alpha helices B and C remain mostly intact along with the disulfide bridge. β-strands forming parallel β-sheets can wrap around in a helical fashion creating a supra secondary structure known as the β-helix. The β-helical conformation allows for stackable trimeric units interacting at the tops and bottoms of the β-helices to form cross β-structure parallel to the long fibril axis [9].

It is possible to look more closely at the residue positions within the β-helix model (Figure 4-3) to compare with the k_q derived accessibility data. *In-silico* mutations and energy minimizations on the computational trimeric model were not performed due to the instability of the model during the energy minimization process. SASA data were

therefore collected on the native residues at those positions to obtain an idea of the exposure of the side chain. While not very obvious in Figure 4-3, W145 is located on the top rung of the β-helix and could form contacts with the bottom rung of an additional β-helix trimer stacked on top, which is the model for fibrillar formation. W145 would therefore be buried, which is consistent with our quenching data. G123W is found within the β-sheet core of the helix and is not very solvent exposed, which is also consistent with the quenching data. In contrast, N159W is on the kink of the turn and is very highly exposed to solvent, which is not compatible with the low k_q measured in our studies. Y150, Y163, and Y218 all fell in the range of ~40-50% exposure, and it does not appear that trimer stacking would cause these residues to become buried from solvent when part of the fibrillar complex; this is not consistent with the respective quenching data predicting solvent exposures for these residues between 7-12% in PrP^{β}. Therefore, even when trimer stacking is considered, the SASA estimations of the β-helix model do not fit with the solvent accessibility data derived from our k_q determinations.

(B) β-Spiral Model

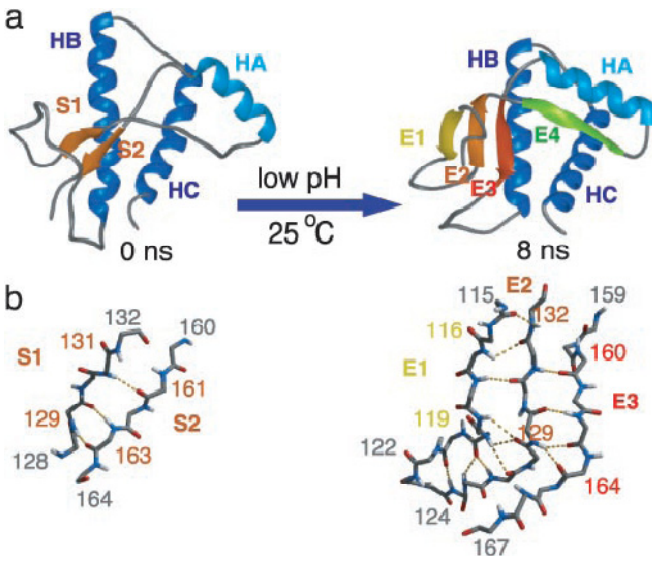

Figure 4-4. Shows simulation of conversion from PrP^{C} to the β-spiral model of PrP^{Sc} (a) with the α-helices labeled HA, HB, HC and the β-strands labeled S1 and S2 in PrP^{C} and E1-E4 (for extended structure) in PrP^{Sc}. (b) shows the hydrogen bonds between the β-strands in PrP^{C} and the β-strands or extended structure in PrP^{Sc} following conversion. Figure taken from [10], copyright 2004 National Academy of Sciences, U.S.A.

The β-spiral model [10-12] is based on the formation of extended β–strand structure in the N-terminal region. Although there are two short β-strands in PrP^{C} (Figure 4-4b), this model predicts that PrP^{Sc} contains an increase in β-sheet extended structure with the formation of additional β-strands (residues 116-132 and 160-164). In contrast with the β-helix model, the structure of helix A is largely unchanged. Though the increased β-sheet structure in the N-terminal region is similar to the β-helix model, there are some major differences between the two models. In contrast to the β-helix model, there is no stacking of the cross-β structure, but rather the spiraling of extending sheets formed by both parallel and antiparallel extended β-strands. Strikingly, residue 123 is

positioned at the turn between E1 and E2 and is highly accessible, in contrast to the β-helix model where G123 is buried within the β-helical structures. To provide further information in the hopes of distinguishing between the two proposed models of PrP^{Sc}, Valerie Daggett and Mari DeMarco, who developed the β-spiral model, calculated SASA of various residues using their own methods [13]. Solvent exposure at specific residues was compared between the two models and positions were chosen that exhibited the largest changes in SASA, and so could most easily distinguish among PrP^{C} and the two models of PrP^{Sc}.

Summary		Solvent Exposure		
		PrP^{C}	Spiral	Beta-helix
GLY	123	exposed	Exposed (76)	buried (6)
TRP	145	exposed	Exposed (89)	buried (15)
ASN	159	buried	buried (12)	exposed (120)

Table 4-3. Shows positions and their corresponding calculated solvent accessible surface area data (SASA) in the β-spiral model and the β-helix model of misfolded PrP. Calculated SASA was provided by Mari DeMarco and Valerie Daggett using their own methods. The SASA data are not recorded as percentages.

In the β-spiral model, both G123 and W145 should be highly exposed, which is not consistent with the quenching data. Quenching data for N159W, however, is consistent with the β-spiral model as this position is predicted to be buried. In contrast, the β-helix model shows residue 123 and 145 as being part of the β-helices and buried, but N159W is on the corner of a loop and will be very solvent accessible. In both models, Y218W is found to still be part of the α-helix with not much conformational

change. The decrease in k_q value upon conversion to a β-enriched isoform may be attributed to the protofibrillar packing in the β-spiral or in the β-helix model the stacking of trimers and/or the packing of protofibrils. Y218W, although still more buried than in PrP^C, had the greatest k_q/solvent accessibility of all the mutants. This seems reasonable according to both of these models. Based on the combined SASA calculations (Table 4-3) and the observable locations of the Trp residues in both models (Figures 4-3 and 4-4), it is seen that the accessibility data derived from the k_q values (Table 4-1) do not fit well with either computational model.

4-4. Experimental Techniques and Related Structural Data

(A) YYR Epitopes

While residues 123, 145, and 159 were chosen because they were predicted to distinguish between the β-helix and β-spiral models of PrP^{Sc}, residues 150, 163, and 218 were chosen for slightly different reasons. Although these three residues have the potential to distinguish between the theoretical models, other studies using antibodies and tyrosine nitration prompted the study of these positions. Y218W is located in the most C-terminal α-helix and doesn't show much change in either model. Because of this, it was originally considered a good "control" position, although its susceptibility to nitration [6] might suggest otherwise. Residues 150 and 163 are tyrosines found within the two YYR motifs in PrP (residues 149-151 and 162-164). Work done by Cashman and colleagues [14] found that there is increased accessibility of one or both of the YYR motifs in PrP^{Sc} compared to PrP^C. Specifically, it was reported that antibody binding targeting the YYR epitope occurs in PrP^{Sc} but not in PrP^C, suggesting that at least one of these repeats becomes more surface exposed in the misfolded state. More recently, the YYR epitope

containing Y150W was found to become more sensitive to tyrosine nitration following conversion to PrP^{β} [6]. In this report, both Y163W and Y150W were designed to investigate the two YYR motifs. It was expected that at least one of these mutants (probably Y150W) would exhibit a large increase in solvent accessibility upon conversion. However, neither mutant displayed any increase in k_q in either PrP^{β} or PrP^{F}; in fact both positions showed a slight decrease in accessibility. These seemingly contrasting results may imply that the other tyrosine in the YYR repeat is the residue responsible for this observed increase in nitratability. This requires closer examination of the various methods involved in accessibility determination for further interpretation.

In the YYR epitope binding study, monoclonal anti-YYR antibodies were used in immunoprecipitation reactions to characterize the specificity for binding PrP^{Sc} over PrP^{C}. It was found that monoclonal YYR antibodies immunoprecipitate PrP^{Sc} but do not select for PrP^{C}. In addition, binding of soluble antigen Tyr-Tyr-Arg to the monoclonal antibodies inhibited their plate binding in an ELISA assay. While soluble antigen Tyr-Ala-Arg showed competitive binding, soluble Ala-Ala-Ala antigen did not show any inhibition [14]. These data could indicate that access to the N-terminal tyrosine or the C-terminal arginine of YYR may be more important than the central tyrosine in binding the antibody, lending support to the hypothesis that tyrosine 149 or 162 would be the more accessible residue.

Concerning the tyrosine nitration studies, it can be seen from the mass spectrometry data that the YYR epitope encompassing residues 149-151 became more readily nitrated upon conversion to PrP^{β}. Upon closer examination, it was also seen that residue 150 was capable of becoming nitrated, but the main nitrotyrosine species detected

in PrP^{β} was at position 149 [6]. Additionally, there are factors other than solvent exposure that significantly influence tyrosine nitration, potentially influencing the results [15]. It is possible that the presence of nearby charged residues would influence the preference to nitrate Y149. Nearby positively charged or sterically hindering residues near a tyrosine will decrease its propensity to react with a nitrating reagent. Since Y150 is adjacent to R151, it is possible that Y149 is less hindered and more able to undergo nitration. Conversely, nearby negatively charged residues will positively influence tyrosine nitration. All in all, there are factors in addition to solvent exposure that determine the ability of a tyrosine to react with nitrating reagents and closer scrutiny of the mechanisms involved provide support for tyrosine 149 as being the residue that is preferentially nitrated. It is also possible that the presence of a more hydrophobic tryptophan molecule in the place of tyrosine would change the structure and reduce this position's solvent exposure, as the fraction of tryptophans found buried at least 95% in proteins exceeds that fraction found for tyrosine residues [15]. Even though Y150 and Y149 are adjacent, it is possible to imagine structures, a simple β-strand being one of them, whereby one residue is buried (facing inwards) and one is facing out towards solvent and is more prone to be nitrated or bind to antibodies.

(B) H/D Exchange, EPR and the Surewicz Model

While both β-helix and β-spiral models were derived through computational methods and map the hydrophobic, β-sheet core of PrP^{Sc} to the N-terminal region (up to residue 175 in the β-helix model), experimental studies have been conducted that provide evidence for a different region comprising this β-sheet core of PrP^{Sc}. Mass spectrometry work by Surewicz using hydrogen/deuterium exchange techniques mapped the cross β-

structural core to residues 169-213, as these residues were most highly protected from exchange. The rapid exchange noted for N-terminal residues 90-140 indicates that this portion of PrP is void of an extensive, stable, hydrophobic backbone structure like a β-sheet stacking interaction [16]. However, when looking at the H/D exchange data for the monomeric PrP^C, it can be seen that while some of the segments containing α-helices are measurably protected, considerable exchange still takes place over the course of 1-2 hours and some α-helical and β-sheet segments exhibit exchange times and deuterium incorporation resembling the fibril exchange data for regions existing outside the β-sheet core (169-213) [16]. This argues that secondary structure outside the highly protected region (169-213) may exist in the form of α-helices or simple β-strands/sheets although not involved in the stacking, cross-β sheet core.

Very recent studies by this group using EPR and spin labeling implicated the presence of parallel, in-register β-strands comprising a cross-β structural core spanning residues ~160-220. These results were seen even after forming fibrils under physiologically relevant, non-denaturing conditions at low pH [17]. Again, residues outside of this site were not seen to possess tight packing or the high degree of order required for single-line spectra spin exchange, but this does not rule out structural organization in the N-terminus (residues ~90-160) as most of these positions did exhibit dipolar broadening [18]. In light of this information (which was not available at the beginning of our experimental design) and the stark contrast with the other two computational models, we therefore sought to compare the Surewicz model with our fluorescence data. The Surewicz studies support the decrease in accessibility of residues 159, 163 and 218. Positions 159, 163, and 218 would be located within the cross-β

structure that has been shown to possess in-register, parallel stacking of β-strands of the individual misfolded monomers. Studies involving prions from yeast [19] and other amyloidogenic peptide fragments including prion have provided evidence of a "steric zipper" structure where one parallel cross β-strand packs adjacent to another parallel cross β-strand forming a dry, hydrophobic, tightly-formed zipper that shields the residues within the core from solvent [20]. If this were the case, tryptophans at 159, 163, and 218 would be found within the hydrophobic zipper structure, be stacked in-register and be highly buried from solvent. This would agree with the SASA data acquired from our k_q values. It is not possible to determine the SASA of the N-terminus using the Surewicz data and so positions 123, 145 and 150 cannot be fully evaluated in context with this model. However, it is plausible that the residues outside the parallel β-sheet core exhibit some secondary structure, and may become more buried upon conversion. It has been shown through FTIR data that there is a significant increase in β-structure upon conversion of PrP^{C} to PrP^{Sc}, but only a slight decrease in α-helicity has been observed [12]. Because of this, it is plausible that conversion of the N-terminus could occur to form α-helical secondary structure.

(C) Antibody Binding

Epitope mapping studies have been performed among the various prion isoforms and can be used as a tool to provide information concerning regions of a protein sequence that bind with an antibody and are thus near the surface. Using the YYR epitope experiments combined with nitration data, it may be possible to elucidate the individual residue accessibilities. However from most other epitope studies, it is not possible to distinguish between accessibilities of individual residues as the antibodies may target

discontinuous or conformational epitopes in the protein. Typical epitopes are 4-6 residues at a minimum. In this respect, it may not be possible to compare the k_q accessibility results of a single residue with antibody studies in which the epitope recognized includes at least 5 residues. While attempting to find positions that report similar or increased solvent accessibility upon conversion, PrP^{Sc}-selective epitopes provide potential positions that undergo a change of accessibility and/or are near the surface. There are only a few PrP^{Sc} specific antibodies that have been found, one of which is the YYR epitope discussed previously. Another, I5B3, is a discontinuous epitope comprising residues 142-148, 162-170, and 214-226 [21]. These residues are accessible in the β-spiral model but do not fit the β-helix model [12]. The Surewicz model has the potential to fit the I5B3 data as well, depending on how the N- and C-Termini pack together around the in-register, stacking β-core protofibrils. Another PrP^{Sc}-selective antibody designated as IgG 136-158 has been shown to bind a fraction of PrP^{F} (23-230). This same antibody is shown to bind to a subfraction of PrP^{β} form as well, although to a lesser extent than PrP^{F} [22]. Although these data show similar binding of PrP^{Sc}-selective antibodies to PrP^{F} and PrP^{β}, there are some differences in conformation as this antibody only bound a fraction of the two isoforms. Nonetheless, it supports these regions as potentially containing accessible residues within the misfolded forms. Also, both these PrP^{Sc} selective antibodies fit the β-spiral model and may fit Surewicz model depending on tertiary conformation but conflict with the β-helix model as residues 136-158 are found within the center of the model [12].

Another PrP^{Sc}-specific antibody is IgG 89-112, mapping to the N-terminus (residues 89-112) of PrP90-231 [22]. This antibody is found to bind PrP^{Sc} but not PrP^{C}

and is shown to bind a fraction of PrP^F as seen from fluorescence studies [22]. Binding of IgG 89-112 to PrP^β was minimal and resembled that of the PrP^F fraction shown not to bind. This demonstrates that conformational differences exist in the various misfolded isoforms. D13 antibody recognizes residues 95-105, and binds to PrP^F (23-231) [22] and to some extent in truncated PrP^F (90-231) [7] but is less accessible in PrP^{Sc} (PrP27-30 - proteinase-K resistant core) [23]. Taken together, the data indicate that although there are slight conformational differences among the misfolded isoforms, there are N-terminal residues that remain or become more solvent exposed upon conversion.

The exposure of C-terminal epitopes has also been explored. While Novitskaya concluded that residues 224-230 in PrP^F (23-230) were buried and resistant to denaturation [22], others have shown it to be accessible in PrP^C as well as in PrP^{Sc} (PrP27-30) and PrP^F (90-231) [7, 12, 23].

To summarize, while antibody binding can map solvent accessible epitopes of a protein, discontinuous or conformational recognition along with the inherent "multi-residue" nature of an antibody epitope makes it difficult to assess individual residue solvent accessibility within a given epitope. At all six of the positions tested here, no tryptophan becomes more accessible upon conversion to the misfolded form. By using antibody data, it becomes possible to predict regions that may remain or become accessible for binding upon conversion, and this information may be helpful in targeting new positions for future Trp quenching studies.

4-5. Summary

Weighted time-resolved k_q values were used to determine the overall accessibility of the tryptophan mutants in the various isoforms. Because k_q values derived for PrP^C

from both steady-state and time-resolved measurements were similar, and because of the presence of static quenching and multiple tryptophan residues in PrP^{β} and PrP^{F} potentially exhibiting unique static and dynamic components, weighted time-resolved k_q values were used to estimate the average Trp exposure in the misfolded isoforms. Using these values, it was possible to correlate SASA with k_q in PrP^{C} and provide an estimate of the SASA of the Trp residues in PrP^{β} and PrP^{F}. Although SASA varied among Trp positions in PrP^{C}, the predicted accessibilities of positions in PrP^{β} and PrP^{F} were very similarly buried, clustering between 4-11% exposure.

All residues examined were seen to become less accessible upon conversion to the misfolded forms, with the largest changes occurring in G123W and W145. This could indicate that the N-terminal residues become more structured and/or form the hydrophobic core of the aggregates. While large accessibility changes were seen to occur at these residues and to a lesser extent at N159W, no residues that we examined were shown to stay as accessible or become more accessible in the misfolded forms. While there may be difficulties with measuring Trp fluorescence and quenching in aggregates, it has been shown that in the oligomeric intermediates of fibril formation with α-synuclein, the Trp residue stays exposed and becomes buried only upon formation of fibrils [8]. Therefore, it should be possible to find a position that shows increased or similar exposure in the misfolded conformers, at least in PrP^{β}. Therefore, if an appropriate residue were chosen, fluorescence quenching could be used to show a change in conformation leading to an increase in exposure. If identified, this position would be an ideal reporter of aggregate formation of the diseased state.

Tryptophan accessibilities were used to evaluate models of PrP^{Sc} and were also compared to data derived from other experimental techniques. It was found that neither computational model of PrP^{Sc} entirely fit our data. We have sought to compare our data with that from the recent Surewicz model of parallel, in-register β-strands comprising residues ~160-220. Because this model is not complete and elicits no structural detail on residues outside this range, it is not possible to fully compare with our data. However, for the residues falling within this area (163, 218 and 159), this model is supported by the decrease in solvent accessibility.

With various pieces of experimental data, it is possible to further refine the conformational criteria for the misfolded isoforms eventually elucidating a structure. In the absence of experimental data, computational methods have been utilized to model the misfolded structure. With experimental methods like H/D exchange and site-directed spin-labeling (SDSL) EPR, structural information on larger segments or regions of proteins can be examined, while other techniques involve looking for changes in residue or epitope exposure among isoforms. Tryptophan fluorescence can give specific information concerning individual residues and can be used in conjunction with the other methods to give detailed accessibility information for further structural elucidation.

4-6. Future Directions

It was an initial aim of my project to identify a position that undergoes a large conformational change between the cellular and misfolded isoforms. This finding could lead to new detection assays using a reporter molecule at the position of the large change to indicate the misfolding of the prion, in conjunction with PMCA [24] or other techniques. While significant changes in solvent accessibility have been observed among

the isoforms, none of the six positions examined was found to be more accessible in PrP^{β} or PrP^{F} than PrP^{C}. The identification of a residue that becomes solvent exposed only in the β-enriched isoforms would be potentially more useful and insightful, because of the potential for a reporter position recognizing conversion to the misfolded isoforms separate from any affects of fibril aggregation. Future directions would be to mutate other positions to accomplish this. A logical "next" experiment would investigate tryptophan fluorescence at residues 162 and 149, as one of these epitopes should be more exposed, based on tyrosine nitration [6] and antibody studies [14]. Because positions 150 and 163 did not become more accessible, it is possible that the adjacent tyrosine is responsible for the increased accessibility noted in these studies.

Also of interest would be the region between residues 90-105 and 225-230, as the antibody binding studies in this region have shown evidence that some residues remain exposed in PrP^{Sc} [22, 23]. This also may provide further information concerning theoretical models, as both the β-helix and β-spiral model invoke the N-terminal region in the formation of β-sheets whereas data from Surewicz indicates that the C-terminal region between ~160-220 is primarily involved in β-sheet formation, not the N-terminus.

A further step would be to use tryptophan screening and mutate every position along the protein deriving accessibility information for every residue. While this would be very illuminating, it may not be very practical due to the time it takes to make and purify each mutant protein, along with analyzing the time-resolved data.

Although it should be possible to find a residue that shows increased accessibility between PrP^{C} and the misfolded isoforms, tryptophan fluorescence quenching may not be the best method for structural determination based the problems inherent to the formation

of large aggregates. Overall, using a multitude of different techniques, including fluorescence, it is possible to examine various models of PrP^{Sc} as they become available. This would bring researchers one step closer to solving the structural mysteries of the misfolded prion protein.

References

1. Koradi R, Billeter M, Wuthrich K: **MOLMOL: a program for display and analysis of macromolecular structures**. *J Mol Graph* 1996, **14**(1):51-55, 29-32.
2. Eftink MR, Ghiron CA: **Exposure of tryptophanyl residues in proteins. Quantitative determination by fluorescence quenching studies**. *Biochemistry* 1976, **15**(3):672-680.
3. James TL, Liu H, Ulyanov NB, Farr-Jones S, Zhang H, Donne DG, Kaneko K, Groth D, Mehlhorn I, Prusiner SB *et al*: **Solution structure of a 142-residue recombinant prion protein corresponding to the infectious fragment of the scrapie isoform**. *Proc Natl Acad Sci U S A* 1997, **94**(19):10086-10091.
4. Alonso DO, DeArmond SJ, Cohen FE, Daggett V: **Mapping the early steps in the pH-induced conformational conversion of the prion protein**. *Proc Natl Acad Sci U S A* 2001, **98**(6):2985-2989.
5. Liu H, Farr-Jones S, Ulyanov NB, Llinas M, Marqusee S, Groth D, Cohen FE, Prusiner SB, James TL: **Solution structure of Syrian hamster prion protein rPrP(90-231)**. *Biochemistry* 1999, **38**(17):5362-5377.
6. Lennon CW, Cox HD, Hennelly SP, Chelmo SJ, McGuirl MA: **Probing structural differences in prion protein isoforms by tyrosine nitration**. *Biochemistry* 2007, **46**(16):4850-4860.
7. Baskakov IV, Legname G, Baldwin MA, Prusiner SB, Cohen FE: **Pathway complexity of prion protein assembly into amyloid**. *J Biol Chem* 2002, **277**(24):21140-21148.
8. Dusa A, Kaylor J, Edridge S, Bodner N, Hong DP, Fink AL: **Characterization of oligomers during alpha-synuclein aggregation using intrinsic tryptophan fluorescence**. *Biochemistry* 2006, **45**(8):2752-2760.
9. Govaerts C, Wille H, Prusiner SB, Cohen FE: **Evidence for assembly of prions with left-handed beta-helices into trimers**. *Proc Natl Acad Sci U S A* 2004, **101**(22):8342-8347.
10. DeMarco ML, Daggett V: **From conversion to aggregation: protofibril formation of the prion protein**. *Proc Natl Acad Sci U S A* 2004, **101**(8):2293-2298.
11. DeMarco ML, Daggett V: **Molecular mechanism for low pH triggered misfolding of the human prion protein**. *Biochemistry* 2007, **46**(11):3045-3054.
12. DeMarco ML, Silveira J, Caughey B, Daggett V: **Structural properties of prion protein protofibrils and fibrils: an experimental assessment of atomic models**. *Biochemistry* 2006, **45**(51):15573-15582.
13. Daggett V, DeMarco ML. In. Edited by McGuirl MA; 2005.

14. Paramithiotis E, Pinard M, Lawton T, LaBoissiere S, Leathers VL, Zou WQ, Estey LA, Lamontagne J, Lehto MT, Kondejewski LH *et al*: **A prion protein epitope selective for the pathologically misfolded conformation**. *Nat Med* 2003, **9**(7):893-899.
15. Souza JM, Daikhin E, Yudkoff M, Raman CS, Ischiropoulos H: **Factors determining the selectivity of protein tyrosine nitration**. *Arch Biochem Biophys* 1999, **371**(2):169-178.
16. Lu X, Wintrode PL, Surewicz WK: **Beta-sheet core of human prion protein amyloid fibrils as determined by hydrogen/deuterium exchange**. *Proc Natl Acad Sci U S A* 2007, **104**(5):1510-1515.
17. Cobb NJ, Apetri AC, Surewicz WK: **Prion protein amyloid formation under native-like conditions involves refolding of the C-terminal alpha-helical domain**. *J Biol Chem* 2008, **283**(50):34704-34711.
18. Cobb NJ, Sonnichsen FD, McHaourab H, Surewicz WK: **Molecular architecture of human prion protein amyloid: a parallel, in-register beta-structure**. *Proc Natl Acad Sci U S A* 2007, **104**(48):18946-18951.
19. Nelson R, Sawaya MR, Balbirnie M, Madsen AO, Riekel C, Grothe R, Eisenberg D: **Structure of the cross-beta spine of amyloid-like fibrils**. *Nature* 2005, **435**(7043):773-778.
20. Sawaya MR, Sambashivan S, Nelson R, Ivanova MI, Sievers SA, Apostol MI, Thompson MJ, Balbirnie M, Wiltzius JJ, McFarlane HT *et al*: **Atomic structures of amyloid cross-beta spines reveal varied steric zippers**. *Nature* 2007, **447**(7143):453-457.
21. Korth C, Stierli B, Streit P, Moser M, Schaller O, Fischer R, Schulz-Schaeffer W, Kretzschmar H, Raeber A, Braun U *et al*: **Prion (PrPSc)-specific epitope defined by a monoclonal antibody**. *Nature* 1997, **390**(6655):74-77.
22. Novitskaya V, Makarava N, Bellon A, Bocharova OV, Bronstein IB, Williamson RA, Baskakov IV: **Probing the conformation of the prion protein within a single amyloid fibril using a novel immunoconformational assay**. *J Biol Chem* 2006, **281**(22):15536-15545.
23. Peretz D, Williamson RA, Matsunaga Y, Serban H, Pinilla C, Bastidas RB, Rozenshteyn R, James TL, Houghten RA, Cohen FE *et al*: **A conformational transition at the N terminus of the prion protein features in formation of the scrapie isoform**. *J Mol Biol* 1997, **273**(3):614-622.
24. Saborio GP, Permanne B, Soto C: **Sensitive detection of pathological prion protein by cyclic amplification of protein misfolding**. *Nature* 2001, **411**(6839):810-813.

Appendix

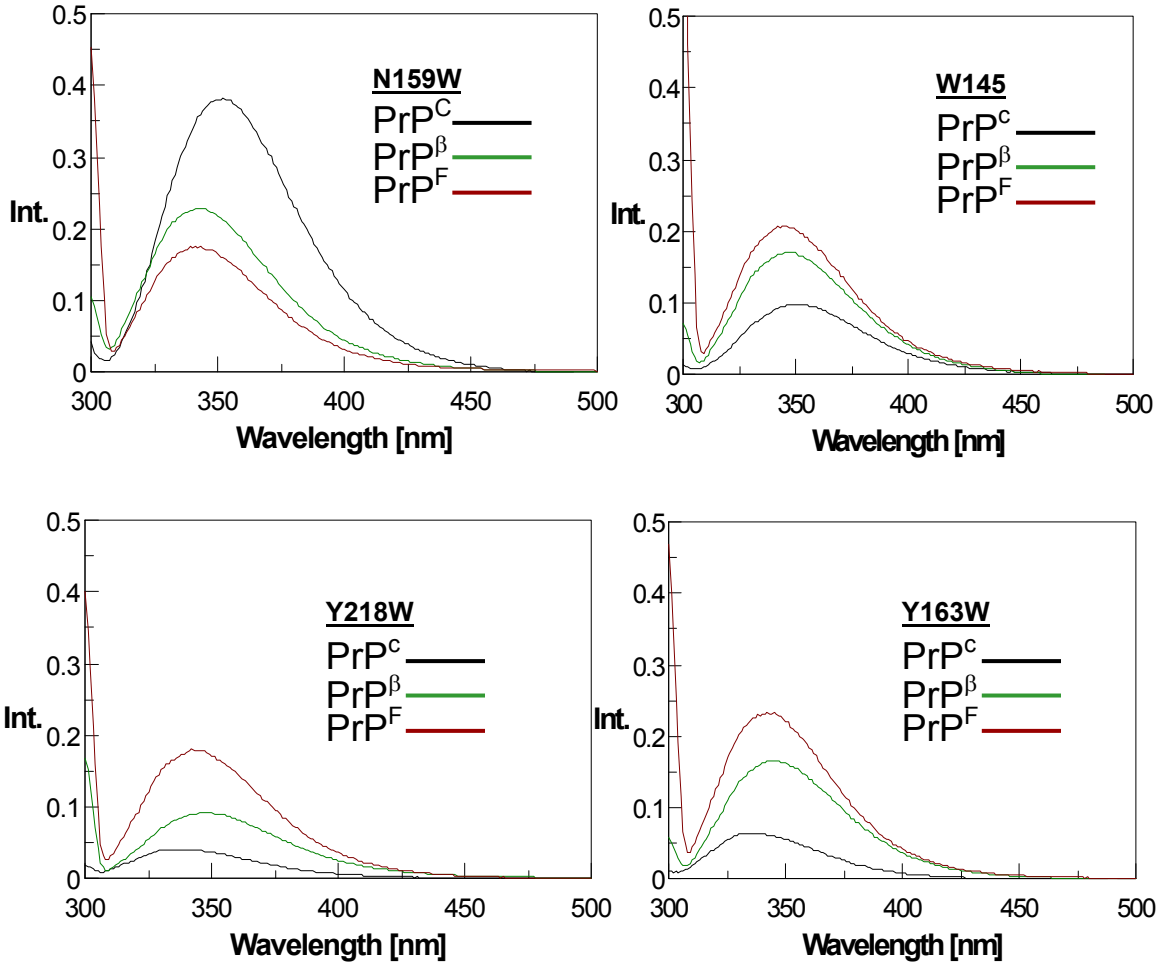

Figure A-1. Steady-state spectra for additional mutants in the three different isoforms PrP^{C}, PrP^{β}, and PrP^{F}. All spectra normalized to 20 μM concentration.

I. Y163W

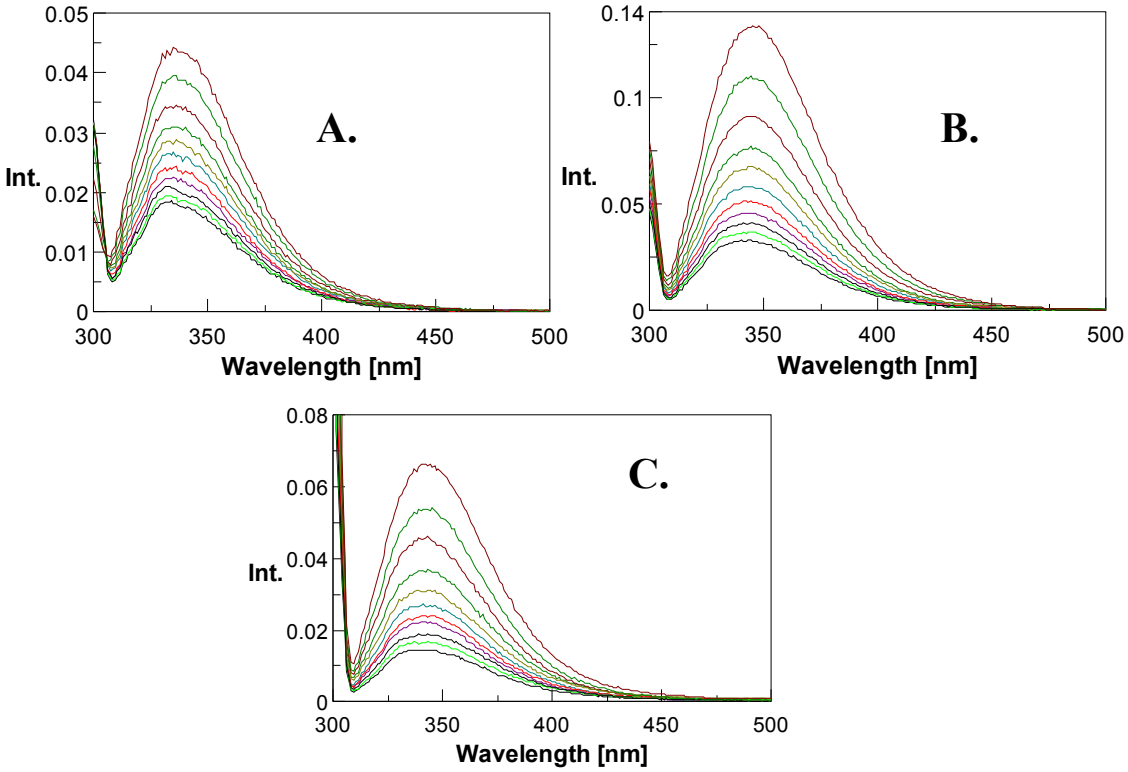
A.
B.
C.
Int.
Wavelength [nm]
0.05
0.04
0.03
0.02
0.01
0
0.14
0.1
0.08
0.06
300
350
400
450
500

II. Y218W

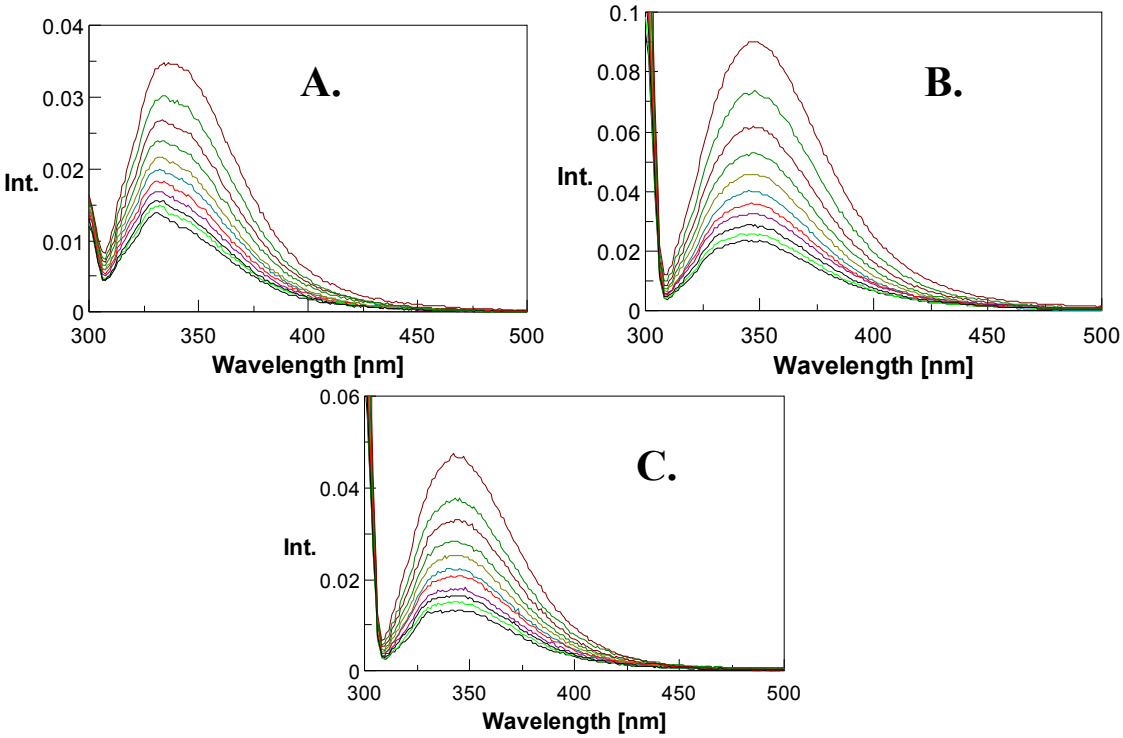
A.
B.
C.
Int.
Wavelength [nm]
0.04
0.03
0.02
0.01
0
0.1
0.08
0.06
0.04
0.02
300
350
400
450
500

III. W145:

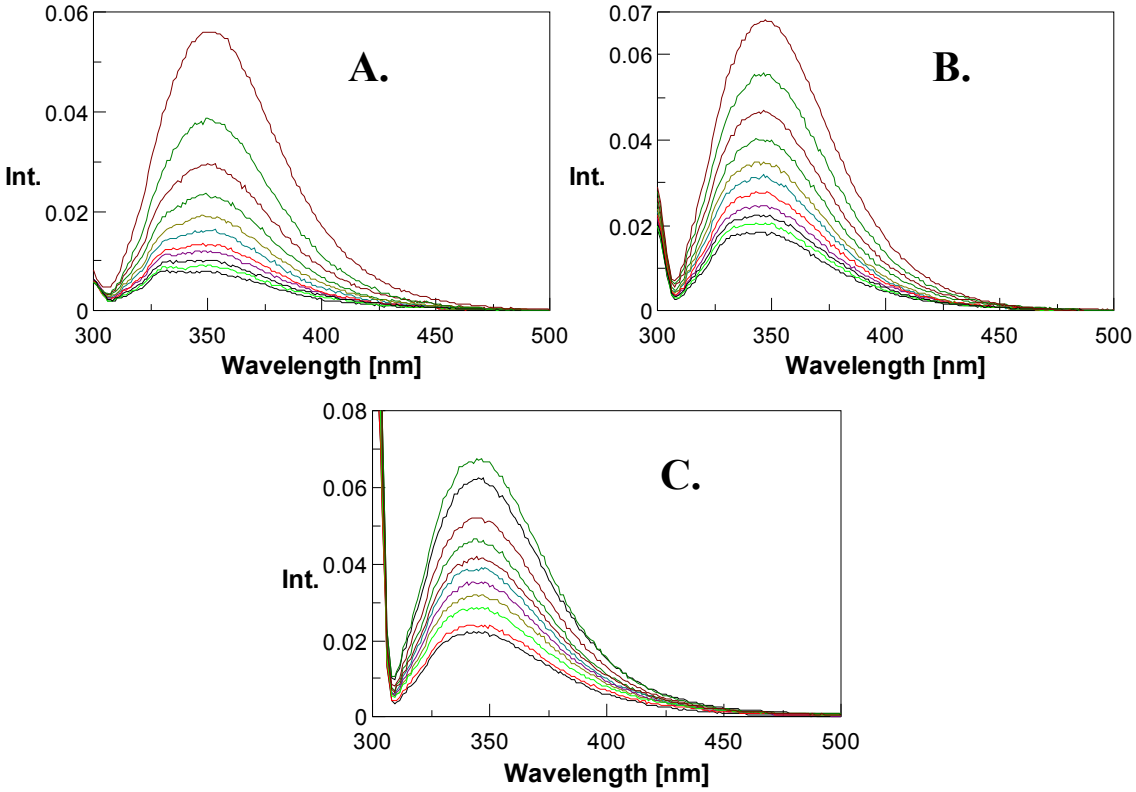

IV. Y150W:

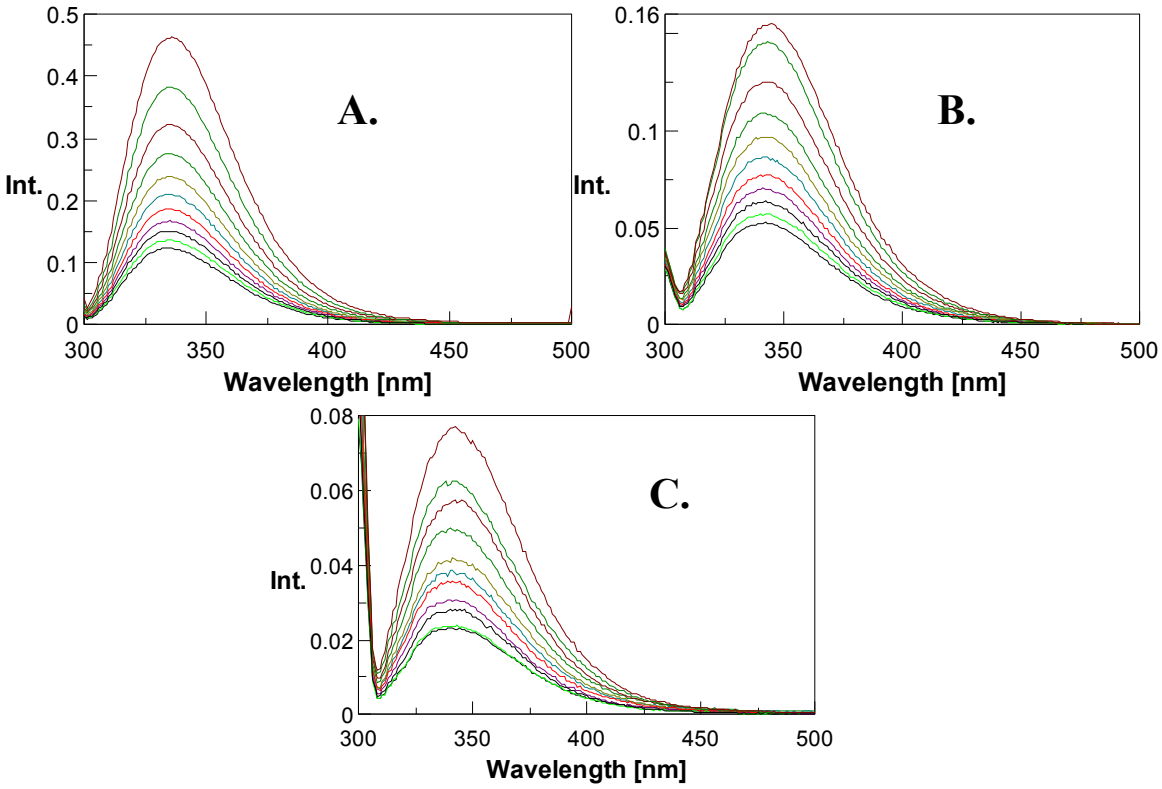
A.
B.
C.
Int.
Wavelength [nm]
0.5
0.4
0.3
0.2
0.1
0
0.16
0.1
0.05
0.08
0.06
0.04
0.02
300
350
400
450
500

V. G123W:

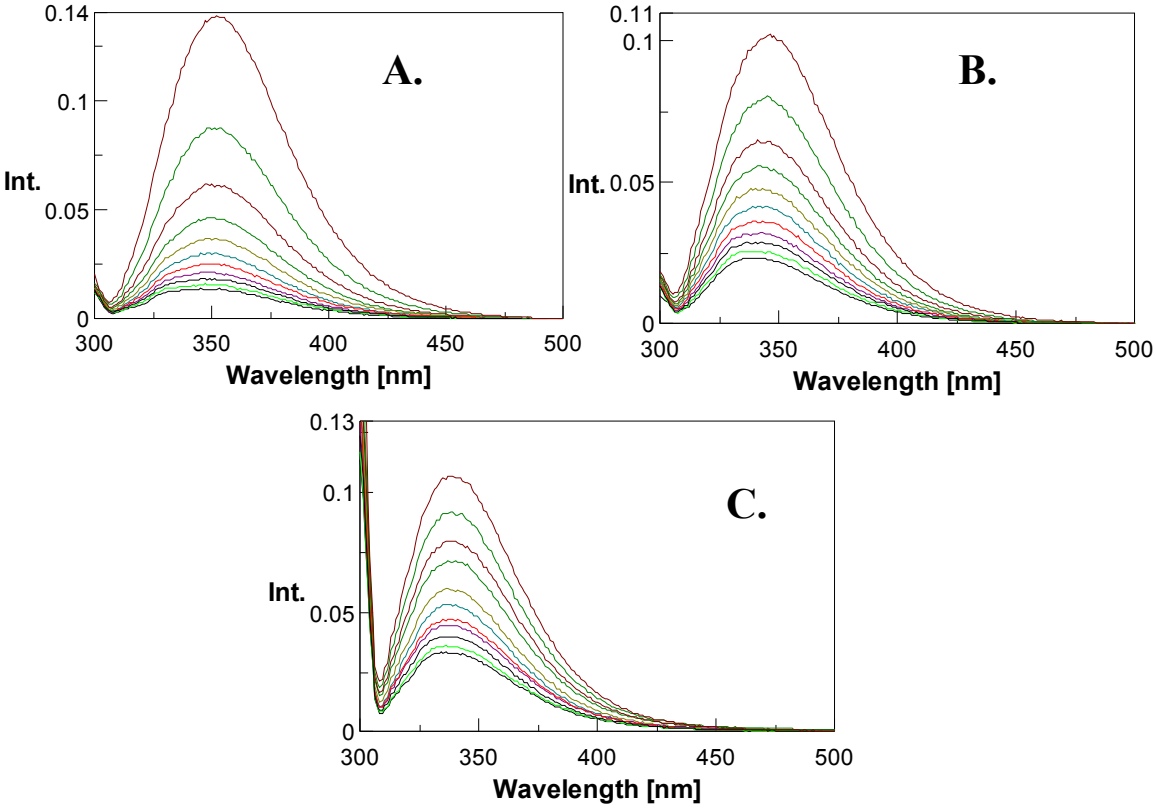

Figures A-2 (I-V). Steady-state quenching spectra for five mutants in (A) PrP^{C}, (B) PrP^{β}, and (C) PrP^{F} isoforms. Acrylamide was added at 0.05 M increments up to 0.5 M concentration total.

I. Y163W

A. **B.**

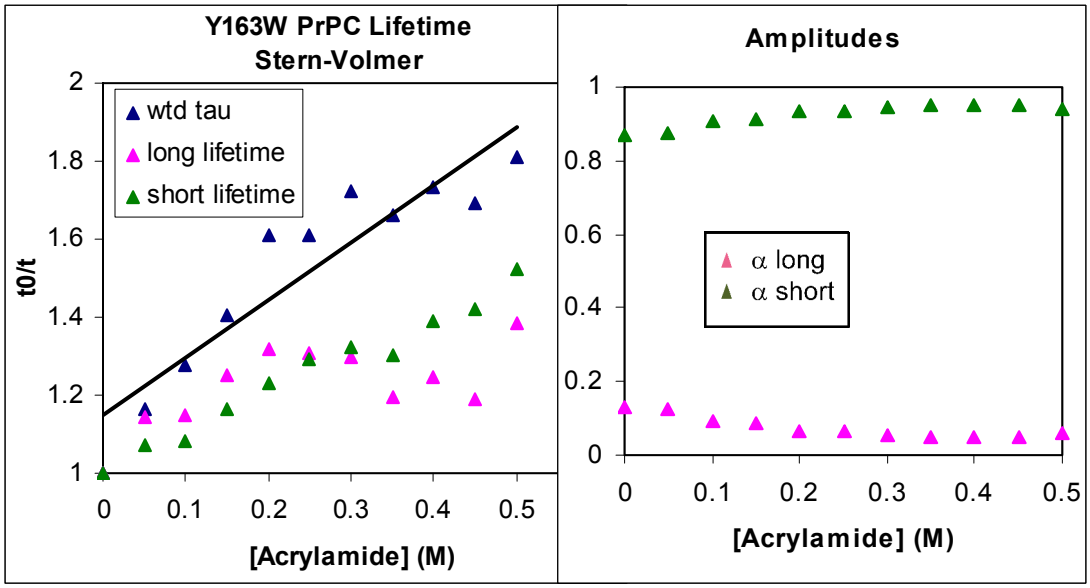
Y163W PrPC Lifetime
Stern-Volmer
wtd tau
long lifetime
short lifetime
t0/t
[Acrylamide] (M)
Amplitudes
α long
α short
[Acrylamide] (M)

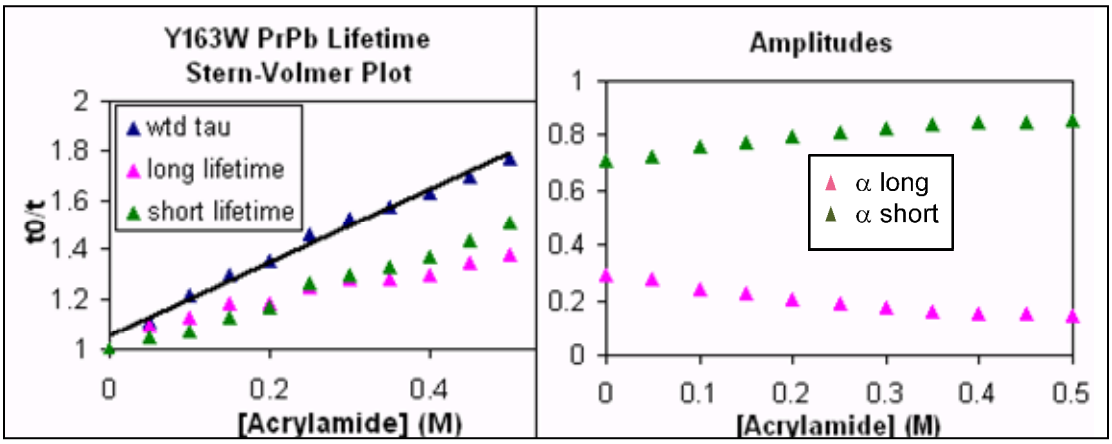
Y163W PrPb Lifetime
Stern-Volmer Plot
wtd tau
long lifetime
short lifetime
t0/t
[Acrylamide] (M)
Amplitudes
α long
α short
[Acrylamide] (M)

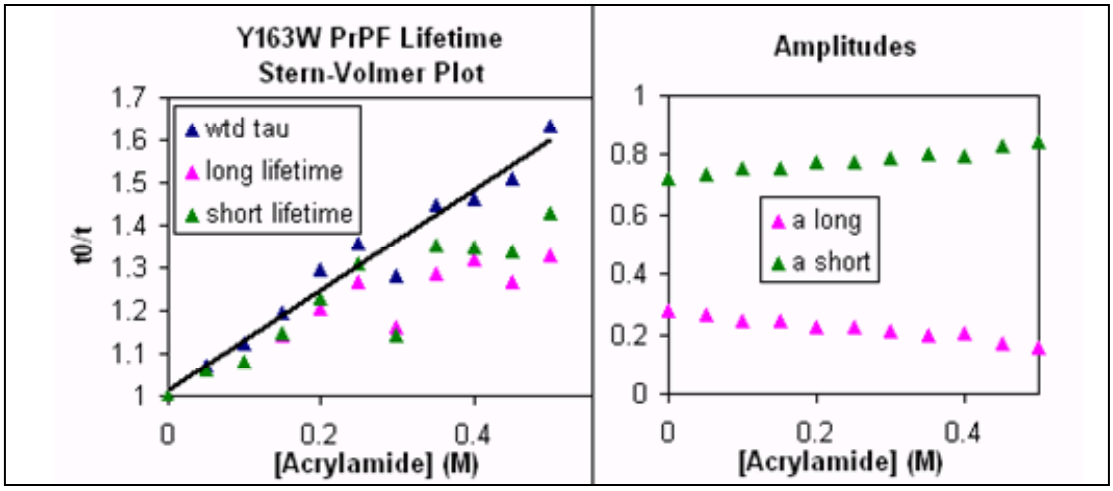
Y163W PrPF Lifetime
Stern-Volmer Plot
wtd tau
long lifetime
short lifetime
t0/t
[Acrylamide] (M)
Amplitudes
a long
a short
[Acrylamide] (M)

II. W145

A. **B.**

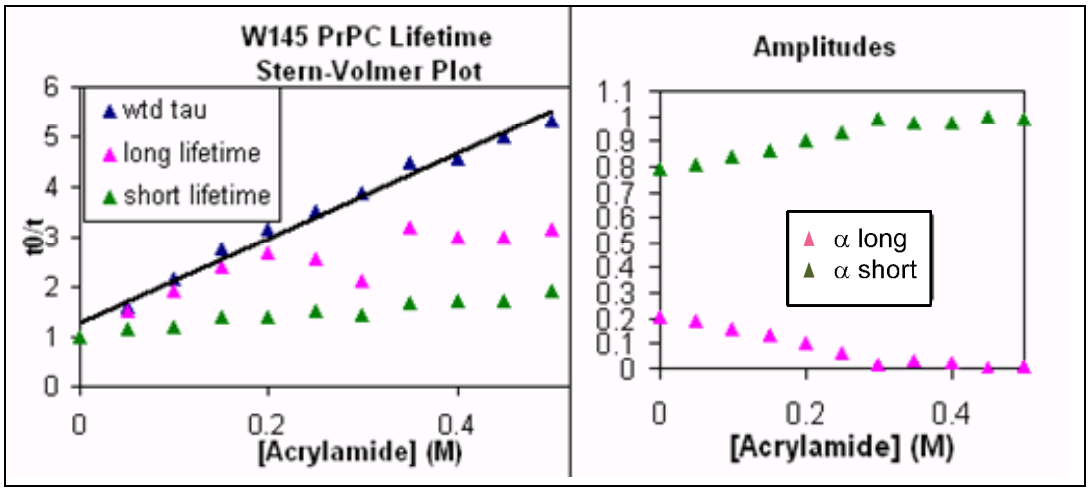
W145 PrPC Lifetime
Stern-Volmer Plot
wtd tau
long lifetime
short lifetime
t0/t
[Acrylamide] (M)
Amplitudes
α long
α short
[Acrylamide] (M)

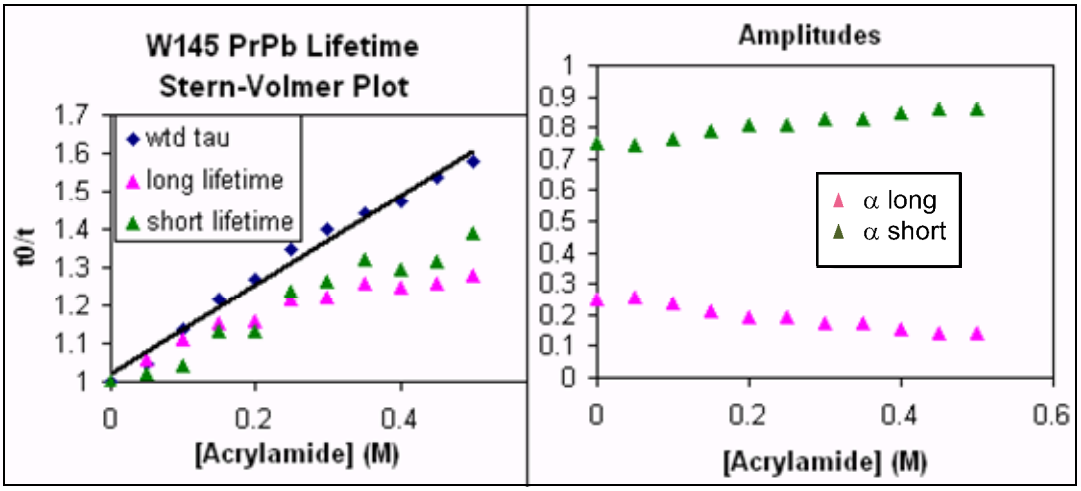
W145 PrPb Lifetime
Stern-Volmer Plot
wtd tau
long lifetime
short lifetime
t0/t
[Acrylamide] (M)
Amplitudes
α long
α short
[Acrylamide] (M)

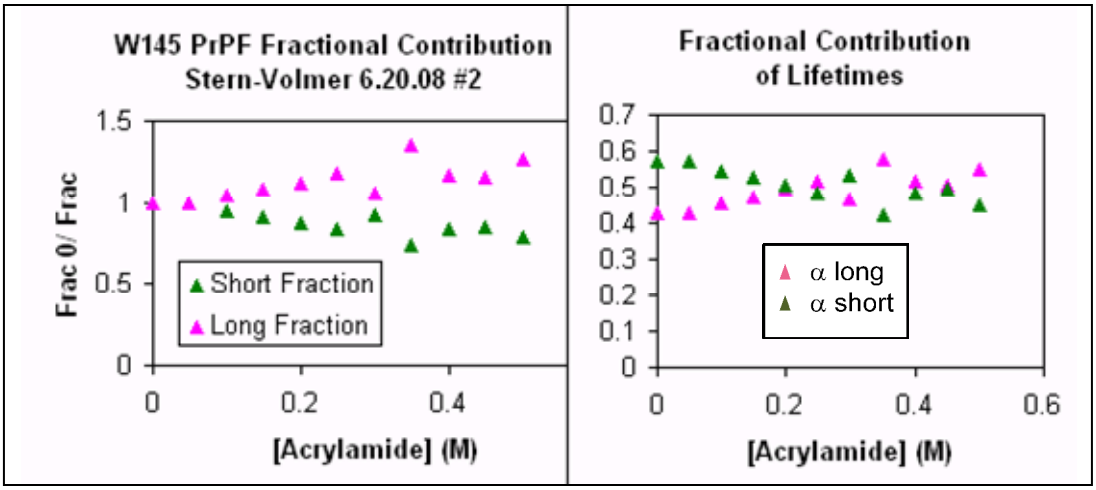
W145 PrPF Fractional Contribution
Stern-Volmer 6.20.08 #2
Frac 0/ Frac
Short Fraction
Long Fraction
[Acrylamide] (M)
Fractional Contribution
of Lifetimes
α long
α short
[Acrylamide] (M)

III. Y150W

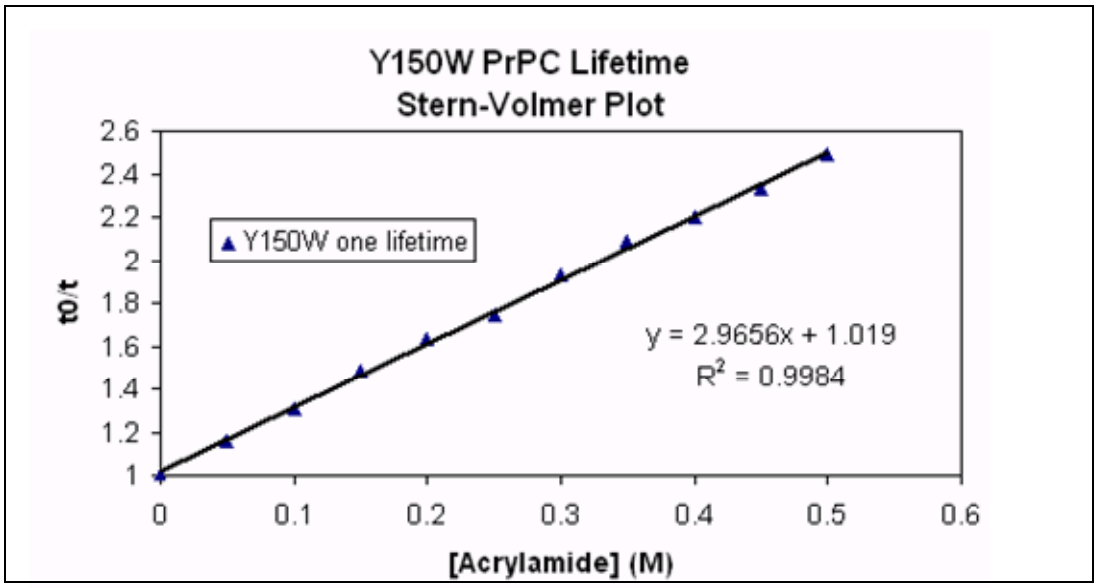
Y150W PrPC Lifetime
Stern-Volmer Plot
Y150W one lifetime
y = 2.9656x + 1.019
R2 = 0.9984
t0/t
[Acrylamide] (M)

A. **B.**

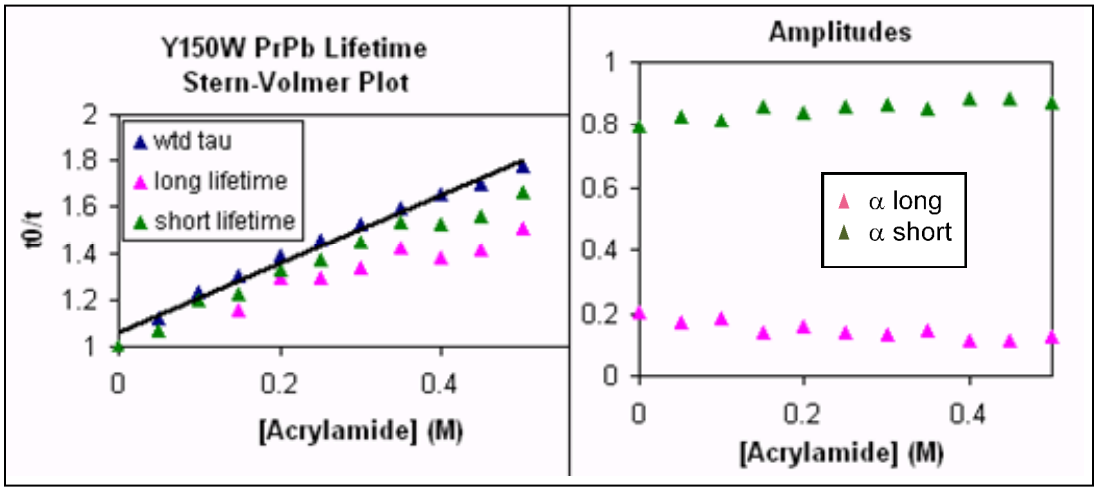
Y150W PrPb Lifetime
Stern-Volmer Plot
wtd tau
long lifetime
short lifetime
t0/t
[Acrylamide] (M)
Amplitudes
α long
α short
[Acrylamide] (M)

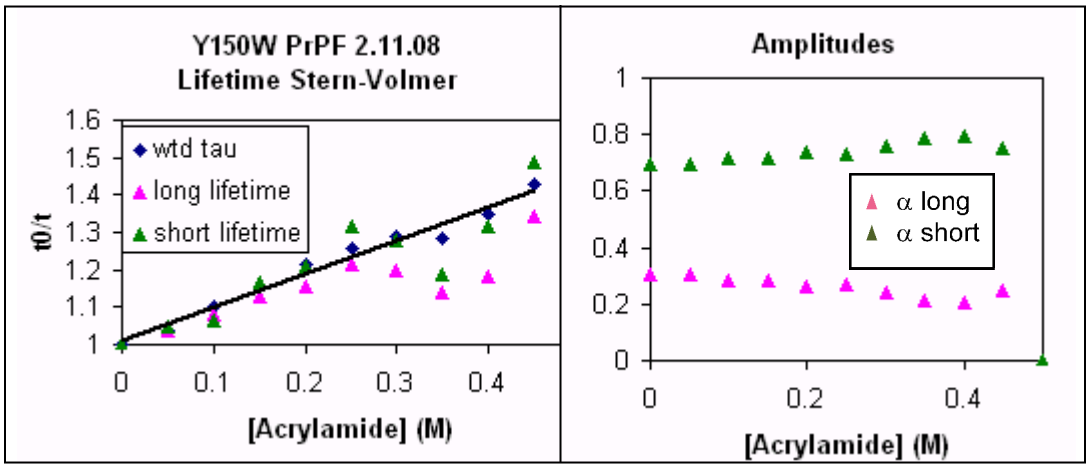
Y150W PrPF 2.11.08
Lifetime Stern-Volmer
wtd tau
long lifetime
short lifetime
t0/t
[Acrylamide] (M)
Amplitudes
α long
α short
[Acrylamide] (M)

IV. G123W:

A. **B.**

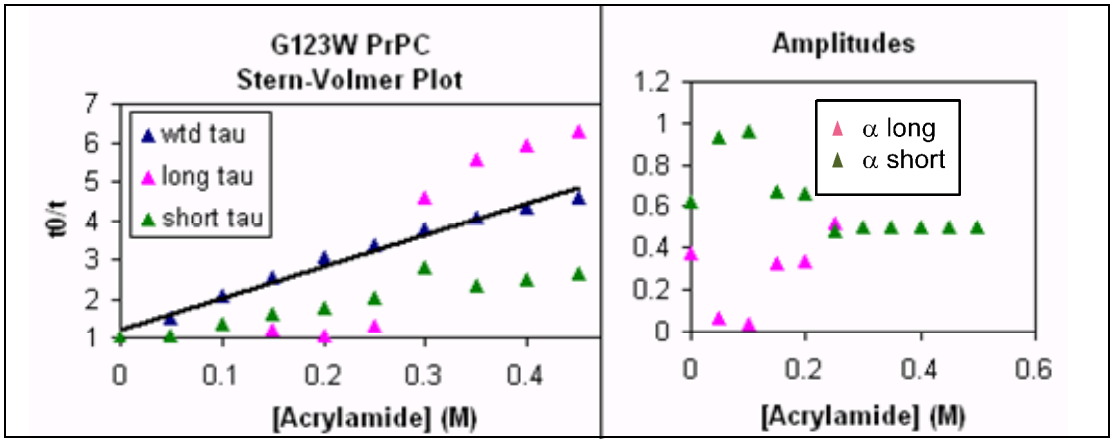
G123W PrPC
Stern-Volmer Plot
wtd tau
long tau
short tau
t0/t
[Acrylamide] (M)
Amplitudes
α long
α short
[Acrylamide] (M)

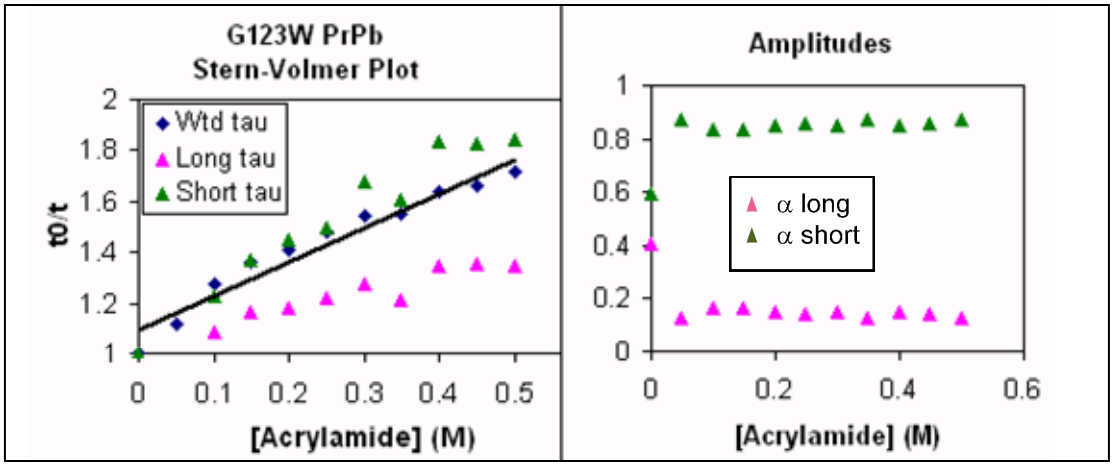
G123W PrPb
Stern-Volmer Plot
Wtd tau
Long tau
Short tau
t0/t
[Acrylamide] (M)
Amplitudes
α long
α short
[Acrylamide] (M)

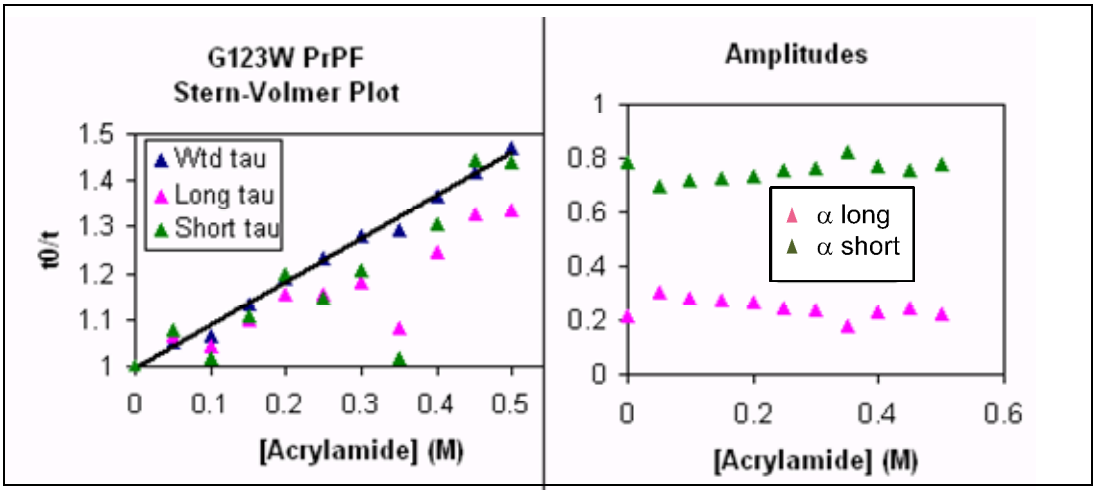
G123W PrPF
Stern-Volmer Plot
Wtd tau
Long tau
Short tau
t0/t
[Acrylamide] (M)
Amplitudes
α long
α short
[Acrylamide] (M)

V. N159W

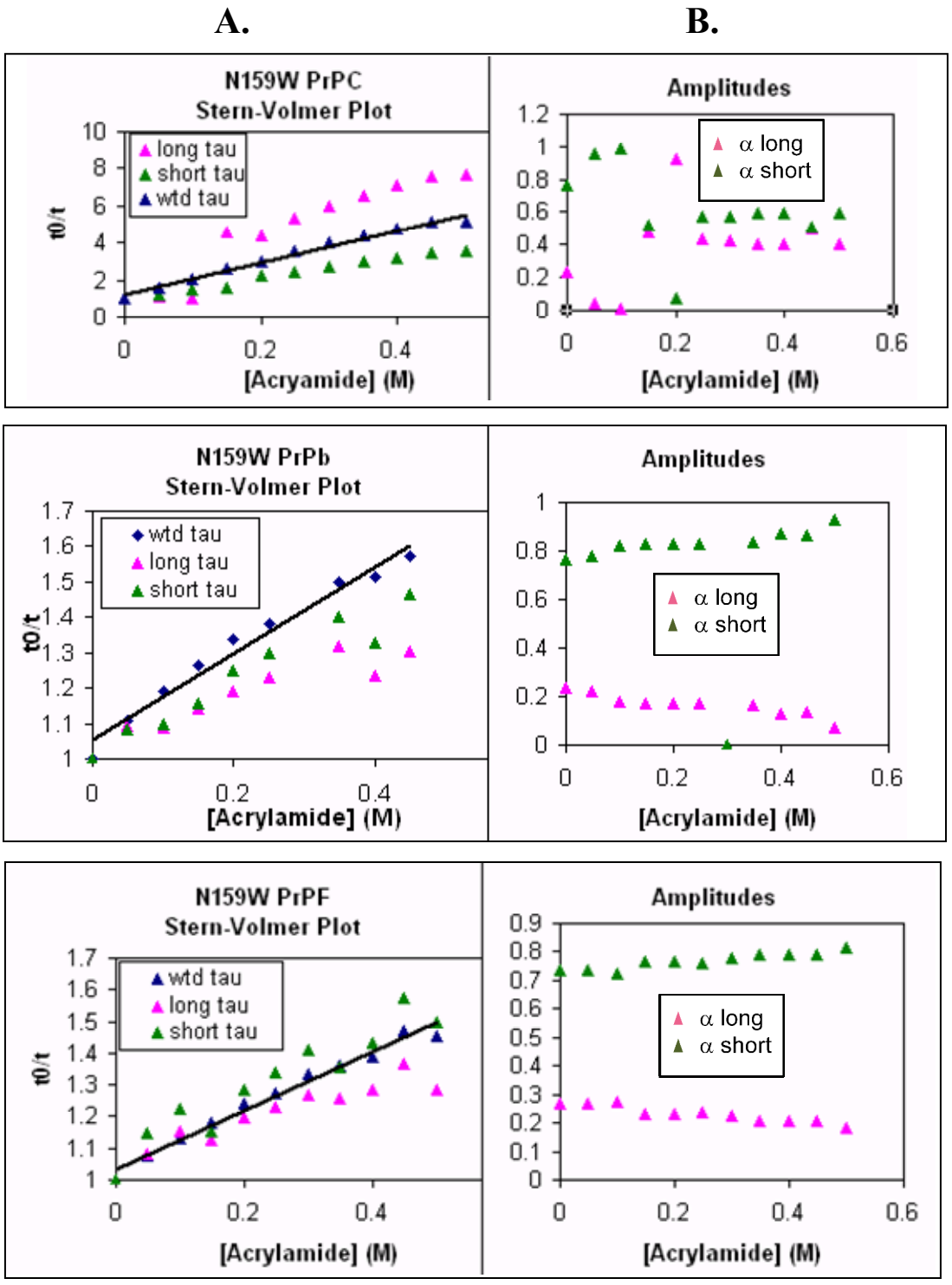

Figures A-3 (I-V): (A) column shows time-resolved quenching Stern-Volmer plots for 5 mutants in PrP^{C}, PrP^{β}, and PrP^{F}. (B) column shows α values of the corresponding lifetime normalized to unity as a function of quencher concentration for 5 mutants in various isoforms.